PERFORMANCE CHARACTERISTICS OF SOLAR AIR HEATED HDH DESALINATION SYSTEM

BY

ISLAM ABDULHAFEZ SHABANEH

A Thesis Presented to the

DEANSHIP OF GRADUATE STUDIES

KING FAHD UNIVERSITY OF PETROLEUM & MINERALS

DHAHRAN, SAUDI ARABIA

In Partial Fulfillment of the
Requirements for the Degree of

MASTER OF SCIENCE

In

MECHANICAL ENGINEERING

JANUARY 2011

KING FAHD UNIVERSITY OF PETROLEUM AND MINERALS

DHAHRAN 31261, SAUDI ARABIA

DEANSHIP OF GRADUATE STUDIES

This thesis, written by Islam Abdulhafez Shabaneh., under the direction of his thesis advisor and approved by his thesis committee, has been presented to and accepted by the Dean of Graduate Studies, in partial fulfillment of the requirements for the degree of **MASTER OF SCIENCE IN MECHANICAL ENGINEERING**.

Thesis Committee

Dr. Mohamed A. Antar (Advisor)

Dr. Syed M. Zubair (Member)

Dr. P. Gandhidasan (Member)

Dr. Amro M Al - Qutub
Department Chairman

Dr. Salam A. Zummo
Dean of Graduate Studies

29/1/11

Date

Dedicated to

My PARENTS,

ADVISOR, BROTHERS

and SISTERS

ACKNOWLEDGEMENTS

I would like to express my gratitude to my advisor Dr. Mohamed A. Antar, for his guidance, support, encouragement, and patience throughout my graduate study. Sincere thanks go to both the members of my committee, Dr. P. Gandhidasan and Dr. S. M. Zubair for their constructive guidance and technical support.

I would further like to express my deep gratitude to Eng. Karam Adham and Eng. Hasan Baig for going out of their way to help me in all possible means. Thanks are also due to the Center of Excellence for Scientific Research Collaboration with MIT for their help and assistance.

Special thanks are due to the support and facilities provided by the National Science, Technology and innovation plan (NSTIP) administered by King Fahd University of Petroleum and Minerals KFUPM under project No. 08-WAT79-4 to carry out this work.

I would like to thanks my senior colleagues at the university Raed and Ahmad Eter who were always there to provide thoughtful solutions to the various problems encountered in my research.

Finally, thanks are due to my parents, my sisters and brothers as well as all my family members for their emotional and moral support throughout my academic career and also for their love, forbearance, encouragement and prayers.

TABLE OF CONTENTS

LIST OF TABLES

LIST OF FIGURES

THESIS ABSTRACT (ENGLISH)

NAME: ISLAM ABDULHAFEZ SHABANEH

TITLE: PERFORMANCE CHARACTERISTICS OF SOLAR AIR HEATED HDH DESALINATION SYSTEM

MAJOR: MECHANICAL ENGINEERING

DATE: JANUARY 2011

Many arid and semi-arid countries such as the Kingdom of Saudi Arabia face shortages of potable water available from natural sources. The limited water resources and the need to balance economic and social development resulted in the emergence of an imbalance between them. Seawater desalination accordingly represents a viable solution to the problem.

In this work, an experimental Setup of HDH solar desalination system was carried out in order to convert the seawater into sweet water. The system consists of nine solar air heaters, a humidifier, a condenser and two water tanks. The system was tested for different experimental operating conditions. A comparison between the experimental and theoretical results of the condenser productivity is made where a close agreement was reported.

Thermal design of two types of heat exchangers (as condensers) was performed, namely a plate fin tube heat exchanger and a shell and tube heat exchanger. Results were compared to the condenser of the experimental setup as well as a condenser designed by a vender. Very good agreement is obtained between the simulation results and the both experimental results and the vender's calculations.

Results of the present study showed that the condensate flow rate increases by increasing the air mass flow rate till an optimum value is reached and then decreases, condensate flow rate also increases by increasing the water mass flow rate.

Furthermore, the condensate flow rate was found to increase by increasing the inlet humid air temperature, whereas it decreases by increasing the inlet water temperature. A sensitivity analysis was performed on both heat exchangers and indicated that changes of the condensate flow rate are influenced by the inlet air temperature followed by the inlet relative humidity. In addition, transverse distance and inlet air velocity have an insignificant effect on the condensate flow rate. Other variables have a negligible effect on the condensate mass flow rate.

Finally, Experimental test of the HDH desalination system indicated high the solar air heater efficiency and condenser effectiveness, whereas the humidifier effectiveness is low. Experimental measurements of temperature and relative humidity for each component in the system are also reported and used in evaluating their performance.

MASTER OF SCIENCE DEGREE
KING FAHD UNIVERSITY OF PETROLEUM and MINERALS
Dhahran, Saudi Arabia

THESIS ABSTRACT (ARABIC)

الاسم : اسلام عبد الحافظ شبانه

العنوان: خصائص اداء انظمه تحليه مياه البحرباستخدام تجفيف ترطيب تسخين الهواء بالطاقه الشميه

التخصص: هندسه ميكانيكيه

التاريخ : كانون الثاني 2011

العديد من البلدان القاحلة وشبه القاحلة مثل المملكة العربية السعودية تواجه نقصا في مياه الشرب المتوفرة من مصادر طبيعية. المصادر المحدوده للمياه والحاجه الى توازن التطور الاقتصادي والاجتماعي ادى الى خطوره عدم الموازنه بينهم . وفقا للك تمثل تحليه مياه البحر حل قابل للتطبيق لهذه المشكله.

في هذا العمل تم بناء نظام تحليه مياه البحرباستخدام تجفيف ترطيب تسخين الهواء بالطاقه الشميه لتغير مياه البحر المالحه الى مياه حلوه. النظام يتكون من تسعه مسخنات هواء بالاضافه الى مرطب واحد ومجفف واحد وخزانان مياه. تم فحص النظام لظروف عمل تجريبيه مختلفه. مقارنه بين النتائج النظريه والعمليه لاتاجيه المكثف تم تدوينها في حين تم تسجيل هذا الاتفاق في الاداء.

توعان من المبادلات الحرايه (كمكثفات) تم تصميمها نظريا وتدعى المبادل الحراري من نوع زعنفه انبوب ونوع قشره وانبوب. تم مقارنه النتائج بالنتائج العمليه للمكثف وكذلك نتائج تصميم المبادل الحراري من قبل مورد.تم التوصل الى اتفاق جيد جدا بين النتائج النظريه والنتائج العمليه وحسابات المورد.

النتائج لهذه الدراسه تظهر بان كميه الانتاجيه تزيد بزياده كميه تدفق الهواء حتى الوصول الى النقطه العليا ثم تقل بعد ذلك، الانتاجيه ايضا" تزيد بزياده كميه تدفق المياه الداخله للمكثف.

علاوة على ذلك، تزيد كميه الانتاجيه بزياده درجه حراره الهواء الرطب الداخل، بينما تقل بزياده درجه حراره المياه الداخله للمكثف. تم عمل تحليل للحساسيه لكل من المبادل الحراري من توع زعنفه انبوب ونوع قشره وانبوب. واظهرت النتائج بان تغير كميه المياه المتكثفه تتأثر بشكل رئيسي بتغير درجه حراره الهواء متبوعه بالرطوبه النسبيه. بالاضافة الى ذلك المسفه المستعرضه وسرعه الهواء الداخل لها تأثير ضئيل على كميه المياه المتكثفه. العوامل الاخرى لها تأثير مهمل على كميه المياه المتكثفه.

في النهايه ، اظهر فحص تجريبي لنظام تحليه المياه عن طريق الطاقه الشمسيه بان فعاليه السخانات الهوائيه الشميه وكذلك المكثف كانت جيده جدا" بينما للمرطب كانت فعالية المرطب قليه. القياسات التجريبيه لكل من الحراره والرطوبه النسبيه عند كل قطعه بالنظام تم تدوينها واستخدمت في تقييم الاداء.

درجة الماجستير في العلوم

جامعه الملك فهد للبترول والمعادن

الظهلران ، المملكه العربيه السعوديه

NOMENCLATURE

Symbol	Definition	unit
A	Heat transfer surface area, area of bare tube without fin	m^2
a_s	Flow area across-tube bundle	m^2
b	Fin height	mm
B	Baffle spacing; parameter in Chisholm correlation for two-phase pressure drop	m
C`	Tube clearance	mm
$C`_{eff}$	Effective clearance for finned-tube bundle	mm
C	Capacitance rate	$W/℃$
Cp	Specific heat	$kJ/kg℃$
$\overline{Cp}$	Average Specific heat	$kJ/kg℃$
D, d	Diameter	mm
D*	Hydraulic diameter of the coil	mm
E	Parameter in Beatty-Katz correlation	mm
F	LMTD correction factor	-
F_1, F_2	Parameters in flooding correlation for reflux condenser	-
FP	Correlating parameter	-
FP(s)	Correlating parameter based on fin spacing	-
f	Friction factor, fin	-
f_i	Fanning friction factor for ideal flow through bank of plain tubes	-
$f_i`$	Fanning friction factor for ideal flow through bank of finned tubes	-

G	Mass flux	$kg/(s.m^2)$
g	Dimensional constant	$kgm/(N.s^2)$
g_c	Unit conversion factor	kg/s^2
H	Coil height	mm
$\hat{H}$	Specific enthalpy	kJ/kg
h	Heat-transfer coefficient, enthalpy	W/m^2℃
I	Solar intensity	W/m^2
i	Latent heat, enthalpy	kJ/kg
j, j-factor	Colburn j factor	-
J(s)	Sensible j-factor	-
$J_i(s)$	Total j-factor	-
j_H	Modified Colburn factor for shell-side heat transfer	-
j^*	Dimensionless vapor mass flux	-
JP	JP parameter	-
k	Thermal conductivity	W/m℃
L	Length, length of the coil	mm
LMTD	Log mean temperature difference	℃
m	Extended surface parameter	-
$\dot{m}$	Mass flow rate	kg/s
N	Number of shell side passes, total number	-
NTU	Number of transfer unit	-
n	Total number	-
p	Atmospheric pressure, heat exchanger parameter	kPa
Pr	Prandtl number	-
P_T	Tube pitch	mm
Q	Volumetric Air flow rate	m^3/s

q	Heat transfer	kW
R	Fin Parameter , fouling factor, thermal resistance	$m^2°C/W$
R_e	Radius of Circular fin	mm
Re, Re_D	Reynolds number	-
$[Re_{Da}]_s$	Reynolds number for air based on fin spacing	-
r	Tube radius	mm
s	Fin spacing, Specific gravity	mm
S	Parameter used to calculate LMTD correction factor	-
Sc	Schmidt number	-
T, t	Temperature	°C
U	Overall heat-transfer coefficient	$W/m^2°C$
$U_D^`$	Modified Design overall heat-transfer coefficient	$W/m^2°C$
V	Total volume of the coil	m^3
v	Fluid velocity	m/s
w	Coil width, Humidity ratio	mm
x_a	Tube transverse distance of heat exchanger	mm
x_b	Tube longitudinal distance of heat exchanger	mm
y	Thickness of the fin	mm
Greek Letters		
Δ	Change, difference	-
β	Fin parameter of plate fin tube heat exchanger	-
ε	Heat exchanger effectiveness	-
Γ	Condensation rate per unit width of surface	kg/ms
Γ́	Modified condensate loading	kg/ms
$\Delta\hat{H}$	Specific enthalpy difference	kJ/kg
ΔP	Pressure drop	kPa

$\Delta T, \Delta t$	Temperature difference	℃
$(\Delta T_{ln})_{cf}$	Logarithmic mean temperature difference for counter flow	℃
ΔW	Humidity ratio difference	-
η	Efficiency, effectiveness	-
θ_{tp}	Tube layout angle	$Degree$
μ	Viscosity	kg/ms
$\overline{\mu_V}$	Average viscosity of vapor	kg/ms
ρ	Density	kg/m^3
τ	Fin thickness	mm
$\emptyset$	Relative humidity	%
ϕ	Parameter used to calculate LMTD correction factor for J- and X-shell exchangers	-
ϕ	Fin parameter	-
ϕ_i	Viscosity correction factor	-
ϕ_L^2	Two-phase multiplier for pressure gradient based on liquid phase flowing alone	-
ϕ_{Lo}^2	Two-phase multiplier for pressure gradient based on total flow as liquid	-
ϕ_{vo}^{-2}	Average two-phase pressure-drop multiplier	-
ψ	Parameter used to calculate LMTD correction factor for J- and X-shell exchangers	-
ψ	Fin parameter of shell and tube heat exchanger	-
α	Total heat transfer area over total volume, parameter used to calculate LMTD correction factor	m
σ	Free flow area over frontal area	-
Subscript		
a	Air	-
ac	Actual	-

amb	Ambient	-
av	Average vapor of the shell side	-
ave	Average, average vapor of the tube side	-
aw	Average water	-
b	Baffle	-
c	Cut, cold, minimum free flow, coolant, condensate, crossed tube rows, condenser	-
ca	Average condensate	-
D	Designed	-
e	Equivalent	-
f, fin	Flow, fin, film, frictional	-
fg	At average wall temperature	-
fo	Shell side	-
fr	Frontal , Fraction	-
g	Gas, vapor	-
h	Hot, hydraulic ,equivalent height, humidifier	-
i	Inlet ,internal ,inlet state conditions, inside	-
l	Latent, liquid	-
L	Liquid ,condensate	-
Lo	Total flow as liquid	-
m	Mean	-
max	Maximum	-
min	Minimum	-
n	Nozzle	-
n, i, o	Inlet and outlet nozzle	-
o	Outlet, outside, overall	-

p	Prime, passes	-
r	Root , row, return	-
r_e	Equivalent root	
req	Required	-
s	Shell, surface, Saturation, solar, sensible, based on fin spacing	-
so	Surface, solar intensity	-
T, t	Tube, total, thickness	-
tot	Total	-
v	Vapor	
vo	Flow as vapor	-
w	Water, wall, weighted	-
wa	Water average	
wtd	Weighted average of finned surface	-
1	Based on Root-tube, inlet	-
2	Based on fin, outlet	-
2c	Based on corrected fin	-

CHAPTER 1

INTRODUCTION

1.1 Background

Water is an important resource for use of mankind in Saudi Arabia, with a population of more than 27 million, growing at an annual rate of 3.8%, the highest in the world. It is essential for agricultural and industrial growth, as well as for supporting growing populations who require a safe drinking water supply. It is found that 97% of all water in oceans, 2% in glaciers and ice caps, and the rest in lakes, rivers and underground. Natural resources cannot satisfy the growing demand for low-salinity water with industrial development, together with the increasing worldwide demand for supplies of safe drinking water. This has forced mankind to search for another source of water. In addition, the rapid reduction of subterranean aquifers and the increasing salinity of these non-renewable sources will continue to exacerbate the international water shortage problems in many areas of the world. Desalination techniques are capable of providing the solution. “Desalination” or “Desalinization” refers to water treatment processes that remove salts from saline water. Desalination has already become an acceptable solution for shortages in conventional water resources.

1.2 Conventional desalination technologies

Desalination of seawater or brackish water is generally performed by either of two main processes: by evaporation of water and condensation of vapor or by use of a semi-permeable membrane to separate fresh water from a concentrate. In the phase-change or thermal processes, the distillation of seawater is achieved by utilizing a heat source. The heat source may be obtained from a conventional fossil-fuel, nuclear energy or from a non-conventional source like solar energy or geothermal energy. In the membrane processes, electricity is used either for driving high pressure pumps or for establishing electric fields to separate the ions.

The most important commercial desalination processes based on thermal energy are multi-stage flash (MSF) distillation, multiple effect distillation (MED) and vapor compression (VC), in which compression may be accomplished thermally (TVC) or mechanically (MVC). The MSF and MED processes consist of many serial stages at successively decreasing temperature and pressure. The MSF process is based on the generation of vapor from seawater or brine due to a sudden pressure reduction (flashing). When seawater enters an evacuated chamber the process is repeated stage-by-stage at successively decreasing pressures. Condensation of vapor is accomplished by regenerative heating of the feed water. This process requires an external steam supply, normally at a temperature around 100℃. The maximum operating temperature is limited by scaling formation, and thus the thermodynamic performance of the process is also limited. For the MED system, water vapor is generated by heating the seawater at a given pressure in each of a series of cascading chambers. The steam generated in one stage, or "effect," is used to heat the brine in the next stage, which is at a lower pressure. The

thermal performance of these systems is proportional to the number of stages, with a capital cost limiting the number of stages to be used. In TVC and MVC systems, after vapor is generated from the saline solution, it is thermally or mechanically compressed and then condensed to generate potable water.

The second important class of industrial desalination processes uses membrane technologies. These are principally reverse osmosis (RO) and electro dialysis (ED). The former requires power to drive a pump that increases the pressure of the feed water to the desired value. The required pressure depends on the salt concentration of the feed. The pumps are normally electrically driven. The ED process also requires electricity to produce migration of ions through suitable ion-exchange membranes Both RO and ED are useful for brackish water desalination; however, RO is also competitive with MSF distillation processes for large-scale seawater desalination.

1.3 The Humidification Dehumidification desalination technology

The solar irradiation of the sun evaporates water from seas, rivers and lakes and also from the soil and plants on the land. The water turns into an invisible gas called water vapor, which humidifies the air. This process is called "Evaporation ".The water vapors cool as they rise into the atmosphere. Cool air cannot hold as much water vapor as warm air, so some of the vapors turn into water droplets (‘dehumidify’ as rain). The process is called "Condensation". In the sky the tiny water droplets from clouds. If these droplets combine to form larger droplets, they will fall to earth as rain, hail or snow. Much of the water that falls on the land flows to the sea in streams and rivers. Some soak into the ground and some stay as ice. The water eventually finds its way into rivers and seas, where the water cycle begins again.

The solar HDH is a thermal water desalination method. It is based on evaporation of seawater or brackish water and consecutive condensation of the generated humid air, mostly at the ambient pressure. The solar HDH process also called the multiple-effect humidification-dehumidification process, solar multistage condensation evaporation cycle (SMCEC) or multiple-effect humidification (MEH), is a technique that mimics the natural water cycle on a shorter time frame by evaporating and condensing water to separate it from other substances. The driving force in this process is thermal solar energy to produce water vapor, which is later condensed in a separate chamber. In sophisticated systems, waste heat is minimized by collecting the heat from the condensing water vapor and pre-heating the incoming water source. This system is effective for small- to mid-scale desalination systems in remote locations because of the relative inexpensiveness of solar collectors. The process of HDH desalination has many advantages, such as the simple equipment working under normal pressure, the cost of investment and operation is moderate, the flexible scale, the low-grade energy available, and so on. Therefore, it has a good developing prospect.

1.4 Classifications of the HDH systems

HDH systems are classified under three broad categories. One is based on the form of energy used such as solar, thermal, geothermal, or hybrid systems. This classification brings out the most promising merit of the HDH concept: the promise of water production by use of low grade energy, especially from renewable resources. The second classification of HDH processes is based on the cycle configuration.

The third classification of the HDH systems is based on the type of heating used water or air heating systems. The performance of the system depends greatly on whether the air or

water is heated. While there are many decades of experience and wisdom on solar water heating devices, relatively little work has been done on the solar collectors for air heating considering their importance to the overall HDH system performance.

1.4.1 Closed-air open-water (CAOW) water heated systems

The air stream is heated and humidified using the energy from the hot water stream which is supplied to the humidifier .The humidified air is then fed to the dehumidifier and is cooled in the dehumidifier using seawater as the coolant. The seawater gets preheated in the process and is further heated in a solar collector before it irrigates the humidifier. The dehumidified air stream from the dehumidifier is then circulated back to the humidifier.

1.4.2 Multi effect closed-air open-water (CAOW) water heated system

To enhance heat recovery, air from the humidifier is extracted at various points and supplied to the dehumidifier at the corresponding point. This enables continuous temperature stratification resulting in a small temperature gap to keep the process running. This is turning results in a higher heat recovery from the dehumidifier. In fact, most of the energy needed for the humidification process is regained from the dehumidifier bringing down the energy demand.

1.4.3 Closed-water open-air (CWOA) water heated system

In this system, air is heated and humidified in the humidifier using the hot water from the solar collector and then is dehumidified using outlet water from the humidifier. Water,

after being preheated in the dehumidifier, enters the solar collector, thus working in a closed loop. The dehumidified air is released to be ambient.

One disadvantage of the CWOA is that when the humidification process does not cool the water sufficiently the coolant water temperature to the inlet of the dehumidifier goes up. This limits the dehumidification of the humid air resulting in reduced water production compared to the open water cycle. However, when efficient humidifiers at optimal operating conditions are used, water may be potentially cooled to temperature below the ambient temperature (up to the limit of the ambient wet-bulb temperature). Under those conditions, the closed water system is more productive than the open water system.

1.4.4 Closed-air open-water (CAOW) air heated systems

Another class of HDH systems which has attracted much interest is the air heated system is the CAOW systems. These systems are of two types' single and multi-stage systems. Air is heated in a solar collector to a temperature of 80 to 90°C and sent to a humidifier. In the humidifier, the air is cooled and saturated.

A major disadvantage of this cycle is that the absolute humidity of air that can be achieved at these temperatures is very low (<6% by weight). This impedes the water productivity of the cycle.

1.5 Objectives of the Present Study

The main objectives of the present study are:

- Performing thermal design of a plate finned-tube heat exchanger. The design of the unit will be compared with existing data [69] to validate the model.

- Performing thermal design of a shell and tube heat exchanger. The design of the unit will be compared with existing data [75] and validated.

- Building an experimental setup of Humidification Dehumidification solar desalination system at KFUPM beach and test it in local weather conditions.

CHAPTER 2

LITERATURE REVIEW

Due to the widespread use of solar desalination systems using HDH over the span of several decades, considerable studies, both experimental as well as theoretical, have been conducted regarding the various aspects of these systems. Furthermore, several studies, observations and recommendations of onsite field engineers, directly involved with the solar desalination systems using HDH process have also been published. A brief account of the major work concerning the primary objectives of this research is presented in the following section.

2.1 Solar air heated systems

Water desalination using HDH processes has proven to be an efficient technique of obtaining fresh water from saline water. This technique presents several advantages such as flexibility in capacity, moderate installation and operating costs, simplicity, and possibility of using low temperature energy sources. The HDH processes are appreciated when the fresh water demand is rather small. The current HDH installations are in very compact units containing two exchangers: an evaporator where air is humidified and a condenser where distilled water is recovered. Compared to other distillation processes, the HDH process functions at the atmospheric pressure so that the components are not

submitted to mechanical solicitations. Several studies have been carried out to investigate the characteristics and performance of HDH desalination systems.

Nawayseh et al. [1] have constructed a simulation program in which the set of nonlinear equations describing the desalination unit were solved numerically. The results of the simulation have been found to agree with the experimental results of two different units constructed in Jordan and Malaysia. Energy obtained either from solar or an electric heating source and the air was the heated fluid. The air flow rate was found to have an insignificant effect on the productivity of desalinated water. Increasing the water flow rate was found to decrease productivity. In a later study, Nawayseh et al. [2] have used the simulation program to optimize the unit performance by studying the effect of condenser and humidifier areas as well as the feed water flow rate on the performance. Ben Bacha et al. [3] have modeled and simulated a solar multiple condensation evaporation system (SMCES). An experimental validation has been carried out to verify the accuracy of the model, and a few requirements have been suggested for the best operation and production for the SMCEC desalination unit. Dai et al. [4] have derived a mathematical model for the open air cycle to simulate the performance numerically. The results revealed that a large error occurred at high inlet temperature of feed water. The water productivity and the hourly water production behave differently with regard to the variation of mass flow rate of air. Optimum mass flow rate of air exists only for hourly water production. The optimum value of the mass flow rate increased with the decrease of the temperature of the inlet water feed to the humidifier. Farid et al. [5] have carried out a simulation study to investigate the performance of solar multi-effect humidification units based on the HDH principle. The study has focused on analyzing the effects of

various components involved in the process along with the study of the effect of water flow rate on the desalination production. Nafey et al. [6] have presented a numerical investigation of the HDH desalination process in which water is heated using a solar concentrator, and the air is heated using a flat-plate solar air heater. It has been reported that the productivity of the unit is strongly influenced by the air flow rate, cooling water flow rate and total solar energy incident through the day. Fath and Ghazy [7] investigated theoretically the performance of a solar desalination system using HDH technique. The system consists of a solar air heater, humidifier and dehumidifier. They concluded that productivity of the system is significantly affected by the solar air heater efficiency. The air heater used in this work was assumed to be consisting of two air conduits. The main idea behind this assumption is to improve the air heater effectiveness. The authors also concluded that the feed water flow rate and dehumidifier effectiveness have an insignificant influence on the system productivity.

Solmus [8] theoretically studied a HDH desalination system configured by a double-pass flat plate solar air heater with two glass covers. The main goals behind this study are to develop a computer simulation program that is based on the mathematical model of the system and, by using this simulation program, to investigate the effect of different system operating conditions, types of air heater, some different design parameters and a weather condition (wind speed) on the solar water desalination system performance under the climatologically conditions of Ankara, Turkey.

Solmus [9] experimentally studied an experimental setup that consists of a double-pass flat plate solar air heater with two glass covers, pad humidifier, dehumidifying exchanger and water storage tank was designed and manufactured. Working principle of the setup is

based on the idea of closed water and open-air cycles. A series of tests were performed on it in the outdoor environment, in order to assess the effect of mass flow rate of the feed water, process air and cooling water, double-pass flat plate solar air heater, initial water temperature and amount of the water inside the storage tank on the productivity of the system. Additionally, an evacuated tubular solar water heater unit was integrated to the existing system and the effect of this integration on the performance of the system was examined. Solar radiation, wind speed, relative humidity, mass flow rate of the feed water, process air and cooling water, mass of condensate water and temperatures at various locations were obtained during the experiments. The results of the experimental study showed that under certain operating conditions, the system productivity decreases about 15% if double-pass solar air heater is not used and significant improvement on the productivity of the system is achieved by increasing the initial water temperature inside the storage tank. In addition, productivity of the system increases with increasing the feed water mass flow rate and quantity of water inside the storage tank. However, productivity of the system remains approximately the same when the air mass flow rate is increased. Moreover, increasing the cooling water mass flow rate results in the improvement on the productivity of the system investigated. Finally, results obtained from the present investigation were compared with the theoretical study and a good agreement between them is observed.

Recently, Chafik [10-12] presented a procedure which consists of several steps (stages) of air heating and humidification that lead to high vapor concentration in the airflow. The present work deals with a study of a water desalination system by solar energy using the HDH principle. The proposed system is a modular one and has the following independent

components: two solar collectors, an evaporator and a condenser. It was reported that, by this way, the airflow rate through the plant can be reduced and low investment and operating costs can be achieved. Moreover, the main equipment of the system, such as solar air collectors, humidifiers and dehumidifier, were designed and tested. Condensing equipment has been designed to recover desalinated water out of the humidified air. The study has two parts. The first one is concerned with the presentation of the characteristics of the designed and constructed components of the desalination system. Some experimental results are analyzed. In the second part, a general mathematical model for the system is presented. It includes the models of the different components of the developed system from the governing heat and mass transfer equations.

2.2 Solar water heated systems

There have been extensive analyses of the performance of solar water heaters, both experimentally and analytically by numerous researchers. Some of the most important are shown here. Gupta and Garg [13] developed a model for thermal performance of a natural circulation solar water heater with no load. They represented solar radiation and ambient temperature by Fourier series, and were able to predict a day's performance in a manner that agreed substantially with experiments. Ong [14-15] performed two studies to evaluate the thermal performance of a solar water heater. He instrumented a relatively small system with five thermocouples on the bottom surface of the water tubes and six thermocouples on the bottom surface of the collector plate. A total of six thermocouples were inserted into the storage tank, and a dye tracer mass flow meter was employed. Ong's studies appear to be the first detailed ones on a thermosyphonic system. Kudish et al. [16] in their study measured the thermosyphon flow rate directly by adapting a simple

and well-known laboratory technique, a constant level device, to a solar collector in the thermosyphon mode. The thermosyphon flow data gathered were utilized to construct a standard efficiency test curve, thus showing that this technique can be applied for testing collectors in the thermosyphon mode. They also determined the instantaneous collector efficiency as a function of time of a day.

Morrison and Braun [17] have studied system modeling and operation characteristics of thermosyphon solar water heater with vertical or horizontal storage tank. They found that the system performance is maximized when the daily collector volume flow is approximately equal to the daily load flow, and that the system with a horizontal tank did not perform as well as a vertical one. Hobson and Norton [18] in their study developed a characteristic curve for an individual directly-heated thermosyphon solar energy water heater obtained from data of 30 days' tests. Using such a curve, the calculated annual solar fraction agreed well with the corresponding value computed from the numerical simulation. Furthermore, the analysis was extended, and they produced a simple but relatively accurate design method for direct thermosyphon solar energy water heaters.

Shariah and Shalabi [19] have studied optimization of design parameters for a thermosyphon solar water heater for two regions in Jordan represented by two cities, namely Amman and Aqaba through the use of a simulation program. Their results indicate that the solar fraction of the system can be improved by 10±25% when each studied parameter is chosen properly. It was also found that the solar fraction of a system installed in Aqaba (hot climate) is less sensitive to some parameters than the solar fraction of a similar system installed in Amman (mild climate).

2.3 Solar air and water heated systems

Solar water desalination processes, such as active and passive basin type solar stills and systems working on HDH principle, have been used to produce fresh water from sea or underground saline water. Among these processes, water desalination systems based on HDH technique using solar energy is one of the simple and most efficient techniques. Moreover, performance of these systems has been studied and improved by several researches.

Orfi et al. [20] studied theoretically and experimentally a solar water desalination system based on HDH principle. The system consists of one water solar collectors, one solar air collector, an evaporator and a condenser. In order to improve the productivity of the system, the authors utilized the latent heat of condensate water vapor in the condenser to preheat the feed water. In addition, they concluded that the global efficiency of the system depends on the efficiency of each component (solar water and air heaters, evaporator and condenser). Nafey et al. [21] have presented experimental study of a single-stage humidification–dehumidification solar desalination process. The effect of solar intensity, ambient temperature, wind speed, the dehumidifier effectiveness, air circulation flow rate, feed water rate and temperature on the system productivity have been investigated. It has been reported that increasing the solar intensity and ambient temperature and decreasing wind velocity increase system productivity. Increasing the air flow rate up to 0.6 kg/s increases the productivity, after which it has no significant effect. The feed water flow rate has an insignificant influence on system productivity.

Muller et al. [22] have used a simulation program to study the effect of varying the operating conditions of the unit constructed in the Canaries. The simulation was based on

an open-water closed-air system operating in 24 h mode using storage tanks. The only two parameters, which have been investigated, are the evaporator inlet temperature and load. The production was improved by operating the unit at higher evaporator temperatures due to the more efficient evaporation and condensation at such conditions. However, the drop in the efficiency of the collector at higher temperatures would limit such improvement. The water inlet temperature was assumed to be available at 40°C and rise approximately to 75°C in the condenser and 85°C in efficient solar collectors. The collectors were replaced by a waste heat source at night. The operating temperature in the unit was not allowed to increase beyond 85°C because the plate-type condenser was made of polypropylene. The simulation was limited to the existing design of the unit in an objective to maximize its production or minimize production cost. There was no attempt to study the effect of varying the size of the components of the unit such as the surface area of the collector condenser and humidifier.

2.4 The humidifier

Many devices are used for air humidification, including spray towers, bubble columns, wetted-wall towers and packed bed towers [23]. The principle of operation for all of these devices is same. When water is brought into contact with air that is not saturated with water vapor, water diffuses into the air and raises the humidity of the air. The driving force for this diffusion process is the concentration difference between the water-air interface and the water vapor in the air. This concentration difference depends on the vapor pressure at the gas-liquid interface and the partial pressure of water vapor in the air. Any of the above mentioned devices can be used as a humidifier in the HDH system. A spray tower, for instance, consists essentially of a cylindrical vessel in which water is

sprayed at the top of the vessel and moves downward by gravity dispersed in droplets within a continuous air stream flowing upward. These towers are simple in design and have the minimal pressure drop on the gas side. However, there is a considerable pressure drop on the water side due to the spray nozzles. Also, mist eliminators are always necessary due to the tendency of water entrainment by the air leaving the tower. It is generally known that this device has high capacity but low efficiency. The low efficiency due to the low water holdup due to the loose packing flow [24]. The diameter-to the length ratio is a very important parameter in spray tower design. For a large ratio air will be thoroughly mixed with the spray. Small diameter-to-length ratio will let the spray quickly reach the tower walls, forming a film becoming ineffective as a spray. Design of spray towers requires knowledge of heat and mass transfer coefficients as well as the contact surface area of the water droplets. Many empirical correlations and design procedures are given in Kreith and Boehm [24].

Younis et al. [25] and Orfi et al. [20] used a spray tower as the humidifier in their HDH systems. And tested the spray tower humidifier by varying the ratio of water-to-dry air mass flow rate and keeping the inlet water temperature and absolute humidity constant the inlet air temperature (80°C) was higher than the water spray temperature (60°C). They found that increasing the amount of water sprayed increased the absolute outlet humidity. However, further increase in the water quantity resulted in air cooling and this condensed some of the water vapor content in the air. This means a decrease in the absolute humidity, although the outlet air is always saturated. Therefore, for air heated HDH cycles there is an optimum value of the mass flow ratio which gives maximum air

humidity. This fact promotes the use of multi-stage air heater and humidifier combinations to increase the fresh water production.

Exactly opposite, in principle, to the spray tower is the bubble column. In the bubble column, a vessel is filled with water and air bubbles are ejected from several orifices located at the bottom of the vessel. Water diffuses into the air bubbles and causes the outlet air to be humidified. These columns are simple in design; however, the diffusion of water into the air bubbles depends on many parameters such as the bubble diameter, bubble velocity, gas hold-up (the ratio of air bubbles-to-water volume), water and air temperatures as well as the heat and mass transfer coefficients. In HDH desalination systems, bubble columns have not been used as humidifiers so far. However, El-Agouz and Abugderah [26] investigated experimentally the performance of a single stage bubble column using air bubbles passing through seawater. They studied the influence of operating conditions on the vapor content difference and the humidification efficiency, which showed strong dependence on saline water temperature and the air velocity. Moreover, the inlet air temperature has a small effect on the vapor content difference. The maximum experimentally obtained vapor content difference of the air was 222 g/kg of dry air at 75 °C of water and air temperatures. However, other geometrical factors such as the orifice diameter, number of orifices, water head height and column diameter were not considered. It is important to mention that there are many empirical correlations for these parameters in Treybal [23] and Lydersen [27]. Therefore, an optimum design and performance evaluation study can be carried out before using the bubble columns in HDH systems.

Wetted-wall towers have been used as a humidifier in HDH systems by Muller et al. [28] and Orfi et al. [20]. In a wetted-wall tower, a thin film of water is formed running downward inside a vertical pipe, with air flowing either co-currently or counter-currently. Water is loaded into the top of the tower, and a weir distributes the flow of water around the inner perimeter of the tube that wets the inner surface of the tube down its length. Such devices have been used for theoretical studies of mass transfer, since the contact area can be calculated, accurately. In [27] heated water was distributed onto vertically hanging fleeces made of polypropylene and trickled downwards. The air move in countercurrent flow to the brine through the humidifier and becomes saturated at the outlet. On the other hand, Orfi et al. [20] used a different design for their wetted-wall humidifier. To improve the heat and mass exchange process, they covered the wooden vertical wetted-walls with a cotton wick to reduce the water flowing velocity and use the capillary effect to keep the vertical walls always wetted. Their design shows higher performance with about 100 % humidification efficiency.

2.5 The dehumidifier

For the design of a thermal system, it is often necessary, for selection purposes, to predict the heat transfer rates of heat exchangers under specific operating conditions. Heat exchangers are complex devices, the complexity being due to both to the geometry and to the physical phenomena involved in the transfer of heat. Many experimental studies have been carried out to study the heat and mass transfer characteristics of the dehumidifying heat exchangers.

2.5.1 Plate fin tube heat exchanger

McQuiston [29] studied the dehumidification in evaporators to correlate the total j factor or sensible j factor with the air flow and heat exchanger characteristics. The accuracy of predicting condensate flow rate varies according to changing in air flow rate and fin spacing. Rich [30] studied the effect of fin spacing on the heat transfer of multi-row, smooth-plate fin-and-tube heat exchangers and found that the heat transfer coefficient is independent of the fin spacing within the range from 3 to 21 fins per inch at a given air mass flux. Later on, Rich [31] studied the effect of the number of rows on heat transfer performance and pointed out that the average heat transfer coefficient for a deep coil may be higher or lower than that for a shallow coil, depending upon the Reynolds number. McQuiston [32] developed a solution for efficiency of a tin plate of uniform cross section and concluded that mass transfer decreases fin efficiency, especially for very moist air with a low evaporator temperature. Saboya and Sparrow [33] in their study of heat transfer characteristics of two-row plate fin and tube heat exchanger configurations, found that a boundary layer on the forward part of the tin plate and a vortex system that develops in front of the tubes provide high mass transfer rates. Subsequently, McQuiston [34-35] performed a series of experiments to study the heat and mass transfer of plate tin tube heat exchangers. Both the total j factor and the sensible j factor were correlated with a parameter that combined tube diameter, tube transverse distance, and fin spacing. He also developed a correction factor for n-row heat exchangers based on the j factors for four-row plate-fin tube heat exchangers.

Webb et al. [36] developed a theoretical model to predict the condensation coefficient on horizontal integral-fin tubes designed for surface tension-induced drainage from the fin.

Eckels and Rabas [37] correlated the wet and dry sensible heat transfer coefficients with the transverse velocity of condensing water vapor and found that the transverse velocity has a significant effect on heat, mass, and momentum transfer augmentation in a typical air-cooling operations. Both wet and dry sensible heat transfer coefficients are linearly increased with the standard face velocity. Coney et al. [38] did a numerical investigation on fin performance with condensation from humid air and presented their results of average condensate heat transfer coefficients and overall air heat transfer coefficients in terms of bulk air velocity. A correlation of the enthalpy Colburn j factor has been developed by Jacobi and Goldschmidt [39]. This correlation characterizes the heat and mass transfer performance of the integral high-finned tube, evaporator, or dehumidifying heat exchanger at low Reynolds numbers. They concluded that although the sensible j factor is deleteriously affected by condensate retention at low Reynolds numbers, the overall heat transfer rates are much higher when condensation occurs. Mirth and Ramadhyani [40-41] showed that wet-surface heat transfer coefficients scatter around the dry surface correlation; the trends were inconclusive with respect to whether or not the wetted surface causes heat transfer enhancement or degradation. They also investigated the heat and mass characteristics of wavy fin heat exchangers where results showed that the Nusselt numbers were very sensitive to the change of inlet dew point temperatures and the Nusselt number decreases with an increase of dew point temperatures. Similar results were reported by Fu et al. [42]. In dehumidifying heat exchangers having a louver fins configuration. They reported a pronounced decrease of the wet sensible heat transfer coefficients with the increase of the inlet relative humidity. On the contrary, the experimental data of Seshimo et al. [43] indicated that the Nusselt number was relatively

independent of inlet conditions. Wu and Bong [44] derived an analytical solution for calculating overall fin efficiency for a partially wet fin, and suggested that the overall fin efficiency must be determined separately for the dry region and the wet region. Nevertheless, the effects of face velocity and of when and where the maximum condensate flow rate occurs had not been discussed in their work.

A better and more common procedure is to collect information about the heat transfer coefficients by means of correlations so that variations with respect to the operating parameters can be taken into account through standard non dimensional groups. Usually the form of the correlation cannot be totally justified from first principles; it is selected based on simplicity and common usage. Estimated errors in heat rates from correlations are normally larger than the experimental error, being mainly due to the data compression that occurs through the correlation process. Another reason for the inaccuracy in predictions is that, for most forms of correlating functions that are used, a least square analysis of the error gives multiple sets of values for the constants indicating that a local, rather than a global, optimum set of values may have been found. The problem of accuracy in condensing heat exchangers predictions is addressed by an alternative approach using artificial neural networks (ANNs) [45].

ANNs have been developed in recent years and used successfully in many application areas, among them thermal engineering Previous work on the prediction of heat rates in heat exchangers without condensation has been reported by Zhao et al. [46] and Diaz et al [47].The most attractive advantage of the method is that it allows the modeling of complex systems without requiring detailed knowledge of the physical processes. Kim and Song [48] found that the total heat and mass transfer rate from the plate increased

with the ratio of fin pitch to the tube diameter. Mon and Gross [49] studied the effects of fin pitches on four-row annular finned-tube bundles in staggered and inline alignments. They found that the boundary layer and horseshoe vortices between the fins were substantially dependent on the Reynolds number and the ratio of fin pitch to the height. Kim [50] measured the heat transfer characteristics of plate finned-tube heat exchangers with continuous fins having large fin pitches. He developed an empirical air side heat transfer correlation for continuous plate finned-tube heat exchangers with large fin pitches. Xie et al. [51] studied air side heat transfer and friction characteristics of continuous finned-tube heat exchangers for1–6 tube rows. Yang et al. [52] studied fin pitch optimization of a continuous finned-tube heat exchanger under frosting conditions for fin pitches greater than 5 mm. Finned-tube heat exchangers having discrete plate fins with large fin pitches have been widely used to enhance the heat transfer performance of evaporators in refrigerators and freezers under dry and frosting conditions.

2.5.2 Shell and tube heat exchanger

Kern [53] provided a simple method for calculating shell-side pressure drop and heat transfer coefficient. However, this method is restricted to a fixed baffle cut (25%) and cannot adequately account for baffle-to-shell and tube-to-baffle leakage. Kern method is not applicable in the laminar flow region where the shell-side Reynolds number is less than 2000. Although the Kern equation is not particularly accurate, it does allow a very simple and rapid calculation of shell-side heat transfer coefficient and pressure drop to be carried out.

The concept of considering the various streams through the exchanger was originally proposed by Tinker [54]. He suggested a schematic flow pattern, which divided the shell-side flow into a number of individual streams. Tinker's model has been the basis of ''stream analysis method'', which utilizes a rigorous reiterative approach and is particularly suitable for computer calculations rather than hand calculation.

Tinker's original analysis was quite complex and hard to understand. After an extensive series of experiments was carried out, a new method has emerged, commonly described as the Bell– Delaware method [55]. The Delaware method uses the principle of Tinker's model but more suitable for hand calculation. In this method, correction factors for baffle leakage effects, etc., are introduced based on extensive experimental data. This method is widely used and most recommended.

In manual design of an exchange, the thermal design engineer cannot avoid the trial and error routine. Accordingly there is little interest in hand calculation method. For manual design, Saunders [56] proposed very practical method that simple design factors are provided which enable the method proposed by Bell to be used rapidly for a fixed set of geometrical parameters.

In Bell's work, the correction factors for heat transfer and pressure drop correlations are given in the graphic form. For computer applications, Taborek [57] gives the correlations for all correction factors involving Bell's methods. Wills et al. [58] have developed the stream analysis method that is viable for hand calculation. Hewitt [59] provides a more readily accessible version of Wills method.

Reppich and Zagermann [60] offers a computer-based design model to determine the optimum dimensions of segmentally baffled shell-and-tube heat exchangers by

calculating optimum shell side and tube-side pressure drops from the equations provided in his work. The six optimized dimensional parameters are number of tubes, tube length, shell diameter, number of baffles, baffle cut, and baffle spacing. The proposed model carries out also the cost analysis.

Gaddis and Gnielinski [61] presented a new procedure for calculating shell-side pressure drop, which is based principally on Delaware method. However, instead of using diagrams as in the Delaware method to calculate the pressure drop in the tube bank, the present authors use equations previously presented [62].

Li and Kottke [63-64] have carried out series of experimental work on shell-and-tube heat exchangers to analysis shell-side heat transfer coefficient (HTC) and pressure loss. They employed a particular mass transfer measuring technique based on absorption, chemical and color giving reaction in their researches to obtain the local shell-side HTC by applying the extended Lewis analogy between heat and mass transfer to a mass transfer coefficient. They studied local shell-side HTC in shell and tube heat exchangers with disc-and-doughnut baffles and segmental baffles. He also investigated the effect of leakage and baffle spacing on pressure drop and HTC [65-66] respectively. Diaz et al [67] did lots of works in steady dynamic simulation and control heat exchangers using ANNs. Other researches about heat exchangers control by means of ANNs were reported in reference [68]. From aforementioned successful applications, it is shown that ANNs are well suitable to thermal analysis in engineering systems, especially in heat exchangers.

Although the design may be carried out by hand calculation, computer programs are widely employed anymore. These are often proprietary codes produced by design

industry, large processing companies, and international research organizations such as Heat Transfer and Fluid.

Flow Service (HTFS) or Heat Transfer Research Inc. (HTRI) or Tubular Exchanger Manufacturers Association (TEMA). Unfortunately, it is hard to employ them as a heat exchanger subroutine of a computer simulation for any thermal system plant that one of its equipment is heat exchanger. Researchers usually tend to make a mathematical model and a computer simulation of thermal systems for their theoretical analysis and when a heat exchanger exists in the system.

CHAPTER 3

CONDENSER DESIGN

PART ONE: PLATE FIN TUBE HEAT EXCHANGER

3.1 Introduction

The processes of heat exchange between two fluids that are at different temperatures and separated by a solid wall occur in many engineering applications; the device used to implement this exchange is a heat exchanger. In many heat exchangers, the fluids are separated by a heat transfer surface, and ideally they do not mix or leak. Such exchangers are referred to as direct transfer type. In contrast, exchangers in which there is intermittent heat exchange between the hot and cold fluids are referred to as indirect transfer type. Specific application may be found in space heating and air conditioning, waste heat recovery and chemical processing.

Engineers involved in heat exchanger work are primarily concerned with the use of practical heat exchanger solution relations that express the performance parameter such as heat transfer rate, outlet temperature of the fluids and pressure drop in terms of system parameters which include inlet temperature, mass flow rate, fluid properties, geometric

characteristic and extent of fouling deposits for the purpose of evaluating the performance of existing heat exchanger or design new equipment.

Heat exchangers are typically classified according to flow arrangement and type of construction. The simplest heat exchanger is one in which the hot and cold fluids move in the same or opposite directions in a concentric type or double pipe construction. In parallel flow arrangement the hot and cold water enters at the same end, flow in the same direction and leave at the other end. In the counter flow arrangement, the fluids enter at the opposite end, flow in the opposite direction and leave at opposite ends.

Alternatively, the fluids may move in cross flow (perpendicular to each other), by finned and unfinned heat exchangers. The configurations are typically differentiated by an idealization that treats fluid motion over the passages as unmixed or mixed. Another common configuration is the shell and tube heat exchanger. Specific forms differ according to the number of shell and tube passes, and the simplest form involves single tube and shell passes. Baffles are usually installed to increase the convection coefficient of the shell side fluid by inducing turbulence and cross flow velocity component.

A special and important class of heat exchangers is used to archive a very large heat transfer surface area per unit volume; termed compact heat exchangers. These devices have dense arrays of finned tubes or plates and are used when one at least of the fluids is gas and hence characterized by a small convection coefficient. Tubes may be of plate or circular shape. Parallel plates may be finned or corrugated and may be used in single pass or multi-pass modes of operation. Flow passages associated with compact heat exchanger are typically small and the flow is usually laminar.

3.2 Design steps of plate fin tube heat exchanger

The following represents the main parameters calculated in the design steps of the plate fin heat exchanger as follows:

1- Inside heat transfer coefficient
2- JP factor
3- Outside heat transfer coefficient
4- Fin efficiency
5- Surface effectiveness
6- Overall heat transfer coefficient
7- Number of transfer unit
8- FP factor
9- Pressure drop
10- Number of tubes
11- Heat exchanger geometry
12- Sensible j-factor
13- Total j- factor
14- Total heat
15- Sensible l heat

3.3 Design procedure of a plate fin and tube heat exchanger

For the design of a thermal system, it is often necessary, for selection purposes, to predict the heat transfer rates of heat exchangers under specific operating conditions. For a heat exchanger is operating with humid air, e.g. Humidification dehumidification applications, some of the moisture in the air may condense on the fins and tubes. The input data from McQuiston et al. [69] used in the design of water to air cooling heat exchanger of continuous plate fin tube type as shown in Table 3-1.

Table 3-1 Input data from McQuiston et al. [69]

Input data	Values	Unit
Inlet air temperature	37.78	℃
Outlet air temperature	10.0	℃
Inlet water temperature	60.0	℃
Outlet water temperature	65.56	℃
Air face velocity	4.57	m/s
Air flow rate	0.94	m^3/s
Outside tube diameter	13.33	mm
Inside tube diameter	12.27	mm
Inlet water velocity	1.22	m/s
Number of fins	315	fin/m
Fin thickness	1.52	mm
Streamwise tube distance	27.50	mm
Transverse tube distance	31.75	mm
Hydraulic diameter of the coil	4.0	mm
Fin area over total area	0.919	-
Frontal area over minimum flow area	0.555	-

Figure 3-1 is a schematic of typical water to-air cooling heat exchanger that has multiple rows of tubes. Although water may be routed through the tubes in many different ways, the circulation is usually such that counter flow will be approached. Counter flow can usually be assumed when three or more rows are used because the water inlet and outlet connections must be on the same end of the coil.

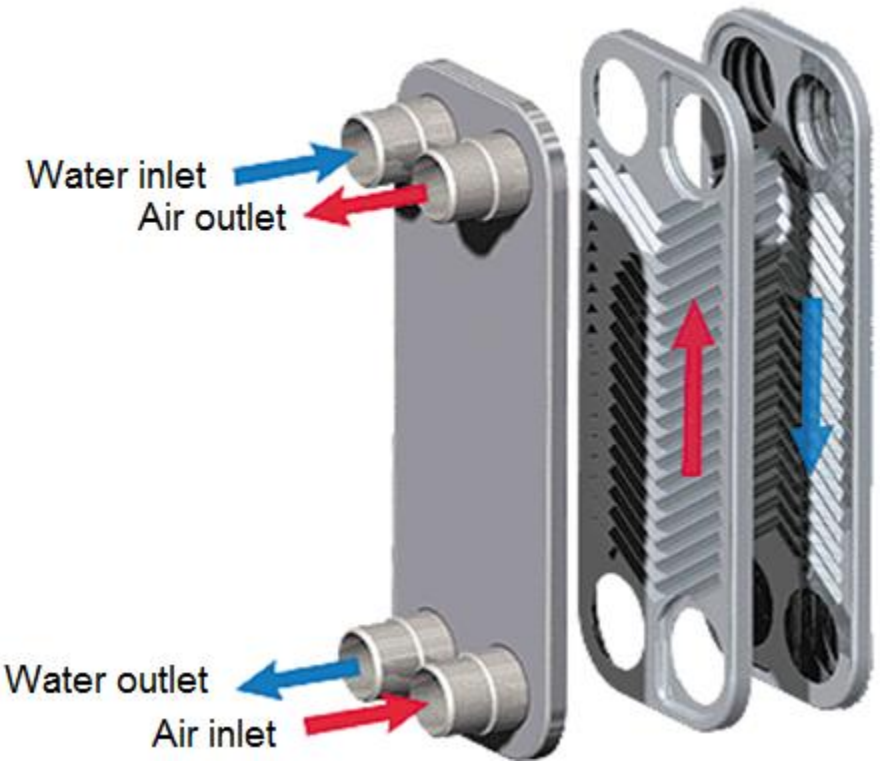

Figure 3-1Typical heat exchanger

In the turbulent region, however, there are a number of expressions available for the Nusselt number. One of the more commonly used correlations for turbulent flow is the Dittus-Boelter equation. This correlation is valid for fully developed flow in circular tubes with moderate temperature variations in Incropera et al. [70]. For plate fin tube heat exchanger, the Dittus-Boelter equation is used to calculate the inside heat transfer coefficient as follows:

The Reynolds number of water based on the inside surface diameter is

$$Re_{Dw} = \frac{\rho_w v_w D_i}{\mu_w} \quad (1)$$

Where μ_w and ρ_w are evaluated at average water temperature.

The Prandtl number is

$$Pr_w = \frac{(\mu_w Cp_w)}{k_w} \quad (2)$$

Since the flow is turbulent the inside heat transfer coefficient for water is calculated using the following equation:

$$h_i = 0.023 \frac{k_a}{D_i} (Re_{Dw})^{0.8} (Pr_w)^{0.3} \quad (3)$$

The work of McQuiston et al. [69] is used as a baseline to evaluate the air-side convective heat transfer coefficient for a plate finned heat exchanger with multiple rows of staggered tubes. The model is developed for dry coils. The heat transfer coefficient is based on the Colburn j-factor.

Two particular parameters in addition to Colburn j-factor seems to be predominating in the outside heat transfer correlations. The first one is the Reynolds number based on the

tube outside diameter. The second one is the ratio of the outside area of the tube without fins to the total surface area.

Calculation of the Reynolds number of the air is used in order to calculate the air-side heat transfer coefficient using the following procedures.

First the calculation of the mass flux based on the minimum flow area using the following equation:

$$G_{fr} = \rho_a v_a \tag{4}$$

$$\dot{m}_a = G_{fr} A_{fr} = G_c A_c \tag{5}$$

$$G_c = G_{fr} \frac{A_{fr}}{A_c} = \frac{G_{fr}}{\sigma} \tag{6}$$

Now the Reynolds number of air based on the outside tube diameter is:

$$Re_{Da} = \frac{G_c D_o}{\mu_a} \tag{7}$$

$\frac{A}{A_t}$: is the ratio of the bare tube area without fins to the total heat transfer area and it is equal to:

$$\frac{A}{A_t} = \frac{4 x_a x_b}{\pi D_h D_o \sigma} \tag{8}$$

The equation by McQuiston et al. [69] is used in order to calculate the JP parameter which is a correlating parameter to be used with the j-factor.

$$JP = (Re_{Da})^{-0.40} \left[\frac{A}{A_t}\right]^{-0.15} \tag{9}$$

The calculation of the Colburn j-factor for smooth plate fin tube heat exchanger with four rows of the tube using equation used by McQuiston et al. [69], or using Figure 3-2 which represents the relation between the JP Parameter and j-factor in a graphical form within ±10% error [69].

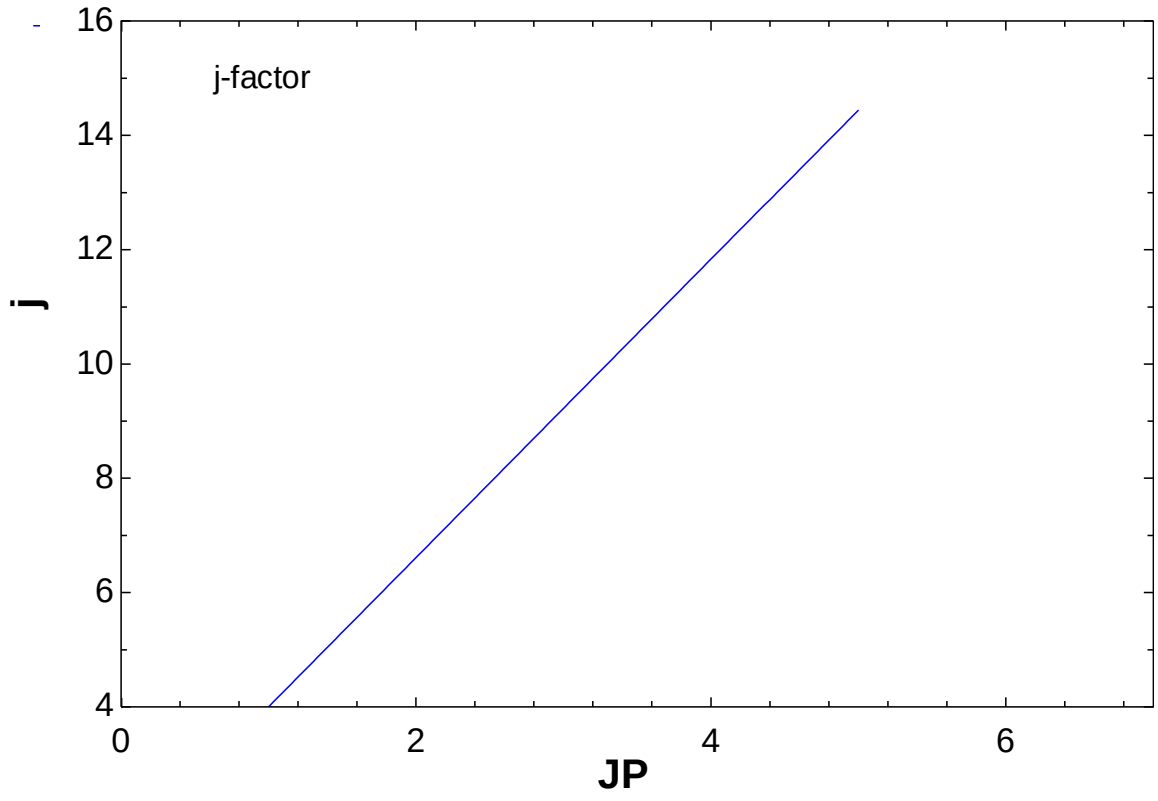

Figure 3-2 Heat transfer correlation for smooth plate-fin-tube coils

Then, the following equation is used to calculate the j-factor [35].

$$j = 0.0014 + 0.2618JP \tag{10}$$

Finally, the air-side heat transfer coefficient can be computed using the following equation:

$$h_o = j[G_c Cp_a][(\mu_a Cp_a/k_a)]^{-2/3} \tag{11}$$

To determine the overall surface efficiency for a finned tube heat exchanger, it is first necessary to determine the efficiency of the fins, as if they existed alone. For a plate-fin-and-tube heat exchanger with multiple rows of staggered tubes, the plates can be evenly divided into hexagonal shaped fins as shown in Figure 3-3. Schmidt and Thannhauser [71] analyzed hexagonal fins and determined that they can be treated as circular fin by replacing the outer radius of the fin with an equivalent radius. The empirical relation for the equivalent radius is given by:

$$\frac{R_e}{r} = 1.27\psi(\beta - 0.3)^{1/3} \tag{12}$$

Where r: is the outside tube radius. The coefficients ψ and β are defined as:

$$\psi = \frac{X_a}{2r_o} \tag{13}$$

And

$$\beta = \frac{1}{X_a}\left[X_b^2 + \frac{X_a^2}{4}\right]^{1/2} \tag{14}$$

Where X_a is the tube spacing in the direction parallel to the direction of air flow, and X_b is the tube spacing normal to the direction of air flow.

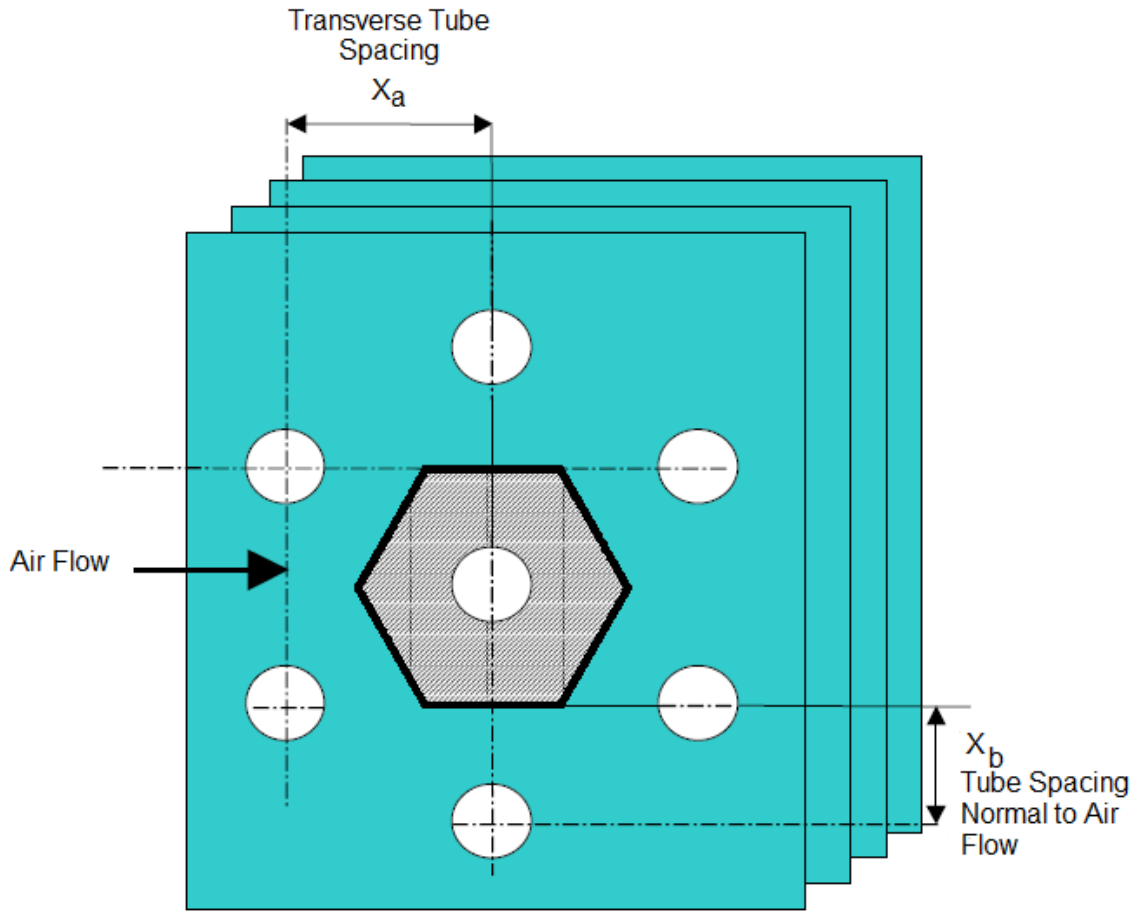

Figure 3-3 Hexagonal fin layout and tube array [69]

Once the equivalent radius is determined, the equations for standard circular fins can be used. For this study, the length of the fins is much greater than the fin thickness. Therefore, the standard extended surface parameter m can be expressed as:

$$m = \left(\frac{2h_o}{k*y}\right)^{1/2} \tag{15}$$

A parameter ϕ can be defined as:

$$\phi = \left(\frac{R_e}{r} - 1\right)[1 + 0.35\ln(R_e/r)] \quad (16)$$

The fin efficiency η_f for a circular fin is a function of m and ϕ, and r can be expressed as:

$$\eta = \frac{tanh[mr\phi]}{mr\phi} \quad (17)$$

The surface effectiveness (η_{so}) is then computed using the following equations:

$$\left[\frac{A_f}{A}\right] = \frac{\pi D_i}{X_a X_a \alpha} \quad (18)$$

$$\eta_{so} = 1 - \left[\frac{A_f}{A}\right](1 - \eta) \quad (19)$$

Where A_f is the total fin surface area, $A_o$is the total air-side surface area of the tube and the fins.

The overall heat transfer coefficient that accounts for the total thermal resistance between the two fluids is expressed as follows:

$$\frac{A_i}{A_o} = \frac{\pi D_i}{x_a x_b \sigma} \quad (20)$$

$$\frac{1}{U_o} = \frac{1}{h_i \eta_{so}} + \frac{R_i}{\eta_{so}} + R_w + \frac{R_o}{\eta_{so}(A_i/A_o)} + \frac{1}{h_o(A_i/A_o)} \quad (21)$$

$R_{i,}R_o$: is the fouling factor inside and outside the tube, R_w is the wall thermal resistance. Neglecting the wall thermal resistance and the fouling factor inside and outside the tube, the overall heat transfer coefficient reduces to:

$$\frac{1}{U_o} = \frac{1}{h_i \eta_{so}} + \frac{1}{h_o (A_i / A_o)} \quad (22)$$

The number of transfer units (NTU) and the fluid capacity rate can be computed using the following equations:

$$\dot{m}_a = \rho_a Q \quad (23)$$

$$C_a = \left(t_{a,o} - t_{a,i}\right) = C_w (t_{w,i} - t_{w,o}) \quad (24)$$

$$\frac{C_{min}}{C_{max}} = \left(t_{a,o} - t_{a,i}\right) = C_w (t_{w,i} - t_{w,o}) \quad (25)$$

$$\varepsilon = \frac{\left(t_{a,o} - t_{a,i}\right)}{(t_{w,i} - t_{a,i})} \quad (26)$$

$$NTU = \frac{U_o A_o}{C_{min}} \quad (27)$$

The total volume of the heat exchanger is given by:

$$V = \frac{A_o}{\alpha} \quad (28)$$

Where α : is total heat transfer area over total volume.

Since the value of face velocity is estimated, the face area is:

$$A_{fr} = \frac{Q}{\bar{v}_{fr}} \quad (29)$$

And the length is:

$$L = \frac{V}{A_{fr}} \quad (30)$$

The number of rows of tubes (N_r) can be calculated using the following equation.

$$N_r = \frac{L}{X_b} \tag{31}$$

The pressure loss of the air flow through the coil can be computed by calculating the following parameter.

$$\left[\frac{A}{A_c}\right] = \frac{\alpha V}{\sigma A_{fr}} \tag{32}$$

The mean density (ρ_m) is approximately equal to:

$$\rho_m = \left[\frac{\rho_{a,i} + \rho_{a,o}}{2}\right] \tag{33}$$

The correlation of friction data for plate fin tube heat exchanger is somewhat more involved than the j-factor. The following equations are used to calculate the FP parameter which is an obtained parameter to be used with the fanning friction factor.

$$D^* = \frac{D\left[\frac{A}{A_t}\right]}{1+\left[\frac{X_a - D}{s}\right]} \tag{34}$$

$$FP = (Re_{Da})^{-0.25}\left[\frac{D}{D^*}\right]^{0.3}\left[\frac{X_a - D}{4(s-y)}\right]^{-0.4}\left[\frac{X_a}{D^*} - 1\right]^{-0.5} \tag{35}$$

Calculation of the friction factor for smooth plate fin tube heat exchanger with four rows of the tube using the equation given by McQuiston [35] or using Figure 3-4, which represent the relation between the FP Parameter and friction factor in a graphical form within $\pm$35% error [69].

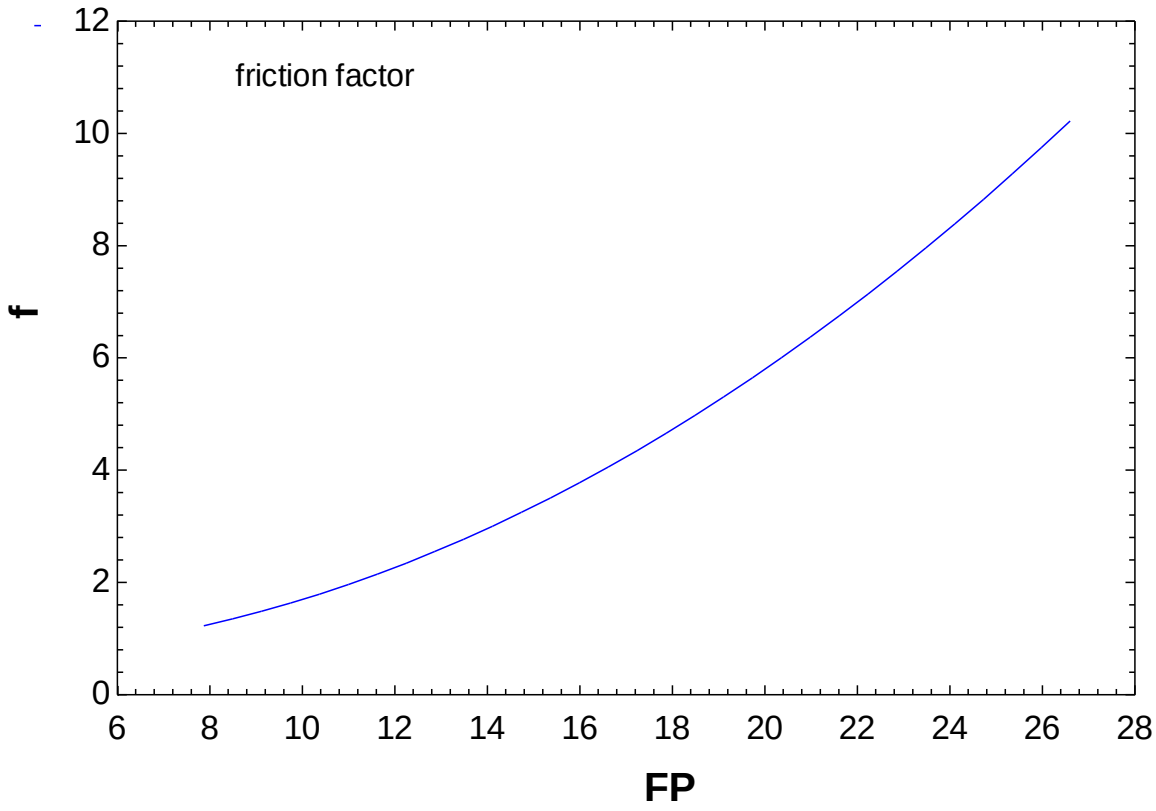

Figure 3-4 Correlation of friction data for smooth plate-fin-tube coil

Friction factor can be given by the equation given by McQuiston [35].

$$f = 4.904 * 10^{-3} + 1.382(FP)^2 \tag{36}$$

Now the pressure loss of the air flow through the coil can be computed using the following equation:

$$\Delta P_o = \frac{{G_c}^2}{2g\rho_{a,i}}\left([1 + (\sigma)^2]\left(\frac{\rho_{a,i}}{\rho_{a,o}} - 1\right) + f * \left[\frac{A}{A_c}\right]\left(\frac{\rho_{a,i}}{\rho_m}\right)\right) \tag{37}$$

The number of tubes can be computed by first calculating the flow cross sectional area. Now the flow cross sectional area of water may be determined from the fluid capacity rate of water and the continuity equation as follows:

$$A_i = \frac{C_w}{\rho_w v_w Cp_w} \tag{38}$$

The number of tubes can be calculated using the following equation:

$$N_t = \frac{4A_i}{\pi D_i^2} \tag{39}$$

The coil geometry can be found using the following equation:

$$H = N_t X_a \tag{40}$$

$$w = \frac{A_{fr}}{H} \tag{41}$$

Research involving plate fin tube surfaces has resulted in correlations that relate dry sensible j-factor and f-factor for wetted dehumidifying surfaces. Expressions were developed that modify the parameters JP and FP for wet surface conditions. It was found that Reynolds number based on fin spacing and the ratio of fin spacing to space between the fins were useful. So the modifying functions are:

The Reynolds number based on fin spacing;

$$[Re_{Da}]_s = Re_{Da}\left[\frac{s}{D}\right] \tag{42}$$

The sensible j-factor that is given as;

$$J(s) = [0.84 + (4 * 10^{-5})[[Re_{Da}]_s]^{1.25}] \tag{43}$$

The total j-factor that is given by;

$$Ji(s) = [0.95 + (4 * 10^{-5})[[Re_{Da}]_s]^{1.25}]\left[\frac{s}{s-y}\right]^2 \tag{44}$$

The friction factor;

$$FP(s) = [1 + [[Re_{Da}]_s]^{-0.4}]\left[\frac{s}{s-y}\right]^{1.5} \tag{45}$$

The design of a heat exchanger for simultaneous transfer of heat and mass is more complicated than for sensible heat transfer because the total energy transfer from the air has two components, namely, latent and sensible heat.

$$q = \dot{m}_w Cp_w\left(t_{w,o} - t_{w,i}\right) = \dot{m}_a Cp_a\left(t_{a,i} - t_{a,o}\right) + \dot{m}_a i_{fg}(w_{a,i} - w_{a,o}) \tag{46}$$

The simplest case occurs when terminal conditions are known, because that

$$q_t = \dot{m}_w Cp_w\left(t_{w,o} - t_{w,i}\right) = \dot{m}_a\left(i_{a,i} - i_{a,o}\right) \quad (47)$$

And

$$q_s = \dot{m}_a Cp_a\left(t_{a,i} - t_{a,o}\right) = U_o A(LMTD) \quad (48)$$

Note:

$$LMTD = \frac{(t_{w,i} - t_{a,o}) - (t_{w,o} - t_{a,i})}{ln\left[(t_{w,i} - t_{a,o})/(t_{w,o} - t_{a,i})\right]} \quad (49)$$

3.4 Validation of plate fin and tube heat exchanger model

McQuiston et al. [69] have designed a water to air heating humidifier of a continuous plate fin tube type. The input data is used to validate the humidifier program developed in this study.

Table 3-2 provides a comparison between the values of the different important parameters and those of McQuiston et al. [69] for the water to air heating coil of a continuous plate fin tube type.

Moreover, this table shows the difference (percentage error) between EES program calculations and McQuiston results. This difference is believed to be as a result of using the built in functions of the air and water properties in the EES program instead of McQuiston constants values.

The maximum percentage error does not exceed 8% between the reported for the humidifier indicating a good agreement between McQuiston results and the results of the current analysis.

The validated model is then used to make a parametric study of a dehumidifier for the existing geometry. The results of the EES program calculation of the parametric study of a dehumidifier is shown in Table 3-3.

Table 3-2 Comparison between McQuiston et al. [69] and EES Program values

Definition	Symbol	McQuiston et al. [69] values	EES program values	Percentage error%
Water density	ρ_w	985.1	981.8	0.34
Water Thermal conductivity	k_w	0.6577	0.6435	2.16
Water Specific heat	Cp_w	4.187	4.153	0.08
Water Viscosity	μ_w	0.00042	0.00045	4.13
Water Prandtl number	Pr_w	2.737	2.91	6.32
Air density	ρ_a	1.246	1.189	4.60
Air Thermal conductivity	k_a	0.02542	0.02542	0.0
Air Specific heat	Cp_a	0.9927	1.004	1.18
Air Viscosity	μ_a	0.0000182	0.0000185	1.37
Air Prandtl number	Pr_a	0.7101	0.7283	2.56
Water Reynolds number	Re_{Dw}	34382	32809	4.58
Inside convection heat transfer coefficient	h_i	7081	6814	3.7
Mass velocity for air in the minimum flow area	G_c	10.27	9.793	4.61
Reynolds number for air	Re_{Da}	7527	7084	5.89
Heat transfer area of bar tube over total heat transfer area	A/A_t	11.58	11.58	0.0
j-factor	j-factor	0.0066	0.006602	0.030
JP parameter	JP	0.01949	0.01997	2.46
Outside convection heat transfer coefficient	h_o	84.49	80.23	5.04
Fin efficiency	η	0.7337	0.79	7.67

Definition	Symbol	McQuiston et al. [69] values	EES program values	Percentage error%
Effectiveness	η_{so}	0.7552	0.81	7.26
Water side area over air side area	A_i/A_o	0.07914	0.07914	0.0
Overall heat transfer coefficient	U_o	57.29	58.09	1.39
Number of rows of tubes	N_r	4.727	4.51	4.59
Number of tube	N_t	9.818	9.517	3.07
FP parameter	FP	0.1259	0.1278	1.51
Pressure drop	ΔP_o	0.1658	0.1578	4.82
Air Reynolds number based on fin spacing	$[Re_{Da}]_s$	1792	1687	5.9
Sensible j-factor	$J(s)$	1.306	1.272	2.6
Total j-factor	$J_i(s)$	1.563	1.525	2.43
Friction factor	$FP(s)$	1.13	1.132	0.177
Modified Sensible j-factor	$JP * J(s)$	0.02546	0.02541	0.196
Modified Total j-factor	$JP * J_i(s)$	0.03046	0.03046	0.0
Modified Friction factor	$FP * FP(s)$	0.1423	0.1446	1.6
Coil height	H	0.3175	0.3175	0.0
Coil width	w	0.6504	0.6504	0.0
Air mass flow rate	$\dot{m}_a$	1.174	1.122	4.4
Water mass flow rate	$\dot{m}_w$	1.411	1.406	0.34
Total heat	q_t	32.847	32.705	0.43
Sensible heat	q_s	25.92	25.82	0.43

Table 3-3 Dehumidifier Parametric study

Definition	Symbol	EES program values
Water density	ρ_w	981.8
Water Thermal conductivity	k_w	0.6435
Water Specific heat	Cp_w	4.183
Water Viscosity	μ_w	0.00045
Water Prandtl number	Pr_w	2.91
Air density	ρ_a	1.189
Air Thermal conductivity	k_a	0.02542
Air Specific heat	Cp_a	1.004
Air Viscosity	μ_a	0.0000185
Air Prandtl number	Pr_a	0.7283
Water Reynolds number	Re_{Dw}	32809
Inside convection heat transfer coefficient	h_i	6814
Mass velocity for air in the minimum flow area	G_c	9.793
Air Reynolds number	Re_{Da}	7084
Heat transfer area of bar tube over total heat transfer area	A/A_t	11.58
j-factor parameter	j-factor	0.006602
Definition	Symbol	EES program values
JP parameter	JP	0.01997
Outside convection heat transfer coefficient	h_o	80.23
Fin efficiency	η	0.79
Effectiveness	η_{so}	0.81

Water side area over air side area	A_i/A_o	0.07914
Overall heat transfer coefficient	U_o	58.26
Number of rows of tubes	N_r	4.488
Number of tube	N_t	9.508
FP parameter	FP	0.1278
Pressure drop	ΔP_o	0.1339
Reynolds number for air based on fin spacing	$[Re_{Da}]_s$	1687
Sensible j-factor	$J(s)$	1.272
Total j-factor	$J_i(s)$	1.525
Friction factor	$FP(s)$	1.132
Modified Sensible j-factor	$JP * J(s)$	0.02541
Modified Total j-factor	$JP * J_i(s)$	0.03046
Modified Friction factor	$F * FP(s)$	0.1446
Air mass flow rate	$\dot{m}_a$	1.122
Water mass flow rate	$\dot{m}_w$	1.406
Condensate mass flow rate	$\dot{m}_c$	0.042
Total heat	q_t	32.7
Latent heat	q_l	6.89
Sensible heat	q_s	25.81

3.5 Parametric study of plate fin and tube heat exchanger

Figure 3-5 shows the relation between the air mass flow rate and the condensate flow rate. It can be observed in this figure that the productivity of the system increases by increasing the air mass flow rate to an optimum value and then decreases. The increase in the productivity is due to an increase in the rate of water vapor carried by additional air. Then as more warm and humid air enters to the shell side of the condenser, the water average temperature increases, this decreasing the driving force for heat transfer within the condenser leading to a decrease in the condensate.

Increasing the water mass flow rare at a fixed air mass flow rate increases the productivity of the condenser. This is due to decreases average cooling water temperature that results in an increase in the temperature difference between the two fluids. Cooling water will then lower the tubes surface temperature and this will increase the rate of condensation.

Figure 3-6 is a cross plot of the previous figure (3-5). It shows the effect of changing the water mass flow rate on the condensate flow rate. The figure shows that increasing the water mass flow rate at a constant air flow rate increases the condensation rate. It is worth of mentioning that the selected values of the air flow rate shown in this figure are the values that correspond to $\dot{m}_a > \dot{m}_{a,optimum}$. That explains the decreasing trend of the condensate with $\dot{m}_a$.

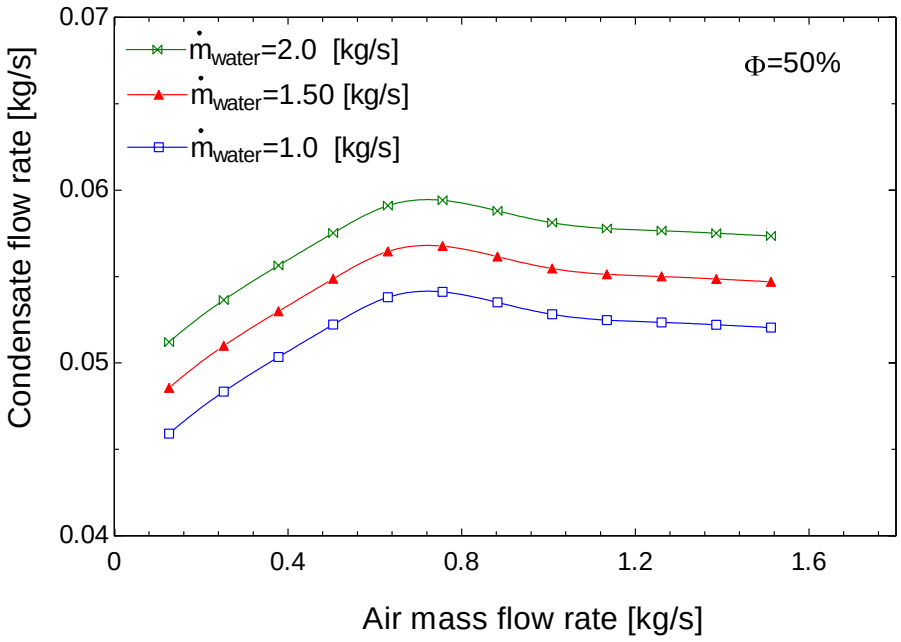

Figure 3-5 Change of condensate flow rate with the changes in the air mass flow rate

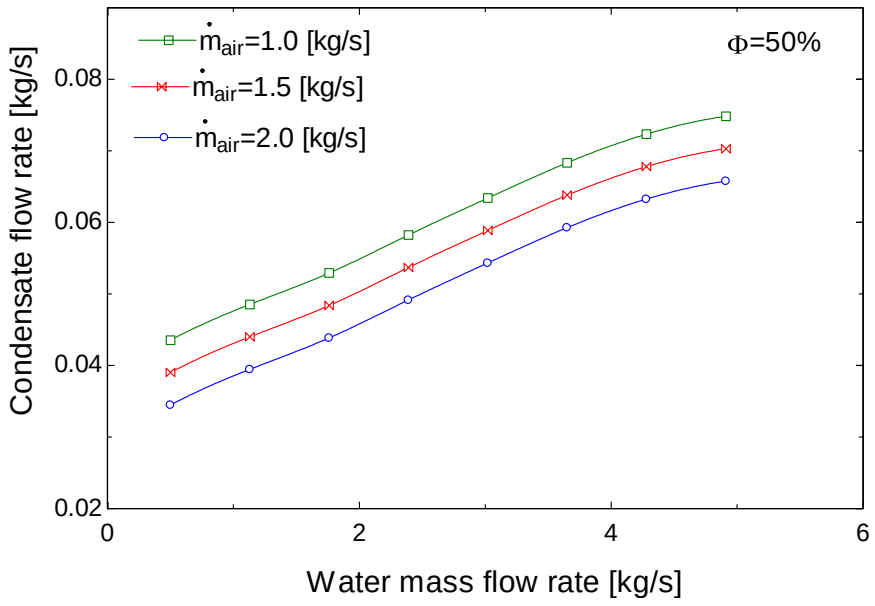

Figure 3-6 Change of condensate flow rate with the changes in the water mass flow rate

Figure 3-7 shows the effect of changing the air inlet temperature on the condensate flow rate for selected values of the air mass flow rate. The figure indicates that increasing the air inlet temperature while maintaining the air mass flow rate constant increases the condensate flow rate. This is because the difference between the average air temperature and the average water temperature increases, thus increasing the heat transfer rate and potential of water vapor condensation. In addition, increasing the air inlet temperature leads to an increase in the average air temperature. Accordingly, the heat capacity and the ability of air to absorb the water vapor before it enters the heat exchanger will increase. Therefore, productivity increases since the condensate flow rate is the product of the air mass flow rate by the changes in the humidity ratio ($\dot{m}_c = \dot{m}_a \Delta W$).

Furthermore, increasing the air mass flow rate at constant air inlet temperature decreases the condensate flow rate. This is because increasing air flow rate increases the average water temperature and decreases temperature difference between the two fluids leading to a decrease in the productivity of the system.

Figure 3-8 shows the relation between the water inlet temperature and the condensate flow rate. Increasing the water inlet temperature at a given water mass flow rate decreases the condensate flow rate due to decreased temperature difference between the two fluids leading to a decrease in the heat transferred from the warm air entering the condenser to the cooling water. This will then decrease the condensation. Moreover, increasing the water mass flow rate at constant water inlet temperature the condensate flow rate will increase due to the increase in the heat transfer rate from the air side to the water in the condenser.

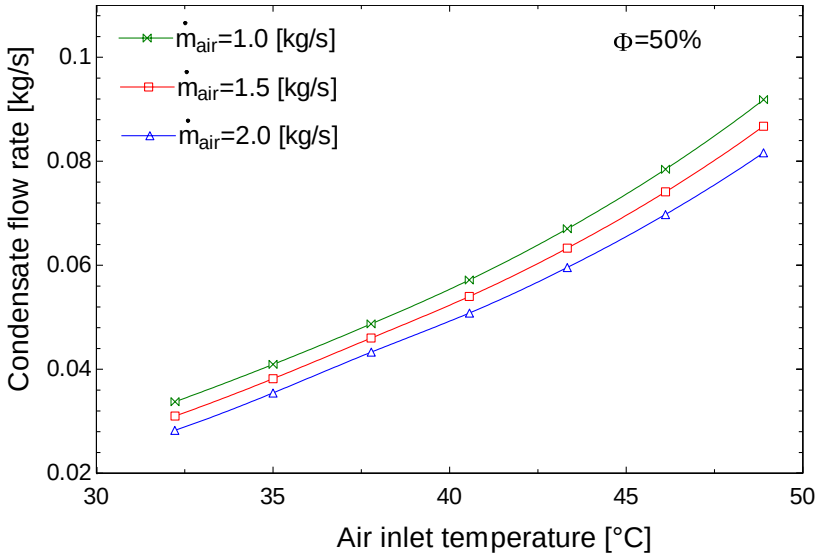

Figure 3-7 Change of condensate flow rate with the changes in the air inlet temperature

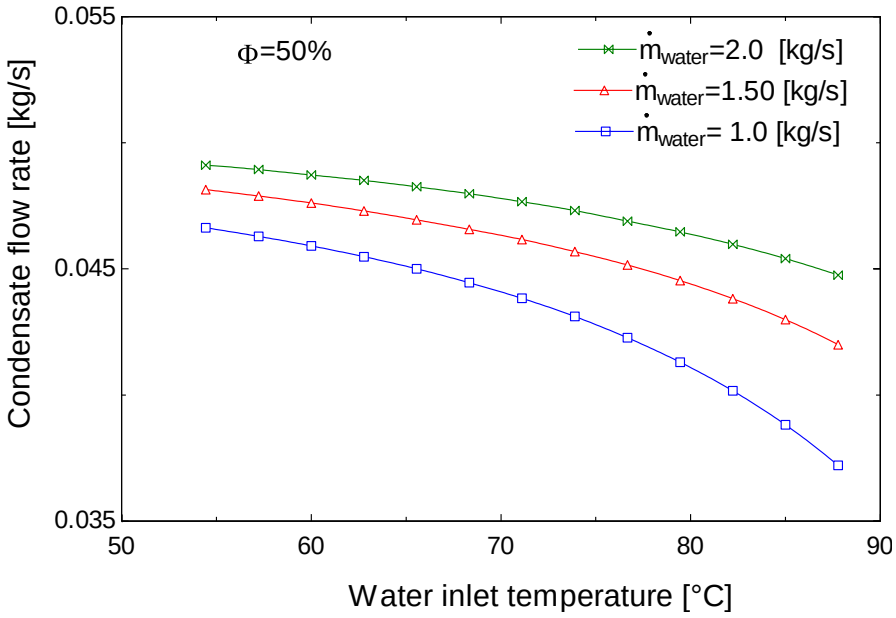

Figure 3-8 Effect of water inlet temperature on the condensate flow rate

3.6 Sensitivity analysis of plate fin and tube heat exchanger

Sensitivity analysis is the study of how a variation (uncertainty) in the output of a mathematical model can be apportioned, qualitatively or quantitatively, to different sources of variation in the input of a model [72]. It is a technique for systematically changing parameters in a model to determine the effects of such changes.

In more general terms uncertainty and sensitivity analyses investigate the robustness of a study when the study includes some form of mathematical modeling. Sensitivity analysis can be useful to computer modelers for the following purposes:

- ✓ Support decision making or the development of recommendations for decision makers
- ✓ Enhancing communication from modelers to decision makers
- ✓ Increased understanding or quantification of the system (e.g. Understanding relationships between input and output variables)
- ✓ Model development (e.g. Searching for errors in the model)

Table 3-4 lists the input parameters used to carry out the sensitivity analysis for the heat exchanger under investigation.

Table 3-4 Input parameters of the sensitivity analysis for the plate fin tube heat exchanger

Item	Symbol	Variability %
Tube inside diameter	D_i	10
Tube outside diameter	D_o	10
Air velocity	v_a	10
Water velocity	v_w	10
Coil width	w	10
Coil height	H	10
Tube length	L	10
Transverse tube distance	x_a	10
Fin spacing	s	10
Streamwise tube distance	x_b	10
Fin thickness	y	10
Tube hydraulic diameter	D_h	10
Atmospheric air pressure	p	10
Relative humidity at the inlet condition	$\emptyset$	10
Inlet air temperature	$t_{a,i}$	$\pm 5℃$
Inlet water temperature	$t_{w,i}$	$\pm 5℃$

The sensitivity analysis of changes in the main variables given bellow is carried out to identify the most significant parameters that affect the plate fin tube heat exchanger performance as shown in Table 3-5.

An equal variability of (10% of the parameter) was assigned to each one of the parameters, except for the inlet temperature of air and water, which have been assigned another percentage uncertainty of $(\pm 5℃)$. The corresponding effect on the main response variables (condensate flow rate, inside and outside heat transfer coefficient, overall heat transfer coefficient, pressure drop and total heat transfer) was monitored and the percentage weighted changes are calculated using EES Software [73] that has a built-in capability to carry out uncertainty analysis [74]. For example, by performing the sensitivity analysis for the condensate mass flow rate as a response variable (first column), changes in condensate mass flow rate are influenced by the inlet air temperature (89.25%) followed by the coil width (2.20%) and inlet relative humidity (1.80%). In addition transverse distance (1.35%), inlet air velocity (1.06%) and atmospheric air pressure (1.06%) has an insignificant effect on the condensate mass flow rate .The other variables have a negligible effect on the condensate mass flow rate. The same argument is used for the rest of the response factors listed in Table 3-4. On the other hand, different parameters are the most influential parameter on the changes in the remaining response variables. (Each responsible parameter has its own major influential parameter). Thus a designer can determine the most influential parameters that control the plate fin tube heat exchanger and accordingly improve the unit performance.

Table 3-5 Sensitivity analysis of plate fin tube heat exchanger

	Response variable, %					
Parameter	$\dot{m}_c$ kg/s 0.042 $\pm$ 0.028	h_i W/m^2°C 6808.0 $\pm$ 935.8	h_o W/m^2°C 80.57 $\pm$ 10.47	U_o W/ m^2°C 58.26 $\pm$ 7.16	ΔP kPa 0.13 $\pm$ 0.096	q_t kW 32.7 $\pm$ 7.60
$\frac{A_f}{A_{tot}}$ 0.92 $\pm$ 0.092	0.04	0.0	0.0	2.94	0.0	0.82
A_{fr} 0.55 $\pm$ 0.055	0.31	0.01	39.12	23.69	0.16	6.60
D_h (mm) 0.33 $\pm$ 0.033	0.01	0.0	0.85	0.51	10.68	0.14
D_i (mm) 1.02 $\pm$ 0.102	0.01	3.05	0.0	0.46	0.0	0.13
D_o (mm) 1.11 $\pm$ 0.111	0.02	0.0	2.25	1.40	6.89	0.39
α 170 $\pm$ 17.0	0.72	0.02	0.01	0.60	3.79	15.08
H (m) 0.31 $\pm$ 0.031	0.01	0.0	0.0	0.0	0.0	0.0
L (m) 0.13 $\pm$ 0.013	0.90	0.02	0.02	0.01	1.81	27.92
P (kPa) 101 $\pm$ 10.1	1.06	0.01	27.11	16.41	0.82	4.57
∅ (%) 0.90 $\pm$ 0.09	1.80	0.0	0.0	0.0	0.0	0.0

Parameter	$\dot{m}_c$ kg/s 0.042 ± 0.028	h_i $W/m^2℃$ 6808.0 ± 935.8	h_o $W/m^2℃$ 80.57 ± 10.47	U_o $W/m^2℃$ 58.26 ± 7.16	ΔP kPa 0.13 ± 0.096	q_t kW 32.7 ± 7.60
$s\ (mm)$ 3.17 ± 0.317	0.0	0.0	0.0	0.0	13.61	0.0
$t_{a,i}$ (℃) 37.78 ± 5.0	89.25	0.0	1.64	1.01	0.04	0.28
$t_{w,i}$(℃) 10 ± 25.0	0.02	64.57	0.0	0.97	0.0	0.32
$v_a\ (m/s)$ 4.57 ± 0.457	1.06	0.01	27.09	16.40	5.31	4.57
$v_w\ (m/s)$ 1.22 ± 0.122	0.01	32.25	0.0	0.48	0.0	0.13
$w\ (m)$ 0.65 ± 0.065	2.26	0.02	0.0	0.0	0.0	28.50
$x_a\ (mm)$ $31.7 + \pm 3.17$	1.35	0.01	0.94	15.19	45.92	5.00
$x_b\ (mm)$ 27.5 ± 2.75	0.24	0.01	0.96	18.24	10.97	5.08
$y(mm)$ 0.15 ± 0.015	0.02	0.0	0.0	1.68	0.0	0.47
Summation	100	100	100	100	100	100

PART TWO: SHELL AND TUBE HEAT EXCHANGER

3.7 Introduction

A shell and tube heat exchanger is a class of heat exchangers design. It is a common type of heat exchangers in water desalination, refrigeration and other large chemical processes, and is suited for higher-pressure applications. As its name implies, this type of heat exchanger consists of a shell (a large pressure vessel) with a bundle of tubes inside. Two fluids, of different inlet temperatures, flow through the heat exchanger. One flows through the tubes (the tube side) and the other flows outside the tubes but inside the shell (the shell side). The set of tubes is called a tube bundle, and may be composed by several types of tubes: plain, longitudinally finned, etc.

Heat is transferred from one fluid to the other through the tube walls, either from tube side to shell side or vice versa. The fluids can be either liquids or gases on either the shell or the tube side. In order to transfer heat efficiently, a large heat transfer area should be used, leading to the use of many tubes. This way, waste heat can be put to use. This is an efficient way to conserve energy. To be able to transfer heat well, the tube material should have good thermal conductivity. Because heat is transferred from a hot to a cold side through the tubes, there is a temperature difference through the tubes. Because of the tendency of the tube material to thermally expand differently at various temperatures, thermal stresses occur during operation. This is in addition to stresses from high pressures from the fluids themselves. The tube material also should be compatible with both the shell and tube side fluids for long periods under the operating conditions (temperatures, pressures, etc.). To minimize deterioration such as corrosion, all of these requirements

call for careful selection of strong, thermally-conductive, corrosion-resistant, high quality tube materials, typically metals, including copper alloy, stainless steel, carbon steel, non-ferrous copper alloy. Bad choice of tube material could results in a leak through a tube between the shell and tube sides causing fluid cross-contamination and possibly loss of pressure.

Heat exchangers with only one phase (liquid or gas) on each side can be called one-phase or single-phase heat exchangers. Two-phase heat exchangers can be used to heat a liquid to boil it into a gas (vapor), sometimes called boilers, or cool a vapor to condense it into a liquid (called condensers), with the phase change usually occurring on the shell side. Boilers in steam engine locomotives are typically large, usually cylindrically-shaped shell-and-tube heat exchangers. In the humidification dehumidification system shell and tube surface condensers are used to condense the exhaust saturated air from the humidifier into condensate water in the dehumidifier.

3.8 Design steps of shell and tube heat exchanger

The following represents the main parameters calculated in the design steps of the shell and tube heat exchanger as follows:

1- Latent heat
2- Total heat
3- LMTD correction factor
4- Design overall heat transfer coefficient
5- Heat transfer area
6- Number of tubes
7- Number of tube passes
8- Vapor velocity
9- Required heat transfer coefficient
10- Inside heat transfer coefficient
11- Outside heat transfer coefficient
12- Fin efficiency
13- Correction of sensible heat
14- Tube side pressure drop
15- Shell side pressure drop
16- Required length

3.9 Design procedure of a shell and tube heat exchanger

Various strategies are applied for the design and cost estimation of heat exchangers. The main objective in any heat exchanger design is the estimation of the minimum heat transfer area required for a given heat duty, as it governs the overall cost of the heat exchanger.

Several researchers have concluded that the area of the heat exchanger bears a strong relation to the total cost and while it considerably impacts the cost, therefore, the estimation of the cost of purchase is usually based on estimations of the heat transfer surface, and on previous knowledge and experience of exchanger manufacturing. In addition, the shell diameter and tube diameter also become important factors influencing directly the area of the exchangers under development. On the other hand, the pitch and configuration of the bundle are also clearly important factors for the cost of the new heat exchanger. Finally, the heat exchanger type is identified as one of the main key parameters.

A shell-and-tube heat exchanger consists of a bundle of pipes or tubes enclosed within a cylindrical shell. One fluid flows through the tubes, and a second fluid flow within the space between the tubes and the shell as shown in Figure 3-9.

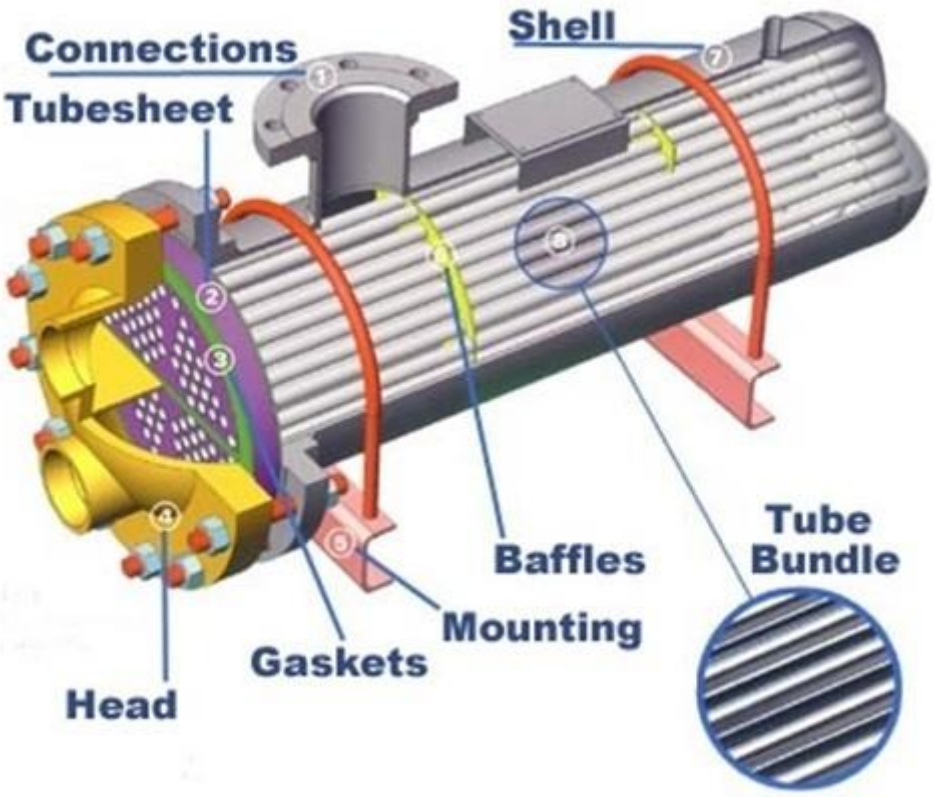

Figure 3-9 Shell and tube heat exchanger [75]

A design of a finned shell and tube heat exchanger type for the following specification

1- Fluid placement: A horizontal shell-side condenser is used. Therefore, the condensing vapor is placed in the shell side and cooling water flows in the tubes [75].
2- Tubing: 19.05 mm, 16 BWG (Birmingham Wire Gauge), 1024 fpm (fin per meter) tubing is selected. A tube length of 4.88 meter and a triangular layout with tube pitch of 23.8 mm are also specified.
3- Tube layout: since the shell-side fluid is clean, triangular pitch is specified. A tube pitch of 23.8 mm can be used. This value is selected because it provides more heat-transfer surface for a given shell size.
4- Baffles: Tube support plates are used in a cross-flow exchanger rather than standard baffles. A sufficient number of plates must be provided for adequate tube support and suppression of tube vibration. Considering the potential for tube vibration problems in this application, a plate spacing of 609.6 mm is a reasonable initial estimate, but this figure has no effect on the thermal or hydraulic calculations.
5- Construction materials: The 90/10 copper -nickel alloy specified for the tubes will provide corrosion resistance and allow a maximum water velocity of 3.0 m/s [75]. For compatibility, this material is also specified for the tube sheets. Finned carbon steel is adequate for the shell, heads, and all other components.

Table 3-6 The input data for the previous design problem from Serth [75]

Input data	Values	Unit
Inlet vapor temperature	84.17	℃
Outlet vapor temperature	75.56	℃
Inlet water temp	29.45	℃
Outlet water temp	48.89	℃
Outside area per length	0.596	m^2/m
Saturated vapor flow rate	22.68	kg/s
Outside tube diameter	19.05	mm
Inside tube diameter	13.26	mm
Root tube diameter	16.56	mm
Length	4.88	m
Number of fins	1024	fin/m
Fin thickness	0.33	mm
Tube pitch	23.80	mm
Tube inside fouling resistance	0.000176	$\mathrm{W/m^2℃}$
Tube outside fouling resistance	0.0000881	$\mathrm{W/m^2℃}$
Total area over inside area	4.35	-
Average two phase pressure drop multiplier	0.33	-
Number of tubes	534	-

The design the previous problem was calculated using the following parameters.

3.9.1 Energy balances.

The duty is calculated using the given enthalpy difference between saturated vapor and saturated liquid. Condensate sub cooling is very small, so we can neglect it, as is the effect of pressure drop on saturation temperature:

It is assumed that the latent heat is equal to the total heat since the sensible heat is assumed very small and can be neglected.

The latent heat can be computed using the following equation:

$$q_t = \dot{m}_{s,v}\left(i_{s,v} - i_{s,l}\right) \tag{50}$$

The cooling water mass flow rate is obtained from the energy balance equation:

$$q_t = (\dot{m}cp\Delta T)_w = \dot{m}_{s,v}\left(i_{s,v} - i_{s,l}\right) \tag{51}$$

3.9.2 The LMTD Correction Factor

In multi-pass shell-and-tube exchangers, the flow pattern is a mixture of co-current and counter-current flow, as the two streams flow through the exchanger in the same direction on some passes and in the opposite direction on others. For this reason, the mean temperature difference is not equal to the logarithmic mean. However, it is convenient to retain the LMTD by introducing a correction factor, F, which is appropriately termed the LMTD correction factor:

$$\Delta T_m = F(\Delta T_{ln})_{cf} \quad (52)$$

$$(\Delta T_{ln})_{cf} = \frac{\Delta t_1 - \Delta t_2}{\ln(\Delta t_1/\Delta t_2)} \quad (53)$$

Note that in this relationship, the LMTD is computed as if the flow were counter current. The LMTD correction factor can be computed analytically for any number of shell-side passes and any even number of tube-side passes as follows [76]:

Let

N= number of shell side passes

The F-factor can be calculated by first calculating the R &P factors using the following equations:

$$R = \frac{t_{i,v} - t_{o,v}}{t_{w,o} - t_{w,i}} \quad (54)$$

$$P = \frac{t_{w,o} - t_{w,i}}{t_{i,v} - t_{w,i}} \quad (55)$$

For the R-factor value there are two cases as follows:

For $R \neq 1$, compute

$$\alpha = \left[\frac{1-RP}{1-P}\right]^{1/N} \quad (56)$$

$$S = \frac{\alpha - 1}{\alpha - R} \quad (57)$$

$$F = \frac{\sqrt{R^2+1}\left[\frac{1-S}{1-RS}\right]}{(R-1)\ln\left[\frac{2-S(R+1-\sqrt{R^2+1})}{2-S(R+1+\sqrt{R^2+1})}\right]} \quad (58)$$

For $\mathbf{R = 1}$, compute

$$S = \frac{P}{N-(N-1)P} \tag{59}$$

$$F = \frac{\sqrt{R^2+1}\left[\frac{1-S}{1-RS}\right]}{(1-S)\ln\left[\frac{2-S(2-S\sqrt{2})}{2+S(2-S\sqrt{2})}\right]} \tag{60}$$

In the EES program, the value of $R \neq 1$ so the first case was used.

3.9.3 Approximate design overall heat-transfer coefficient

Consider the section of a double-pipe exchanger shown in Figure 3-10, in which the hot fluid is arbitrarily assumed to flow through the inner pipe. Heat is transferred by convection from the hot fluid to the wall of the inner pipe, by conduction through the pipe wall, and then by convection from the pipe wall to the cold fluid. The driving force for the heat transfer is the difference in temperature between the hot and the cold streams. To describe this overall process, an overall heat-transfer coefficient is used. The resistance is made up of five resistances in series, namely, the convective resistance between the hot fluid and the pipe wall, the conductive resistance of the pipe wall, and the convective resistance between the pipe wall and the cold fluid in addition to the two fouling resistances on the inside and outside surface area of the tube.

Figure 3-10 Section of a double-pipe heat exchanger

The following values are estimated for the film coefficients as initial optional values:

$$h_i = 5678 \frac{W}{m^{2\circ}C} \tag{61}$$

$$h_o = 1420 \frac{W}{m^{2\circ}C} \tag{62}$$

The previous estimated values are recommended in EES Program to make the iteration process more stable and easy to iterate.

And using the previous input data and assuming that $\eta_w = 1$ the initial value of the designed overall heat transfer coefficient can be calculated using the following equation:

$$U_D = \left[\frac{A_{tot}}{h_i A_i} + \frac{R_i A_{tot}}{A_i} + \frac{A_{tot} \ln (D_r/D_i)}{(2\pi K_t L)} + \frac{1}{h_o \eta_w} + \frac{R_o}{\eta_w}\right]^{-1} \tag{63}$$

3.9.4 Heat transfer area and number of tubes

The heat transfer area and the number of tubes are calculated using the estimated value of overall heat transfer area using the following equations:

$$A = \frac{q_t}{U_D \Delta T_m} \tag{64}$$

$$n_t = \frac{A}{\left(\frac{A_{tot}}{L}\right)*L} \quad (65)$$

3.9.5 Number of tube passes and velocity

Assuming two tube passes, there for two tube passes will be sufficient to give turbulent flow in the tubes.

So, the velocity is:

$$v_w = \frac{\dot{m}_w(\frac{n_p}{n_t})}{\rho_w \pi(D_i^2/4)} \quad (66)$$

Since the velocity is in the acceptable range for the tubing material which is less than 3 m/s, two tube passes will be accepted and used.

3.9.6 Shell size

The closest tube counts for the previous calculation is used [75] in order to provide adequate entrance and distribution space for the vapor. However, the next largest shell size is used with this tube bundle to be more appropriate.

3.9.7 Required overall heat transfer coefficient

The Required value of the overall heat-transfer coefficient can be calculated from the following equation:

$$U_{req} = \frac{q_t}{n_t(\frac{A_{tot}}{L})\Delta T_m} \quad (67)$$

Now because the value of the required value of the overall heat-transfer coefficient is less than the designed overall heat-transfer coefficient, which was clearly appeared in the EES Program calculation. The number of tube and the number of tube passes on this value is used to calculate the real value of the inside and outside heat transfer coefficients using the following equations in the following sections.

3.9.8 Inside heat transfer coefficient

The Reynolds number of water based on the inside surface diameter is:

$$Re_{Dw} = \frac{4\dot{m}_w(\frac{n_t}{n_t})}{\pi D_i \mu_w} \quad (68)$$

Where the water properties are evaluated at the average water temperature

Now, The Prandtl number is:

$$Pr_w = \frac{(\mu_w Cp_w)}{k_w} \quad (69)$$

The inside heat transfer coefficient for water can be calculated by assuming the viscosity correction factor ($\phi_i = \left(\frac{\mu}{\mu_w}\right)$) using the following equation:

$$h_i = 0.023 \frac{k_w}{D_i} (Re_{Dw})^{0.8} (Pr_w)^{0.3} \phi_i^{0.14} \quad (70)$$

3.9.9 Outside heat transfer coefficient

For finned tubes, the equivalent diameter defined by the following equation [75].

$$D_e^{-0.25} = \frac{1.30\,\eta_f A_{fin} E^{-0.25} + A_p D_r^{-0.25}}{\eta_w A_{tot}} \quad (71)$$

The fin efficiency for low-fin tubes is usually quite high, unless the material of construction has a relatively low thermal conductivity. Therefore, η_f and η_w have set to unity as a first approximation. The remaining parameters are calculated from the tube and fin dimensions:

$$r_1 = D_r/2 \quad (72)$$

$$r_2 = D_o/2 \quad (73)$$

$$E = \frac{\pi(r_2^2 - r_1^2)}{2r_2} \quad (74)$$

For convenience, the fin and prime surface areas are calculated per inch of tube length:

$$A_f = 2N_f\pi(r_2^2 - r_1^2) \quad (75)$$

$$A_p = 2\pi r(L - N_f\tau) \quad (76)$$

Next, the modified condensate loading is computed:

$$\acute{\Gamma} = \frac{\dot{m}_{s,v}}{L[n_t]^{2/3}} \quad (77)$$

The outside heat transfer coefficient using Beatty-Katz correlation [75] is:

$$h_o = 0.609\left[\frac{k_L^3 \rho_L(\rho_L - \rho_v) g\,\eta_w(A_{tot}/L)}{\mu_L D_e \acute{\Gamma}}\right]^{1/3} \quad (78)$$

3.9.10 Film temperature, average temperature and weighted temperature

The film temperature is computed using the following equation [75].

$$T_f = 0.75T_{wtd} + 0.25T_{av} \quad (79)$$

The average temperature of prime surface is computed using the following equation:

$$T_p = \frac{h_i t_{aw} + h_o \eta_w (A_{tot}/A_i) T_{av}}{h_i + h_o \eta_w (A_{tot}/A_i)} \quad (80)$$

The weighted temperature of finned surface is computed using the following:

$$T_{wtd} = \frac{h_i \eta_w t_{aw} + (h_i(1-\eta_w) + h_o \eta_w (A_{tot}/A_i)) T_{av}}{h_i + h_o \eta_w (A_{tot}/A_i)} \quad (81)$$

3.9.11 Fin efficiency

The fin efficiency is computed using the following equation:

$$r_{2c} = r_2 + \tau/2 \quad (82)$$

$$\psi = (r_{2c} - r_1)\left[1 + 0.35\ln[r_{2c}/r_1]\right] \quad (83)$$

$$m = \left[\frac{2h_o}{k*\tau}\right]^{1/2} \quad (84)$$

$$\eta_f = \frac{\tanh[m\psi]}{m\psi} \quad (85)$$

The weighted efficiency of the finned surface is computed using the following equation:

$$\eta_w = \left[\frac{A_p}{A_{tot}}\right] + \eta\left[\frac{A_f}{A_{tot}}\right] \quad (86)$$

3.9.12 Correction for sensible heat transfer

The effect of interfacial shear was neglected in calculating h_o, which will offset the effect of sensible heat transfer. Hence, this step could be omitted, but is included here to illustrate the procedure. The rate of sensible heat transfer is estimated using the following equation:

$$q_s = 0.5\overline{Cp_v}\dot{m}_{s,v}\left(T_{s,v} - T_{s,l}\right) \tag{87}$$

For convenience, the heat capacity at vapor inlet conditions is used as an approximation for $\overline{Cp_v}$

The Simplified Delaware method is used to calculate h_v. Since the baffle cut is greater than 20%, this method will tend to overestimate h_v. However, the safety factor built into the method will help to compensate for this error:

The vapor flow rate is used to calculate h_v .Physical properties of the vapor are taken at inlet conditions for convenience:

Now h_v can be calculated by computing both the Reynolds number and the Colburn j_H factor using the following equations:

$$Re = \frac{GD_e}{\mu_v} \tag{88}$$

$$j_H = 0.5\left(1 + \frac{B}{d}\right)(0.08Re^{0.6821} + 0.7Re^{0.1772}) \tag{89}$$

Now h_v is computed using the following equation:

$$h_v = j_H\left[\frac{K_v}{D_e}\right]Pr^{1/3}{\phi_i}^{0.14} \tag{90}$$

After the sensible heat is considered the modified overall heat transfer coefficient can be calculated using the following equation:

$$U_D^{`} = \left[U_D^{-1} + \left(\frac{q_s}{q_t}\right) h_v^{-1}\right]^{-1} \quad (91)$$

From the previous calculations, it is found that the value of the designed overall heat transfer coefficient is more than the value of the required designed overall heat transfer coefficient.

Therefore, since $U_D > U_{req}$, the condenser is thermally acceptable and due to this the pressure drop can be calculated.

3.9.13 Tube side pressure drop

Tube side pressure drop is computed using the following equation:

$$f = 0.4137 Re^{-0.2585} \quad (92)$$

$$\Delta P_f = \frac{f n_p L G^2}{7.50 * 10^{12} D_i s \phi_i} \quad (93)$$

$$\Delta P_r = 1.334 * 10^{-13}\left(1.6 n_p - 1.5\right) G^2/s \quad (94)$$

The total tube-side pressure drop is:

$$\Delta P_i = \Delta P_f + \Delta P_r + \Delta P_n \quad (95)$$

3.9.14 Shell-side pressure drop

The ideal tube bank correlations can be used to calculate the pressure drop in a cross-flow shell. The cross-flow area S_m is approximated by a_s with the baffle spacing equal to the length of the shell. For finned tubes, an effective clearance is used that accounts for the area occupied by the fins:

$$C_{eff}^{`} = P_T - D_{re} \tag{96}$$

Where D_{re} is the equivalent root-tube diameter and is calculated using the following equation:

$$D_{re} = D_r + 2n_f b\tau \tag{97}$$

n_f =the number of fins per unit length of tube

Note that $B * C_{eff}^{`}$ is the flow area between two adjacent tubes in one baffle space.

In calculating the Reynolds number for finned tubes, the equivalent root-tube diameter is used in place of D_o in the following equation:

$$Re_v = \frac{GD_e}{\mu_v} \tag{98}$$

The friction factor for plain tubes is obtained using the following equation:

$$f_i = 0.372 \left[\frac{1.33}{P_T D_o}\right]^{0.2134} Re^{-0.123} \tag{99}$$

The friction factor for finned tubes is estimated at 1.4 times the value for plain tubes [77]. Thus,

$$f`_i = 1.4 * f_i \quad (100)$$

The number of tube rows crossed is estimated using the following equation with the baffle cut taken as zero and a shell internal diameter to represent the size of the tube bundle.

$$N = \frac{d_s(1-2B_c)}{P_T \cos\theta_{tp}} \quad (101)$$

The pressure drop for all-vapor flow is calculated using the following equation. The effect of the bundle bypass flow is neglected here:

$$(\Delta P_f)_{vo} = \frac{2f`_i N_c G^2}{g_c \rho_v v \phi_i} \quad (102)$$

The two-phase friction loss is calculated using an average two-phase multiplier of 0.33 for a total condenser:

$$\Delta P_f = \phi_{vo}^{-2} (\Delta P_f)_{vo} \quad (103)$$

Assuming two 4-in schedule 40 nozzles are used for the condensate and allowing half a velocity head for the exit loss, we obtain:

$$G_{n,o} = \frac{0.5\dot{m}_w}{(\pi/4)D_n^2} \quad (104)$$

$$\Delta P_{f_{n,o}} = 0.5 * 1.335 * 10^{-13} \frac{G(n,o)\text{^}2}{s_L} \quad (105)$$

The total shell-side pressure drop is:

$$\Delta P_{f_o} = \Delta P_f + \Delta P_{f_{n,i}} + \Delta P_{f_{n,o}} \quad (106)$$

3.9.15 Required length

All design criteria are satisfied; however, the condenser is somewhat over-sized. The number of tubes cannot be reduced because the tube-side pressure drop is close to the maximum. Therefore, shorter tubes are considered. The required tube length is:

$$L_{req} = \frac{q_t}{n_t(\frac{A_{tot}}{L})U_D \Delta T_m} \quad (107)$$

Hence, the tube length is reduced. This change will decrease the tube-side pressure drop and increase the shell-side pressure drop slightly. Although these changes will not affect the viability of the design, the new pressure drops are calculated here for completeness for the tube and shell side using the iterative method in the EES program.

An iterative method is used in the engineering equation solver program (EES) in order to update all the previous parameter. And then the final overall heat transfer coefficient, pressure drop after all the previous updated values is calculated.

3.10 Validation of shell and tube heat exchanger model

Table 3-7 It provides a comparison between the values given by Serth [75] and the results of the present model developed in this study. Moreover, it shows the percentage deviation between the current calculations and these of Serth [75]. The difference is believed to be due to variable properties in the current model as compared to the constant properties assumption given by Serth.

It should be noted that the maximum percentage error does not exceed 8% between both calculations.

Table 3-7 Comparison between Serth [75] and values of the developed model

Definition	Symbol	Serth [75] values	EES program values	Percentage error%
Total heat	q_t	$7.743 * 10^6$	$7.834 * 10^6$	1.17
Latent heat	q_l	$7.544 * 10^6$	$7.632 * 10^6$	1.16
Sensible hat	q_s	$1.99 * 10^5$	$2.02 * 10^5$	1.51
Water mass flow rate	$\dot{m}_w$	92.7	96.36	3.95
Condensate mass flow rate	$\dot{m}_{s,v}$	22.68	22.68	0.0
Fin efficiency	η_f	0.867	0.8708	0.44
Weighted efficiency	η_w	0.896	0.893	0.33
Mean temperature difference	ΔT_m	71.3	71.55	0.31
Inside convection heat transfer coefficient	h_i	10522.0	10505.0	0.16
Outside convection heat transfer coefficient	h_o	1766.0	1777.0	0.61
Overall heat transfer coefficient	U_{req}	403.2	416.6	3.34
Overall heat transfer coefficient	U_D	491.7	497	1.07
Modified Colburn factor for shell-side heat transfer	j_H	348.4	360.5	3.47
Number of tube passes	n_p	2.0	2.0	0.0
Number of tube	n_t	534	534	0.0
Number of shell side passes	N	1.0	1.0	0.0
Tube Length required	L_{req}	4.0	4.22	5.50
Friction factor of the tube side	f_t	0.0257	0.02495	2.92
Friction factor of shell side	f_s	0.137	0.1372	0.15

Definition	Symbol	Serth [75] values	EES program values	Percentage error%
Frictional pressure drop in straight sections of tubes	ΔP_f	52.74	55.40	5.03
Tube-side pressure drop due to entrance, exit and return losses	ΔP_r	5.447	5.867	7.7
Pressure drop in nozzle	ΔP_n	2.48	2.48	0.0
Total tube-side pressure drop	ΔP_i	60.67	63.75	5.07
Frictional pressure drop for total flow as vapor	$(\Delta P_f)_{vo}$	0.517	0.522	0.85
Frictional pressure in shell	ΔP_s	0.172	0.172	0.0
Pressure losses in inlet nozzle	$\Delta P_{n,i}$	1.83	1.83	0.0
Pressure losses in outlet nozzle	$\Delta P_{n,o}$	0.83	0.83	0.0
Total shell-side pressure drop	ΔP_o	2.82	2.88	2.13

3.11 Parametric study of plate fin and tube heat exchanger

Figure 3-11 shows the relation between the saturated vapor flow rate and the condensate flow rate. It can be observed in this figure that the productivity of the system increases by increasing the saturated vapor mass flow rate to an optimum value and decreases after that value. The increase in the productivity is due to increased moisture carried with the vapor to the shell side of the condenser as it rate increases. Increasing the saturated vapor mass flow rate beyond this optimum value at a given water mass flow rate decreases the condensate flow rate due to increased heat transfer to the water side, thus heating the water that would reduce the temperature difference between the two fluids and accordingly reduce the rate of condensation.

The figure also shows an increase in condensation rate due to higher cooling water flow rate. Since this leads to higher heat removal rate and accordingly more vapor condensates in the shell side. On the other hand, an increase in the water mass flow rare keeping the air mass flow rate unchanged increases the productivity of the heat exchanger (c0ndensate) since the total heat transfer will increase due to increasing the water mass flow rate. This means that more heat will be absorbed from the air side and transferred to the water side this decreasing the temperature of the air side toward the dew point temperature.

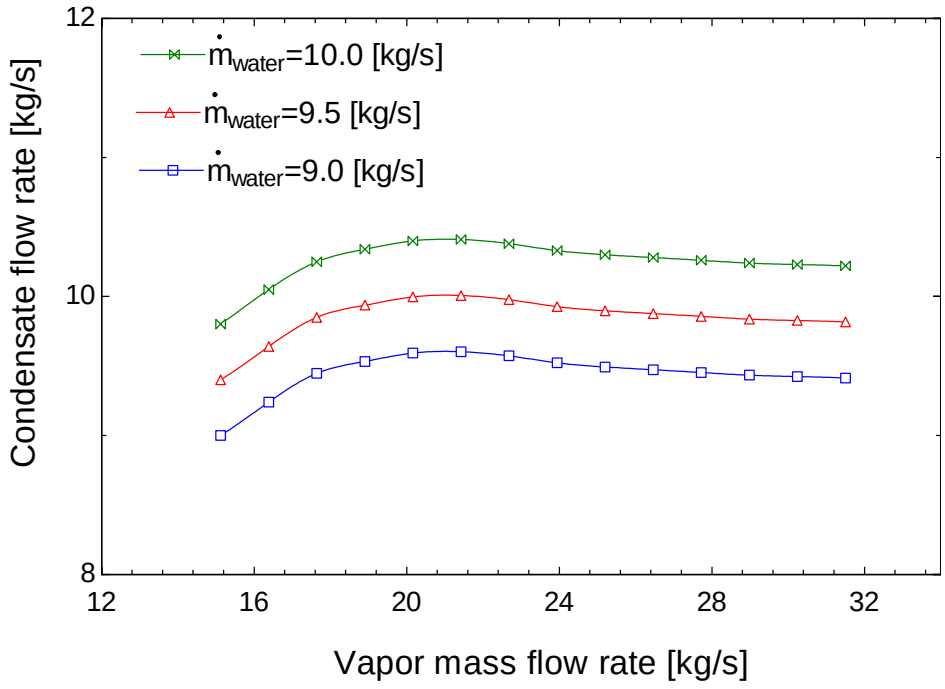

Figure 3-11 Change of condensate flow rate with the changes in the vapor mass flow rate

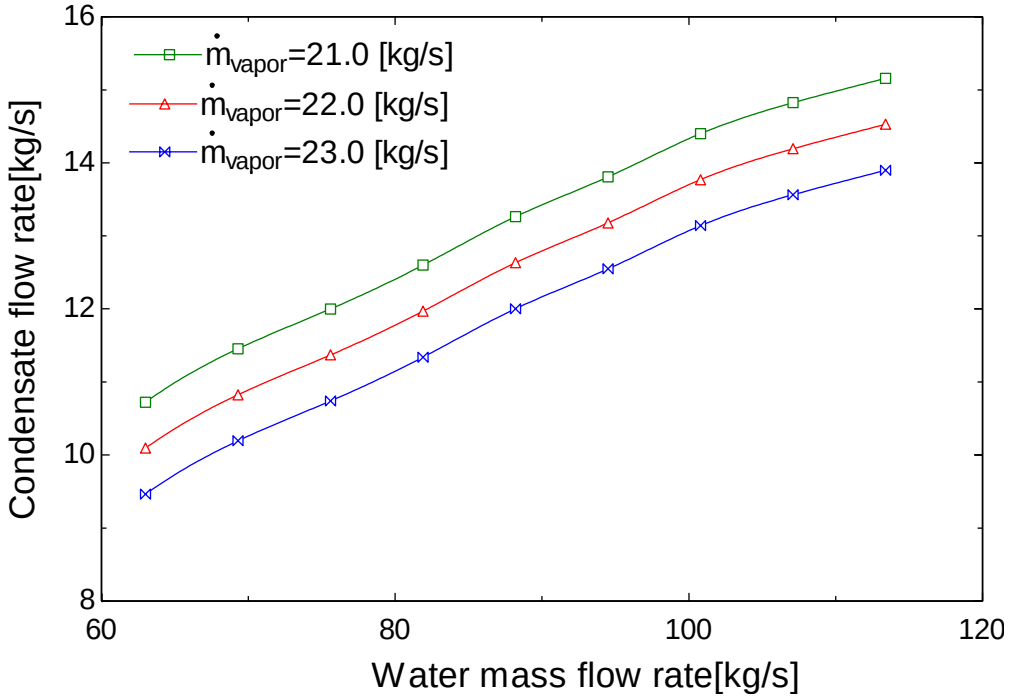

Figure 3-12 Change of condensate flow rate with the changes in the water mass flow rate

Figure 3-12 is a cross plat of Figure 3-11 that indicate the same effect of both fluids flow rate on the condensate production rate.

The effect of humid air inlet temperature to the condenser on the distillate production rate is shown in Figure 3-13. Increasing the saturated vapor inlet temperature for given saturated vapor mass flow rate will increase the condensate flow rate due to increased difference between the average saturated vapor temperature, and the average water temperature leading to more vapor condensation.

It is also shown that increasing the vapor mass flow rate at constant saturated vapor inlet temperature will decrease the condensate flow rate. This is because this additional flow rate will increase the average water temperature and decrease the heat capacity thus leading to a decrease in the productivity of the system.

Figure 3-14 shows the relation between the water inlet temperature and the condensate flow rate. From this figure, it can be seen that increasing the water inlet temperature at constant water mass flow rate decreases the condensate flow rate because of the decrease in the difference between the average water and average saturated vapor temperature. Accordingly less heat transfer rate would results leading to less condensation rate. Figure 3-14 also shows that the water mass flow rate at constant water inlet temperature leads to higher heat removal rate and accordingly more condensate production.

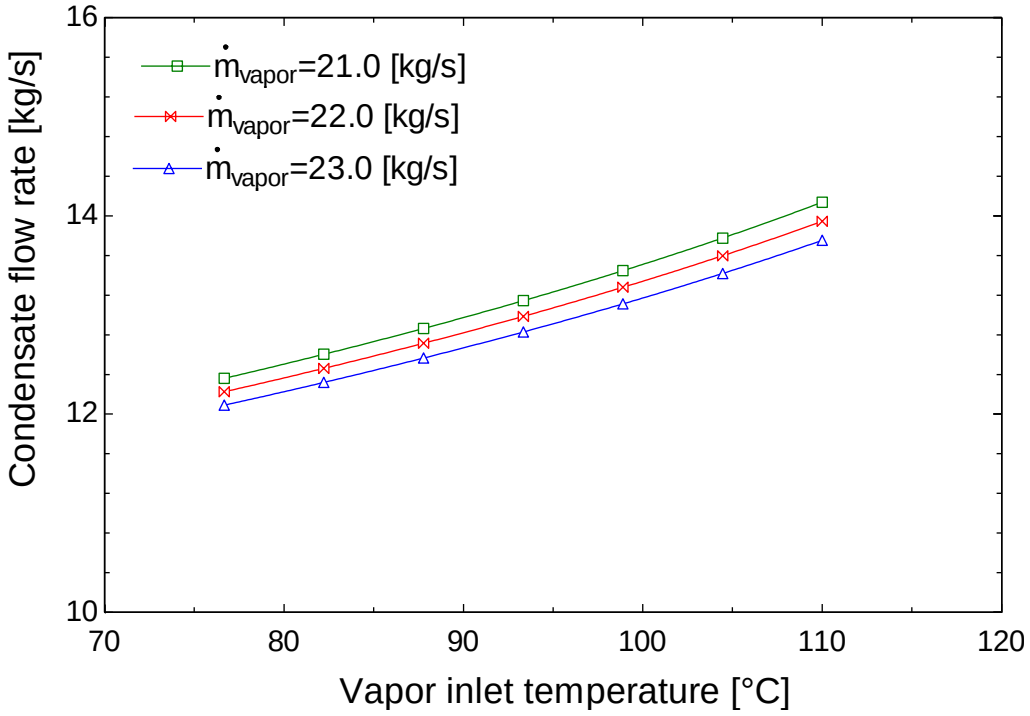

Figure 3-13 Effect of vapor inlet temperature on the condensate

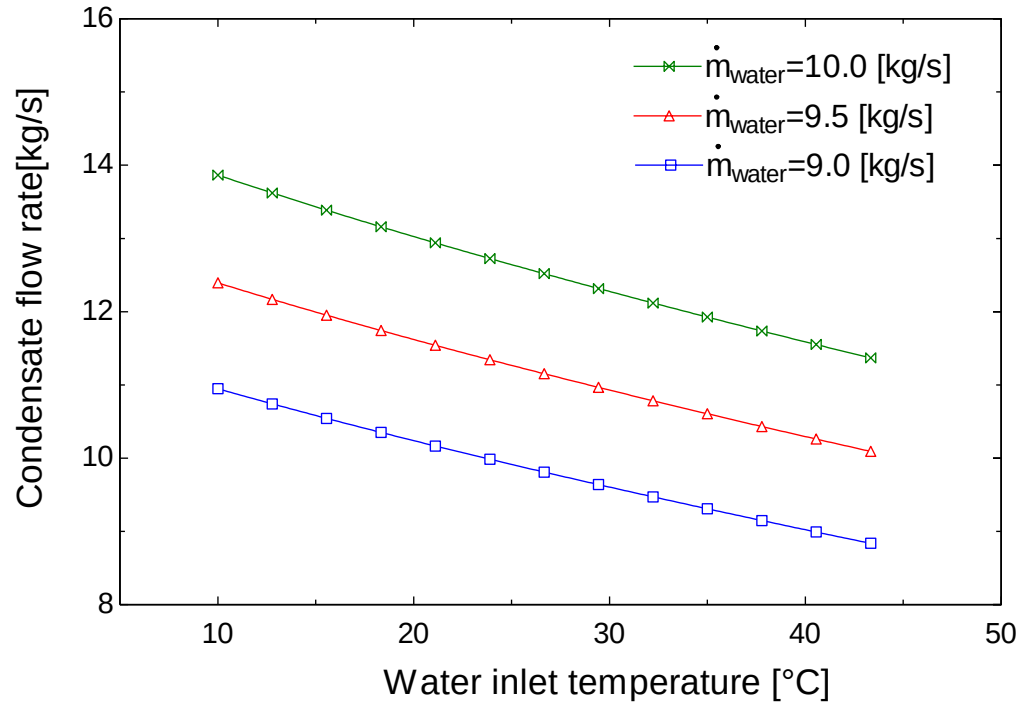

Figure 3-14 Effect of water inlet temperature on the condensate rate

The validated model is then used to make a design of a vertical shell and tube condenser for the experimental setup at KFUPM beach. Table 3-8 represents the input data of the shell and tube condenser that is used to design the shell and tube condenser.

Table 3-8 Input data of the shell and tube condenser

Input data	Values	Unit
Inlet air temperature	70	℃
Inlet water temperature	30	℃
Outlet water temperature	40	℃
Inlet air relative humidity	95	%
Water mass flow rate	1.0	kg/s
Air mass flow rate	0.278	kg/s
Outside tube diameter	19.05	mm
Inside tube diameter	13.26	mm
Number of fins	1024	fin/m
Fin thickness	0.33	mm
Tube pitch	23.80	mm
Tube inside fouling resistance	0.000176	$W/m^2℃$
Tube outside fouling resistance	0.0000881	$W/m^2℃$

A comparison between the developed program output results and the vender output results of the design for the experimental shell and tube condenser at KFUPM beach is shown in the following table.

Table 3-9 Comparison between the model output results and the vender output results

Output data	Vender values	EES program values	Unit
Total heat transfer	42.1	41.83	kW
Outside tube diameter	19.05	19.05	mm
Inside tube diameter	16.56	16.56	mm
Tube length	1.2	1.23	m
Number of passes	6	6	-
Number of tubes	72	72	-
Shell inside diameter	336.0	336.0	mm
Number of shell	1.0	1.0	-
Outside surface area	4.67	4.69	m^2
Pressure drop	47.0	47.54	kPa

3.12 Sensitivity analysis

Sensitivity analysis has been applied for the shell and tube heat exchanger in order to study the changing of output of a mathematical model can be apportioned, qualitatively or quantitatively, to different sources of variation in the input of a model. Table 3-10 represents the input parameter of the sensitivity analysis for the shell and tube heat exchanger.

Table 3-10 Input parameter of sensitivity analysis for the shell and tube heat exchanger

Item	Symbol	Variability %
Tube inside diameter	D_i	10
Tube outside diameter	D_o	10
Internal diameter of shell	d_s	10
Tube root diameter	D_r	10
Nozzle diameter	D_n	10
Fin height	b	10
Vapor mass flow rate	$\dot{m}_v$	10
Water mass flow	$\dot{m}_w$	10
Thermal conductivity of tube wall	k_t	10
Number of fins per unit length of the tube	N_f	10
Number of tube passes	n_p	10
Number of tubes in bundle	n_t	10
Tube pitch	P_T	10
Pressure losses in inlet nozzles	$\Delta P_{n,i}$	10
Density of vapor	ρ_V	10
LMTD correction factor	F	10
Fin Thermal conductivity	k_f	10
Tube inside fouling factor	R_i	10
Tube outside fouling factor	R_o	10
Inlet saturated vapor temperature	$t_{i,v}$	$\pm 5℃$
Inlet water temperature	$t_{i,w}$	$\pm 5℃$

The sensitivity analysis for changes in the main variables is carried out to identify the most significant parameters that affect the shell and tube heat exchanger performance as shown in Table 3-11. An equal variability of (10% of the parameter) was assigned to each one of the parameters, unless the inlet temperature of saturated vapor and water, which have given percentage uncertainty of (± 5℃℃) . The corresponding effect on the main response variables (condensate flow rate, inside and outside heat transfer coefficient, overall heat transfer coefficient, pressure drop of shell side, pressure drop of tube side and total heat transfer) was monitored and the percentage weighted of the change is calculated using EES Software [73]. For example, through performing the sensitivity analysis for the overall heat transfer coefficient as a response variable (fifth column) changes in the overall heat transfer coefficient are influenced by the tube outside diameter (34.15%) followed by the water inlet temperature (18.84%), air inlet temperature (15.86%) and tube root diameter (12.63%). In addition Tube inside fouling factor (5.56%), Fin efficiency (3.91%) and effectiveness (2.89%) have slightly effect on the overall heat transfer coefficient. The other variables have a negligible effect on the overall heat transfer coefficient. The same argument is used for the rest of the response factors listed in the table. On the other hand, different parameters are the most influential parameter on the changes in the remaining response variables. (Each responsible parameter has its own most influential parameter). Thus a designer can determine the most influential parameters that control the shell and tube heat exchanger and accordingly improve the unit performance.

Table 3-11 Sensitivity analysis for the shell and tube heat exchanger

	Response variables, %						
Parameters	$\dot{m}_c$ kg/s (166.5 $\pm$ 30.89)	h_i W/m^2°C (10283 $\pm$ 2680)	h_o W/m^2°C (1789 $\pm$ 479.1)	U_O W/m^2°C (480.4 $\pm$ 67.23)	ΔP_t kPa (60.96 $\pm$ 36.27)	ΔP_s kPa (2.79 $\pm$ 0.48)	q_t kW (7.62 $\pm$ 0.126 $*$ 10^6
$\frac{A_o}{L}$ 0.596 ± 0.0596	0.51	0.02	3.08	0.03	0.0	0.29	4.64
$\frac{A_{tot}}{A_i}$ 4.35 ± 0.435	0.14	0.01	0.07	0.0	0.0	0.08	1.24
$\frac{A_{tot}}{L}$ 0.596 ± 0.0596	0.0	0.0	0.0	0.0	0.0	0.00	0.01
b $1.25 \pm 0.1.25$	0.0	0.0	0.0	0.0	0.0	0.01	0.0
$cos\theta_{tp}$ 0.86 ± 0.086	0.0	0.0	0.0	0.0	0.0	0.12	0.0
D_n 1227.1 ± 122.71	0.0	0.0	0.0	0.0	0.0	44.69	0.0
D_i 13.3 ± 1.33	0.0	47.86	0.0	0.28	56.67	0.0	0.03
D_o 19.1 ± 1.91	0.36	0.01	30.44	34.15	0.0	0.20	3.26
D_r 16.6 ± 1.66	0.13	0.00	19.68	12.63	0.0	2.26	1.21

Parameters	$\dot{m}_c$ kg/s (166.5 $\pm$ 30.89)	h_i W/m²℃ (10283 $\pm$ 2680)	h_o W/m²℃ (1789 $\pm$ 479.1)	U_O W/m²℃ (480.4 $\pm$ 67.23)	ΔP_t kPa (60.96 $\pm$ 36.27)	ΔP_s kPa (2.79 $\pm$ 0.48)	q_t kW (7.62 $\pm$ 0.126 $* 10^6$
d_s 685.8 ± 68.58	0.0	0.0	0.0	0.09	0.0	0.10	0.01
$\Delta P_{n,i}$ 1.83 ± 0.183	0.0	0.0	0.0	0.0	0.0	14.92	0.0
η_f 0.87 ± 0.087	0.04	0.0	20.13	3.91	0.0	0.02	0.37
η_{so} 0.89 ± 0.089	0.03	0.0	14.89	2.89	0.0	0.02	0.28
F 0.98 ± 0.098	0.43	0.02	0.22	0.55	0.0	0.0	3.92
$f_i^{`}$ 0.098 ± 0.0098	0.0	0.0	0.0	0.0	0.0	0.12	0.0
f_t 0.33 ± 0.033	0.0	0.0	0.03	0.0	0.0	0.01	0.01
k_f 51.9 ± 5.19	0.0	0.0	0.0	0.0	0.0	0.0	0.00
k_t 51.9 ± 5.19	0.0	0.0	0.0	0.15	0.0	0.0	0.01
L_{req} 4.12 ± 0.412	0.43	0.02	1.87	0.87	0.0	0.39	3.95
L 4.88 ± 0.488	29.75	0.0	1.92	0.39	2.12	0.47	0.04

Parameters	$\dot{m}_c$ kg/s (166.5 $\pm$ 30.89)	h_i W/m^2°C (10283 $\pm$ 2680)	h_o W/m^2°C (1789 $\pm$ 479.1)	U_O W/m^2°C (480.4 $\pm$ 67.23)	ΔP_t kPa (60.96 $\pm$ 36.27)	ΔP_s kPa (2.79 $\pm$ 0.48)	q_t kW (7.62 $\pm$ 0.126 $*$ 10^6
$m_{s,v}$ 22.7 ± 2.27	39.27	0.05	3.49	0.24	0.0	21.95	11.51
m_{ca} 11.3 ± 1.13	0.0	0.0	0.0	0.02	0.0	0.0	0.0
m_w 93.9 ± 9.39	0.07	7.48	0.03	0.46	8.45	0.04	0.62
N_f 1024 ± 1.02	0.0	0.0	0.26	0.03	0.0	0.01	0.0
n_p 2 ± 0.2	0.01	9.55	0.01	0.99	21.08	0.01	0.09
n_t 534 ± 53.4	17.54	8.74	1.57	1.84	8.22	0.20	3.20
P_T 23.8 ± 2.38	0.0	0.0	0.0	0.13	0.0	4.75	0.01
ϕ_{vo} 0.33 ± 0.033	0.0	0.0	0.0	0.0	0.0	0.12	0.0
$T_{s,v}$ 84.1 ± 0.841	6.88	0.11	0.06	15.86	0.0	3.85	25.66
$T_{w,i}$ 29.9 ± 0.29	4.34	26.13	2.20	18.84	0.85	2.43	39.39

Parameters	$\dot{m}_c$ kg/s (166.5 $\pm$ 30.89)	h_i W/m²°C (10283 $\pm$ 2680)	h_o W/m²°C (1789 $\pm$ 479.1)	U_O W/m²°C (480.4 $\pm$ 67.23)	ΔP_t kPa (60.96 $\pm$ 36.27)	ΔP_s kPa (2.79 $\pm$ 0.48)	q_t kW (7.62 $\pm$ 0.126 $* 10^6$
R_i (0.000176 $\pm$ 0.0000176)	0.06	0.0	0.03	5.56	0.0	0.03	0.53
R_0 (0.0000881 $\pm$ 0.00000881	0.0	0.0	0.0	0.09	2.60	2.79	0.01
Summation	100	100	100	100	100	100	100

CHAPTER 4

EXPERIMENTAL SETUP

4.1 Introduction

The solar HDH is a thermal water desalination method. It is based on evaporation of seawater or brackish water and consecutive condensation of the generated humid air, mostly at an ambient pressure. This process mimics the natural water cycle, but over a much shorter time frame.

The simplest configuration is implemented in the solar still, evaporating of the seawater inside a glass covered box and condensing the water vapor on the lower side of the glass cover. More sophisticated designs separate the solar heat gain section from the evaporation and condensation chamber in order to optimize the design of this system. The humidification dehumidification system in which the solar air or water heater represent the solar heat gain. The humidifier is used to humidify the hot air coming from the solar heater by spraying saline water in the humidifier where it is evaporated in the hot air. The dehumidifier is used to condense the water that is evaporated in the humid air in the humidifier by exposing that air to a temperature less than the dew point of that air and by this fresh or sweet water from the saline water will produce.

4.2 Experimental steps

The following represents the main steps of the experimental setup as follows:

1- Fixing the solar air heaters

2- Connecting the humidifier

3- Connecting the dehumidifier (Condenser)

4- Pipe connections between the devices

5- Sensors for measurements

6- DAS operation

7- Water collection and data reporting

4.3 Experimental Set-up

The experimental setup is prepared to study, monitor and record all parameters needed to perform thermal calculations of the following components:

1- Solar air heaters

2- Humidification tower equipped with structured packing material and seawater

3- Sprayers

4- Flow meters

5- Blowers and pumps

6- Flow valve/controllers

7- Data acquisition system

8- Condenser

9- Temperature sensors

A test loop is set up at KFUPM beach. Moreover, includes a micro-processor based. Data Acquisition System which records all parameters necessary to perform thermal analysis of the system. In general, the parameters recorded in the data acquisition system include:

1- Temperatures at various state points of the solar HDH desalination system, in℃.
2- Relative humidity at various state points of the solar HDH desalination system, %
3- Air flow rate of the humid air, water flow rates of humidifying seawater and cooling water, kg/s
4- Quantity of desalted water produced, kg

The operating conditions can be adjusted subject to the need.

4.4 System description

The solar desalination system with the HDH technique mainly consists of tilted tubular evacuated glass cover solar air heaters, humidifiers, and dehumidifying exchanger. A schematic view of the solar HDH system, which is based on the idea of the closed water and open air cycles, is presented in Fig.4-1. Working principle of this system can be explained as follows:

The process air at the ambient conditions is forced to flow through the pipes of tilted solar air heaters, where it is heated. The heated air leaving the solar air heater enters the humidifier, and it is humidified by saline water, which comes from the storage tank of sea water. The warm air loaded by water vapor is passed through the condenser surface where water vapor condenses the vapor and turns it into fresh water. In addition, the saline water leaving the humidifier is collected in the storage tank and recirculated to the humidifier. In this study, air is heated by solar energy, whereas water is not heated.

Another water tank with water pump has used to supply the condenser with the water needed to condense the humid air in the humidifier.

Fans connected to a photovoltaic (PV) panel (which is a semiconductor device that converts part of the incident solar energy directly into electric energy) are used to circulate air. Therefore, flow rate of the ambient air to the solar air heaters depends on the solar energy falling during the day. Air velocity increases at peak hours and decreases toward sunset and cloudy days.

To keep constant flow rate, another suction fan located at the top of the humidifier. Air flow rate is further controlled by a variable air volume device connected to air blower in order to control the air flow rate that has introduced to the humidifier.

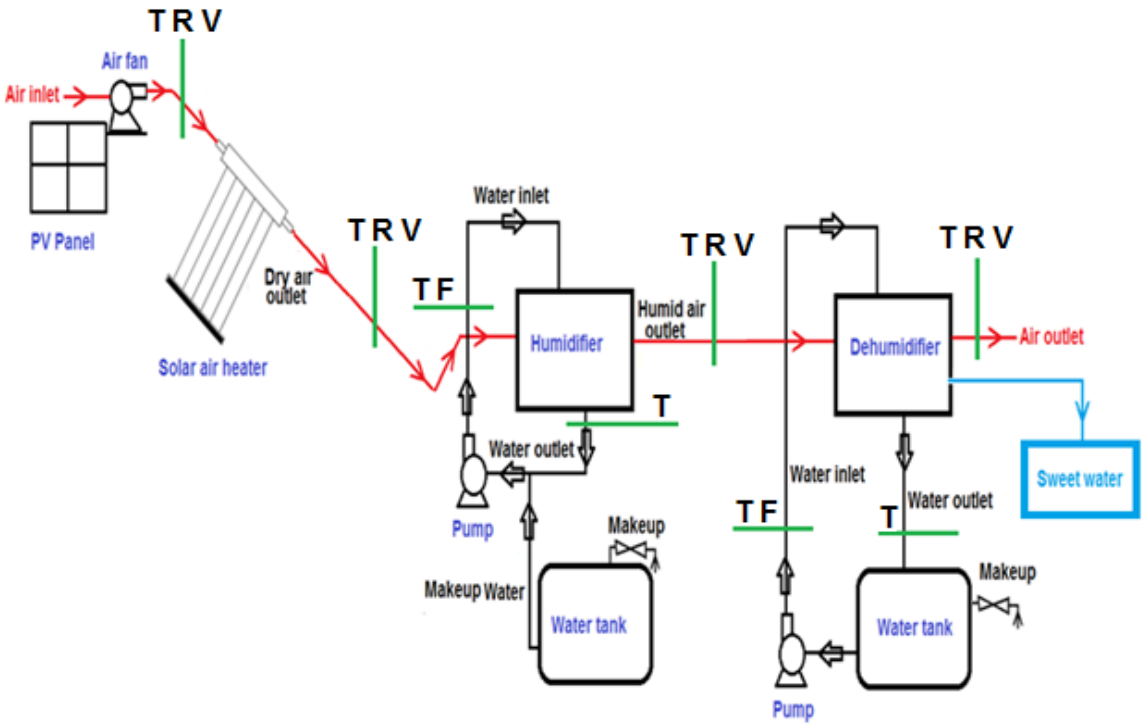

Figure 4-1 Schematic view of the desalination system

Symbols in Figure 4-1 represent as follows:

T: Temperature sensor (thermocouple)

R: Relative humidity sensor

V: Velocity sensor

F: Water flow rate sensor

Another variable (water flow rate) was considered to change the quantity of the water flow rate entering the condenser.

4.5 Heat and mass transfer model

The tilted tubular solar air heater has a simple structure; it absorbs the scattered radiation and direct radiation of the sun at the same time. However, the heat loss which comes from the tubular glass tube is considerable. In order to reduce the heat loss and increase the area of heat-absorbing a tubular collector with an evacuated double glass tube and tilted surface is used.

As shown in Figure 4-2 the solar radiation passes through the double glass tubes, shining on the heat-absorbing tubular stainless steel pipes, so the circular stainless steel pipes are heated. The ambient air flows into the air heater enter the stainless steel pipes in order to preheat the air. Then, this air enters between the stainless steel pipes and the double glass tubes in which a further heating for the air will happen until its temperature arrives to the required outlet temperature of the solar air heaters.

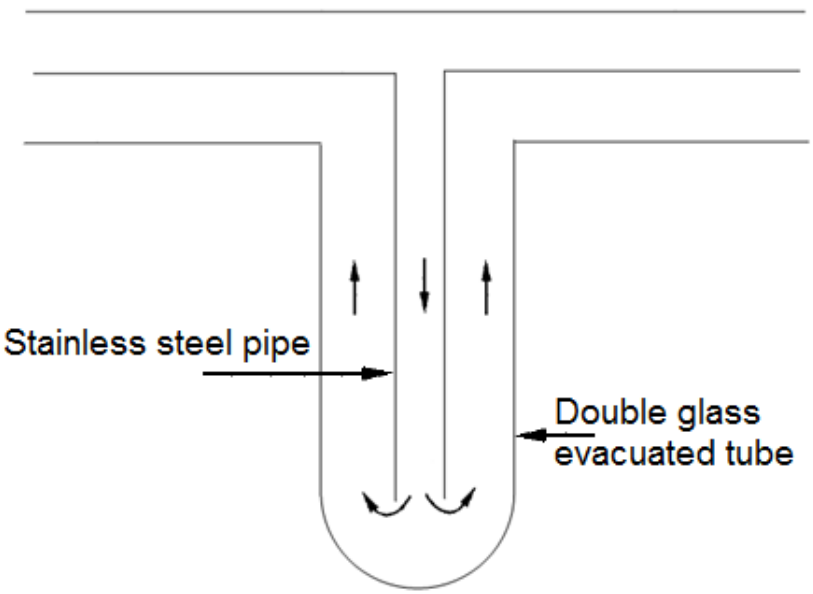

Figure 4-2 Schematic view of solar air heater pipe

Convection heat transfer between the stainless steel pipes and the air inside the stainless steel pipes also convection between the stainless steel pipes and the air between the stainless steel pipes and the double glass tubes will take place. Meanwhile, the stainless steel pipes are making a radiation heat transfer with the double glass tubes. Convection heat transfer between the inside air near the double glass tubes and the double glass tube will take place. The state between the double glass tubes is a vacuum, which only has radiation heat transfer. In addition, heat dissipates into the environment by the convection and radiation heat transfer from the double glass tubes and through the material of the stainless steel pipes by conduction. Radiation heat loss is also minimized by using a low emissivity absorber surface.

4.6 Solar air heaters

A comprehensive study of literature describing solar collectors for air heating was carried out. Efficiencies and prices of commercially available known collectors have been investigated. To use appropriate solar air heaters for the research, the following selection criteria were strictly followed:

1- Resistance against sea climate.

2- Maximum life time.

3- Simple design.

4- Minimum ratio of price to the performance.

4.6.1 Solar air heater system specification

Solar air heaters are used as the source of energy to the system in which air was forced to flow in the solar air heaters using the fans working by the photovoltaic panel .The solar air heaters consist of tubular circular stainless steel pipes surrounded by an evacuated glass tube heated by the energy coming from solar radiation. The evacuated glass is used in order to eliminate the heat losses to the environments by conduction, convection and radiation. Figure 4-3 shows a solar air heater used in the experimental setup.

The solar air heaters that used at KFUPM beach have the following specification:

1- Twenty tubular circular stainless steel pipes inside an evacuated glass pipe to reduce the heat loss to the environments.
2- The total number of solar air heaters used is nine connected in parallel to heat the required flow rate of ambient air before entering the humidifier.
3- The solar air heaters are parallel connected to the humidifier.
4- Nine fans with the nine photovoltaic panels are used to force the ambient air into the solar air heaters.
5- Photovoltaic stand panel is used to change the angle of the photovoltaic panel within the range from 0 to 60 degrees from the horizon.
6- The preferable solar air heater and photovoltaic panel angles for the annual use in Dhahran in Saudi Arabia was $26°16'$ N that matches the latitude (latitude is the angular location north or south the equator).

7- The fan is connected to the photovoltaic panel stand at a height of 78.5 cm from the solar air heater stand level in order to be consistent with the height of the solar air heater inlet pipe center.

Collector dimensions are:

1- Collector length =1.5 m , Collector width=1.42 m
2- Stainless steel pipe inside diameter = 1.7 cm
3- Stainless steel pipe outside diameter = 1.8 cm
4- Glass pipe inside diameter = 4.01cm
5- Glass pipe outside diameter = 4.67 cm
6- Collector inlet diameter = 5 cm

The fans that used have the following specification:

1- Voltage = 6-12 V
2- Power = 30 W

The main parts of the solar air heater that have used in the HDH system as shown in Figure 4-4.

Figure 4-3 Evacuated tube solar air heater

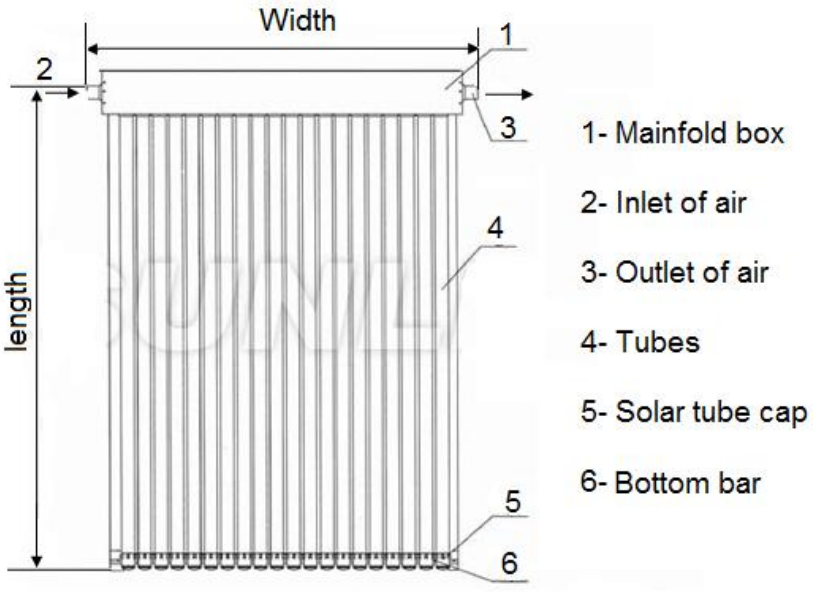

Figure 4-4 Main parts of the solar air heater

4.6.2 Photovoltaic panel

Photovoltaics (PVs) are arrays of cells containing a solar photovoltaic material that converts solar radiation into a direct electric current. Materials presently used for photovoltaics include monocrystalline silicon, polycrystalline silicon, microcrystalline silicon, cadmium telluride, and copper indium selenide/sulfide. Due to the growing demand for renewable energy sources, the manufacturing of solar cells and photovoltaic arrays has advanced dramatically in recent years.

Photovoltaics are best known as a method for generating electric power using solar cells to convert energy from the sun into electric energy. The photovoltaic effect refers to photons of light knocking electrons into a higher state of energy to create electricity. The term photovoltaic denotes the unbiased operating mode of a photodiode in which current through the device is entirely due to the transduced light energy. Virtually all photovoltaic devices are some type of photodiodes.

Solar cells produce direct current from sun light, which can be used to power equipment or to charge a battery. The first practical application of photovoltaics was to power orbiting satellites and other spacecrafts, but today many of photovoltaic modules are used in desalination systems.

Solar panels are normally mounted at an angle (latitude) to receive more energy per unit area instead of a horizontal surface. Cells require protection from the environment and are usually packaged tightly behind a glass sheet.

PV installations can operate for many years with little maintenance or intervention after their initial set-up, so after the initial capital cost of building any solar power plant,

operating costs are extremely low compared to existing power technologies. Solar electric generation is economically superior where grid connection or fuel transport is difficult, costly or impossible.

Figure 4-5 show a photovoltaic panel used in the humidification dehumidification desalination system.

The Photovoltaic panel used in the experimental setup has the following specification at the standard test conditions (STC):

1- Module HYM-040
2- Peak power = 40 W
3- Maximum power current (lmp) =2.27 A
4- Maximum power voltage (Vmp) = 17.64
5- Open circuit voltage (VOC) = 21.6 V
6- Short circuit current (lsh) = 2.49 A

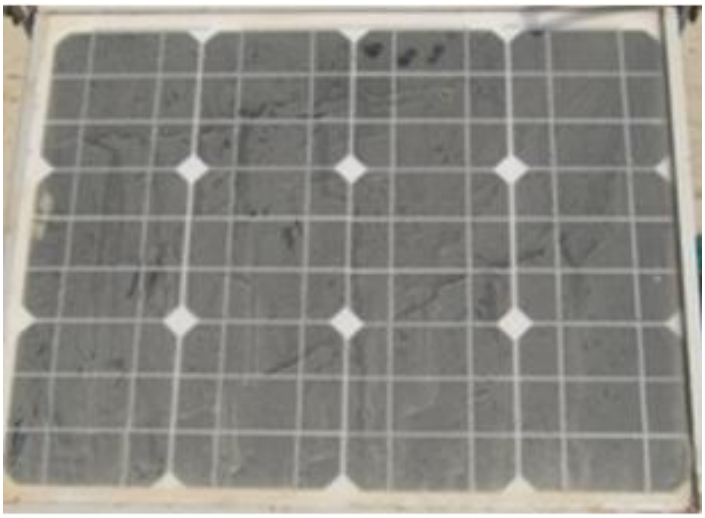

Figure 4-5 Photovoltaics panel

4.7 Packed Bed Humidifier

The heart of the seawater desalination system is the design of a high performance humidifier with seawater-air contact system. The driving force for mass transfer between the air and the seawater is the difference in vapor pressure between air and seawater. As seawater is brought in contact with air, air absorbs the water vapor from the seawater, that is, water evaporates into the air. During this process, heat is evolved due to the latent heat of evaporation of the water. If there is no heat added or removed during this humidification process it will then be adiabatic.

The humidification process can be accomplished using equipment such as a finned-tube surface in a column, spray tower or packed tower. Out of three basic configurations, packed tower configuration has received more attention because of a large rate of heat and mass transfer per unit volume, thus lending them to compact design. In a packed tower humidifier, seawater is distributed from the top and allowed to trickle down through the tower in a thin film covering the packing material surfaces. Different kinds of packing material such as Raschig rings, Lessing rings, Partition rings, Berl saddles, Intalox saddles, Tellerettes, Pall rings, etc. are available in the market. They may be made of ceramic, carbon, plastic or metal in different sizes. Among these packing material, Raschig rings, flexi rings and Berl saddles are widely used in a packed tower.

Although these random packed towers facilitate more mass transfer by providing a large area in a relatively small volume, air pressure drop through the packing is generally high. However, new types of packing's have been introduced recently in contrast to the traditional, randomly placed packing materials. The humidifier column can be packed either randomly, as mentioned earlier or with structured packing. Structured packing

represents the newest development in high efficiency, high capacity packing for mass and heat transfer introduced recently in contrast with traditional, randomly placed packing materials to permit improved control of mass transfer by the use of a fixed orientation of transfer surfaces. They are now widely used in different industrial applications such as crude oil distillation, cryogenic air separation plants, natural gas dehydration plants, acid gas removal in ammonia plants, OTEC research, etc. These new packing materials are fitted in an ordered and structured manner in the column to carefully match its size and operations. They have shown excellent performance characteristics with a relatively low ratio of pressure drop to heat and mass transfer coefficient per unit volume, in addition to easy installation. Recent attempts have been made to use structured packing for dehumidification processes.

Out of these basic configurations for air humidification with seawater, structured packing that combines good heat and mass transfer characteristics with low-pressure drop are used. Figure 4-6 shows the humidifier used in the solar HDH desalination system experimental setup.

The humidifier fan used in the experimental setup has the following specification:

1- Voltage = 220/240 V
2- Revolution per minute =2850 Rpm
3- Frequency =50 HZ
4- Power = 550 W
5- Current= 4.6 A
6- Single phase

The humidifier pump used on the experimental work has the following specification:

1- Motor model C48M2EC1A1
2- Voltage = 115/230 V
3- Power = 1500W
4- Revolution per minute =3450 rpm
5- Frequency =60 HZ
6- Single Phase

4.8 Dehumidifier

A process implemented by which solar heaters are used to heat an air stream blown by fans into the humidifier where sea water was sprayed and vaporized. The vaporized salt-free water is condensed in a condenser where sea water is used as the cooling medium.

Figure 4-7 shows a horizontal shell and tube heat exchanger used in the solar HDH desalination system.

4.9 Dehumidifier specification

A shell and tube heat exchanger is used as a condenser in which one fluid is seawater used as the cooling fluid, whereas the hot fluid is warm air to be condensate. So the condensate hot and humid air flows in the shell side while the seawater flows in the tube side. The design conditions that used for the exchanger are:

Hot side: moist air with inlet air temperature $T_{ai} = 70℃$, relative humidity $\emptyset = 95\%$, and the volumetric air flow rate $V_{ai} = 1000 m^3/h$

Cold fluid: seawater with inlet water temperature $T_{water\ inlet} = 30℃$, outlet water temperature $T_{wo} = 40℃$, water mass flow rate $60kg/min$

Seawater available pressure drop, assuming $< 0.5 - 1\ bar$

Condenser length=1.6 m

Fouling factors, assume values according to TEMA standard

Material selection: Titanium would be ideal with sea water, but it is expensive, so duplex stainless steel (or copper nickel) have used.

Figure 4-6 Humidifier used in the experimental setup

Figure 4-7 Shell and tube heat exchanger (Condenser)

4.10 Data Acquisition System

Data acquisition is the process of recording real world physical conditions and conversion of the resulting samples into digital numeric values that can be manipulated by a computer. Data acquisition and data acquisition systems (abbreviated with the acronym DAS) typically involve the conversion of analog waveforms into digital values for processing. The components of data acquisition systems include:

1- Sensors that convert physical parameters to electrical signals.

2- Signal conditioning circuitry to convert sensor signals into a form that can be converted to digital values.

3- Analog-to-digital converters, which convert conditioned sensor signals to digital values.

Data acquisition applications are controlled by software programs developed using various general purpose programming languages such as BASIC, C, Fortran, Java, Lisp, Pascal. COMEDI is an open source API (application program Interface) used by applications to access and controls the data acquisition hardware. Using COMEDI allows the same programs to run on different operating systems, like Linux and Windows.

Specialized software tools used for building large scale data acquisition systems include EPICS. Graphical programming environments include ladder logic, Visual C++, Visual Basic, MATLAB and. Lab VIEW.

In the solar HDH desalination system experimental setup the Lab VIEW Program has used to convert the physical conditions into digital numeric values that have manipulated by a computer.

So a data acquisition system used to get the reading for the following parameters

1- Air and water Temperatures using thermocouple's sensors
2- Air flow rate using air flow rate sensors
3- Air speed using air speed sensors
4- Water flow rate sensor
5- Solar intensity sensor

So about twenty seven thermocouples type -k- have distributed as follows:

1- Nine thermocouples type -k- at the collector's air outlets, six at the humidifier air inlets, two at the humidifiers air outlet, one at the condenser air outlet, one at the condenser water inlet, one at the condenser water outlet, one at water tank, one at the ambient temperature, two at the humidifier water inlet and outlet.
2- Relative humidity sensors at humidifier air inlet and air outlet and one at the condenser air outlet.
3- Air speed rate sensors at humidifier air inlet and air outlet and one at the condenser air outlet.
4- One water flow rate sensor at the humidifier water inlet and one at the condenser water inlet.
5- One solar intensity sensor.

Figure 4-8 shows the data acquisition system used in the solar HDH desalination system experimental setup.

Figure 4-8 Data acquisition system

CHAPTER 5

RESULTS AND DISCUSSION

All the measurements were performed in Dhahran (26°16'N and longitude 50°10'E), Saudi Arabia. The parameters, solar intensity, ambient temperature and relative humidity, air velocity and water flow rate were measured as input and output parameters to the solar air heater's system which is run between 9 a.m. to 16 p.m.

In this study, seven experimental operation conditions were carried out. Each one was repeated for three days to ensure and validate trends. As a primary test of the experimental setup the raw water has used instead of seawater.

Seven experiment operation conditions were carried out by changing the value of humidifier inlet air mass flow rate, condenser inlet water mass flow rate and humidifier inlet water mass flow rate.

Table 5-1 Experiment operation conditions

Humidifier inlet air mass flow rate l/h	Condenser inlet air mass flow rate l/h	Humidifier inlet water mass flow rate l/h
350	5000	6770
350	5000	6770
350	500	6770
350	5000	3170
350	5000	3170
350	4000	6770
350	5000	3170
350	4000	6770
350	4000	6770
280	5000	6770
280	5000	6770
280	5000	6770
350	5000	4970
350	5000	4970
350	5000	4970
350	3000	6770
350	3000	6770
350	3000	6770
210	5000	6770
210	5000	6770
210	5000	6770

Table 5-2 Salinity range of different types of water

Water type	Salinity value (ppm)
Seawater	30000 - 70000
Raw water –water tank	2000 - 4000
Fresh water - experimental setup	13 - 15
Bottled drinking water - company	100 - 150
Available Drinking water - tap	Up to 500

5.1 Parametric study

A parametric study was carried out by changing the following parameters; humidifier inlet air mass flow rate, humidifier inlet water mass flow rate and condenser inlet cooling water mass flow rate. Each experimental operation condition was reported three times to ensure the trend leading to three readings for each parameter.

5.1.1 Input and output data of the Solar HDH desalination system

Figure 5-1 represents the solar intensity profile on tilted solar air heater and the changes of ambient temperatures with time for three different typical days. The figure indicates that the recorded values change with time, since they depend on the solar energy.

It is observed that at the beginning of the operation time the ambient temperate and solar intensity increases from low values since the sun change its angle as the time pass until noon time in which they are at the peak value. After that their values start to decrease in the afternoon till the sunsets.

Figure 5-2 represents the changes of ambient relative humidity with time for three typical days. It is observed that the values of relative humidity decrease near noon time since both the ambient temperature, and solar intensity are at the peak values. After that the values of relative humidity increases with time as the solar energy flux and ambient temperature decrease.

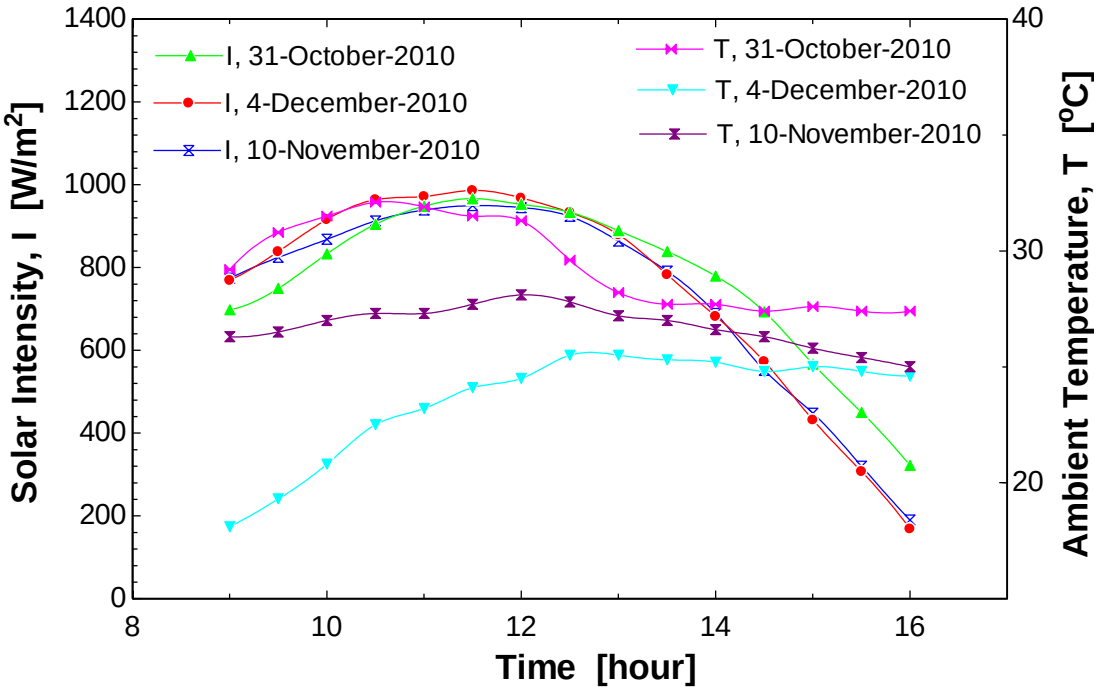

Figure 5-1 Solar intensity and ambient temperature profiles for three different days

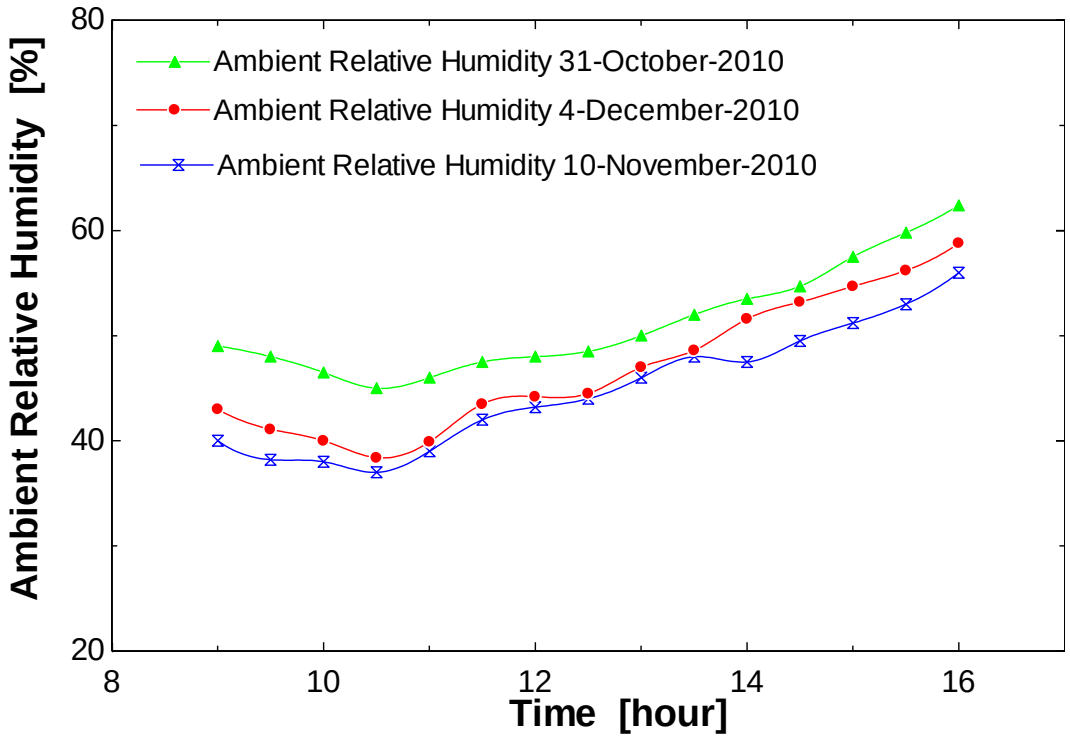

Figure 5-2 Relative humidity profiles for three different days

Figure 5-3 represents the changes of the measured humidifier inlet air temperatures with time. It is noticed that as the system starts to operate, the humidifier inlet air temperature decreases since there is stored energy in the solar HDH system.

After that, the humidifier inlet air temperatures start to change with time since both the solar intensity and ambient temperatures also change with time. The measured values of the humidifier inlet air temperatures are taken for three typical days, and clearly the trend is almost the same.

Figure 5-4 represents the changes of humidifier outlet air temperatures with time. As the experiment starts, the humidifier outlet air temperature decreases since there is stored energy in the solar HDH system in the few hours before the system is operated resulting in a high temperature that decreases as the air is drawn across the solar collector, thus slightly decreasing the air temperature

Then, the humidifier outlet air temperatures increase or decrease with time since both the ambient temperature and the humidifier inlet air temperatures also increase or decrease with time.

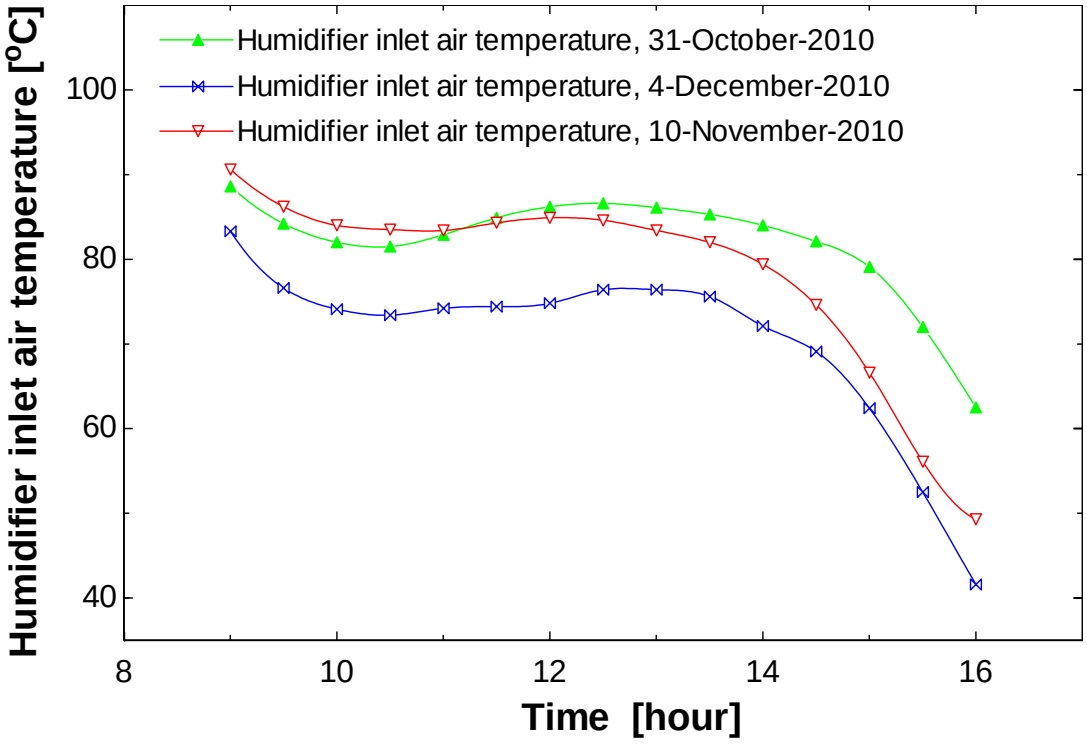

Figure 5-3 Humidifier inlet air temperature for three different days

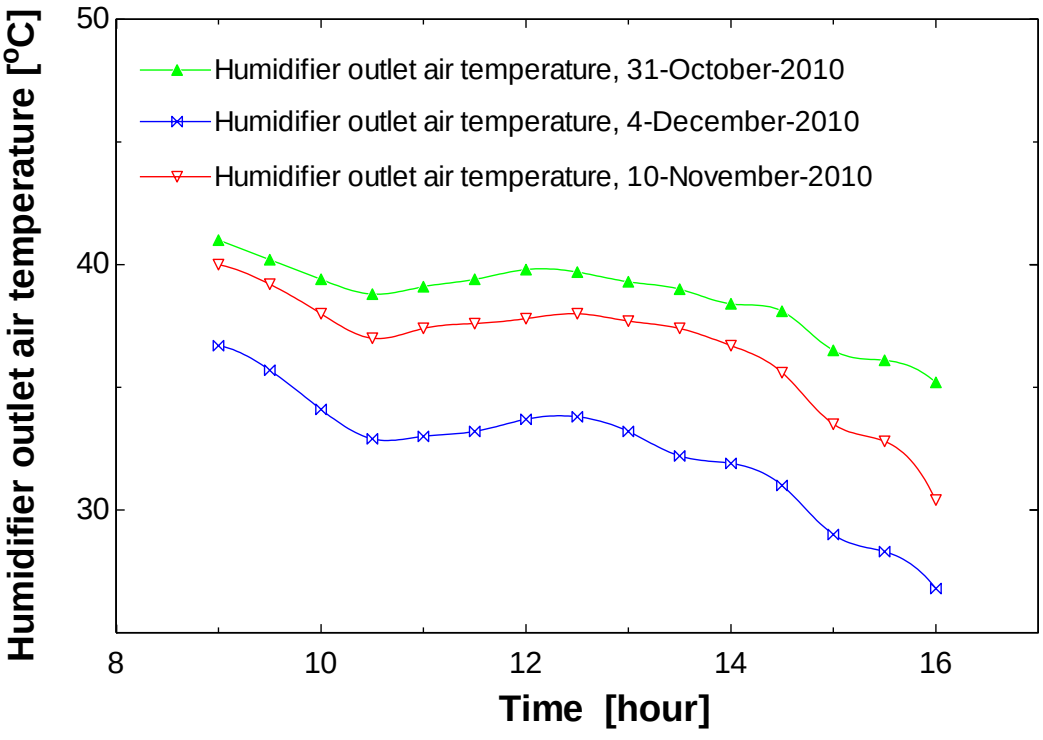

Figure 5-4 Humidifier outlet air temperatures for three different days

Figure 5-5 represents the changes of the measured condenser outlet air temperatures with time. It is shown that at the beginning of the system operation time the condenser outlet air temperatures decrease with time. This decrease is a result of the decrease in the humidifier temperature at the same period. Then, the temperature profiles changes due to ambient and humidifier temperatures' changes.

Figure 5-6 represents the changes of the measured humidifier inlet air relative humidity with time. It is shown that the values of the humidifier inlet air relative humidity are low in the morning (due to high ambient temperature and increased solar intensity) until noon time. Then during afternoon, the humidifier inlet air relative humidity increased since the system became cooler due to the decrease of the solar heat flux and, accordingly, the decreases in the ambient temperature cause sharp increases at the end of the day.

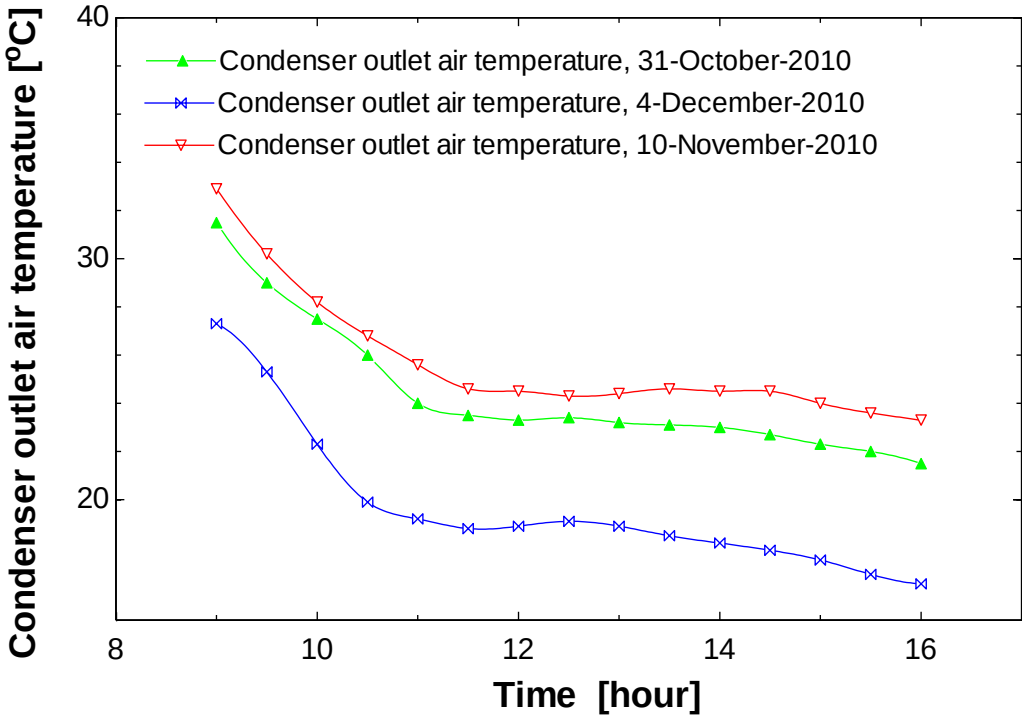

Figure 5-5 Condenser outlet air temperatures for three different days

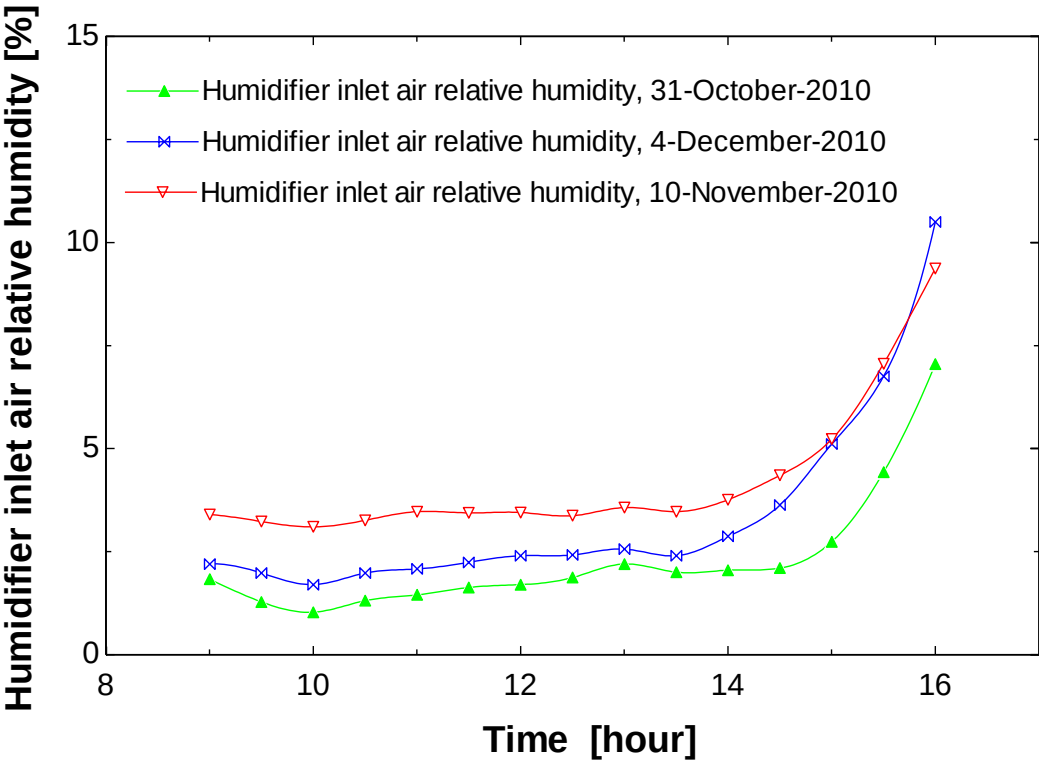

Figure 5-6 Humidifier inlet air relative humidity for three different days

Figure 5-7 represents the changes in the measured humidifier outlet air relative humidity with time. The difference between the measured values of the humidifier outlet air relative humidity of the three trends is due to measuring the humidifier outlet air relative humidity for three different days. However, the same trend is observed qualitatively.

On the other hand, the values of the humidifier outlet air relative humidity were affected by the values of both ambient relative humidity, and the humidifier inlet air relative humidity.

Figure 5-8 represents the changes of the measured condenser outlet air relative humidity with time. It is shown that the values of the condenser outlet air relative humidity are insignificantly changed with time. It is noticed that the values of the condenser outlet air relative humidity are high compared to the humidifier outlet air relative humidity which has approximately the same value of the condenser inlet air relative humidity in the HDH solar system. This can be explained since there is a sensible cooling was carried out during the condenser stage. This increases the air relative humidity. It is important to point out the absolute humidity has decreased due to the condensation process and collection of desalinated water at the exit of the shell side of the condenser.

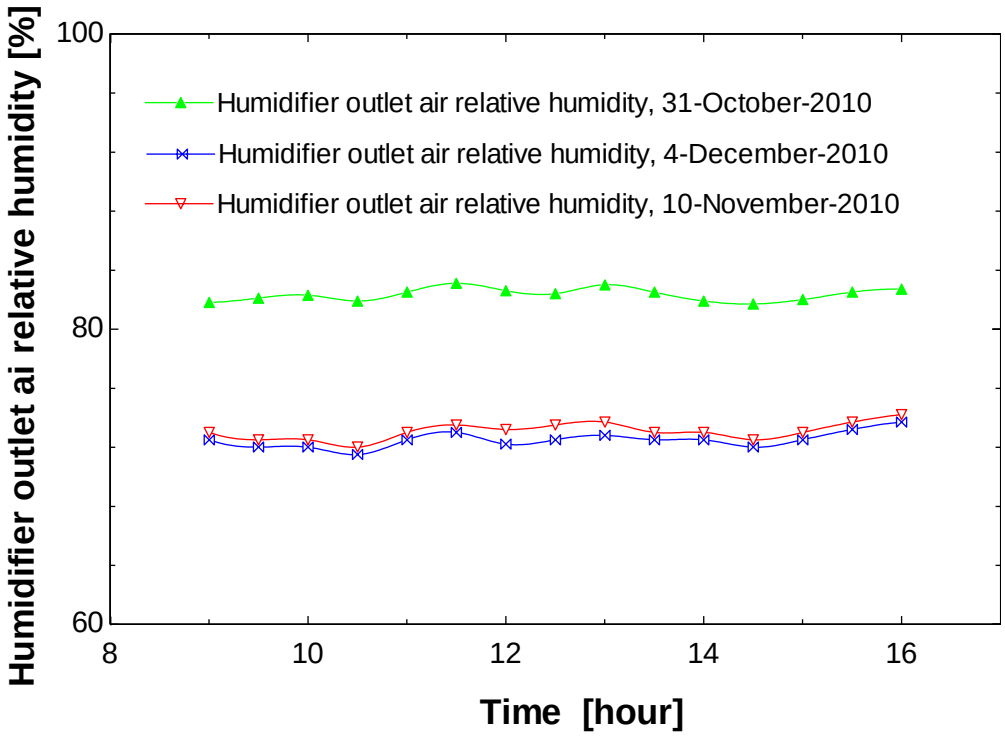

Figure 5-7 Humidifier outlet air relative humidity for three different days

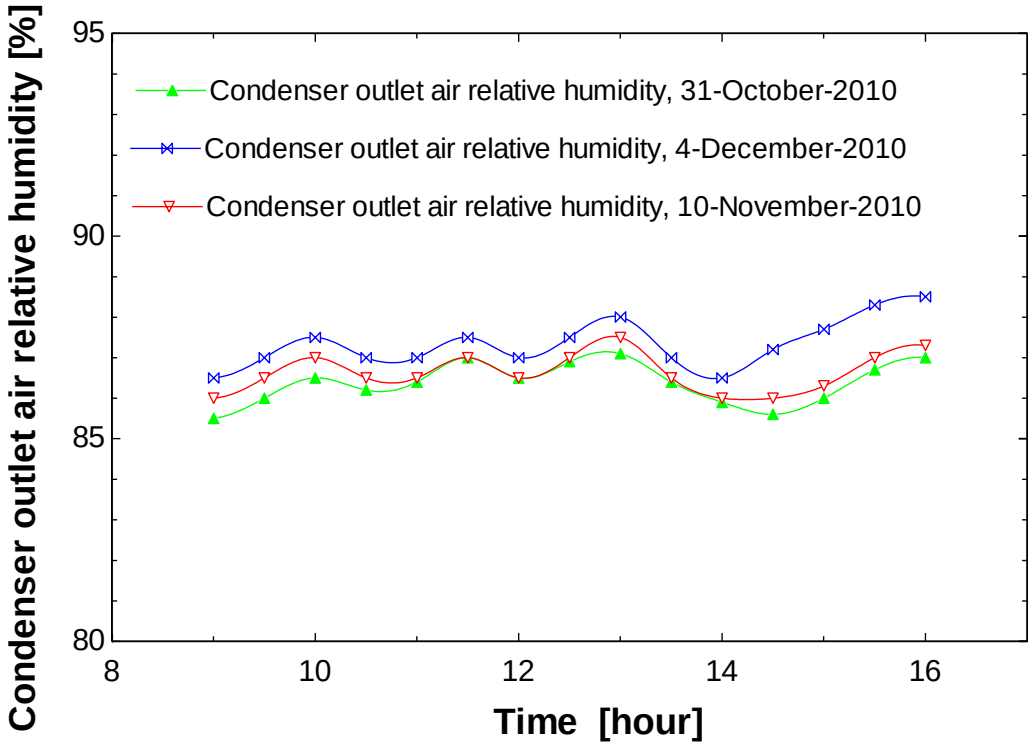

Figure 5-8 Condenser outlet air relative humidity for three different days

5.2 Humidifier inlet water mass flow rate

The effect of changing the humidifier inlet water mass flow rate on the hourly system productivity at constant humidifier inlet air mass flow rate, constant condenser inlet water mass flow rate is shown in Figure 5-9.

It can be noticed that the productivity of the system is increases up to a maximum values then start to decrease after that since the solar intensity, ambient temperature and relative humidity change with time. Moreover, it shows that the productivity of the system decreases with the increases in the values of humidifier inlet water mass flow rate.

Air is brought in contact with the water in the humidifier. As a result, the humidity of the air leaving the humidifier increases. This is due to the increase in the humidifier inlet water mass flow rate. Then, as the water flow rate further increases beyond a peak value, flooding effect may occur, thus decreasing the humidity of air leaving the humidifier.

The accumulated productivity for the HDH system at constant humidifier inlet air mass flow rate, constant condenser inlet water mass flow rate and variable humidifier inlet water mass flow rate is as shown in Figure 5-10. So as the time passes the accumulated productivity increases due to more distilled water produced.

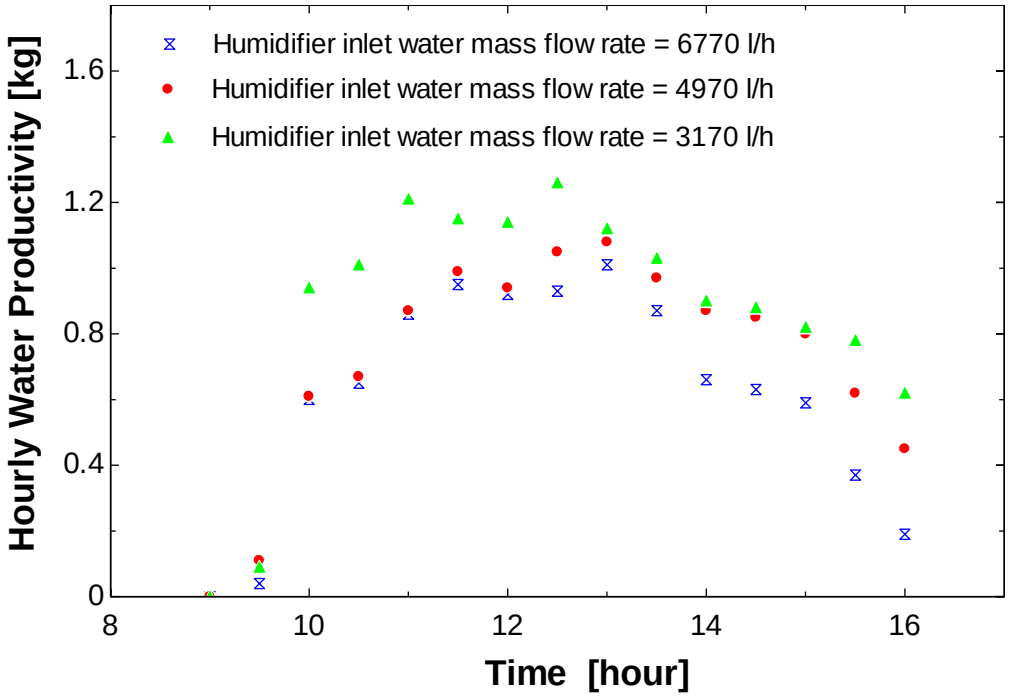

Figure 5-9 Hourly water productivity for different humidifier inlet water mass flow rates

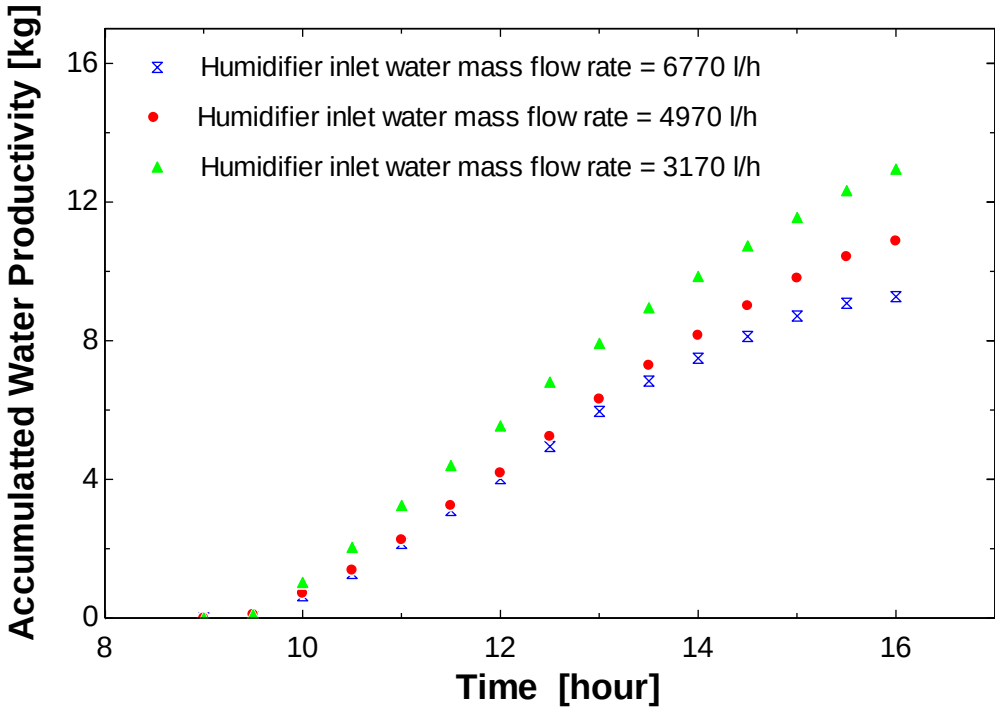

Figure 5-10 Accumulated water productivity for three different humidifier inlet water mass flow rate

5.3 Humidifier inlet air mass flow rate

The effect of the changes in the humidifier inlet air mass flow rate on the hourly system productivity at constant humidifier inlet water mass flow rate and constant condenser inlet water mass flow rate is shown in Figure 5-11. It can be observed that the productivity of the system increases by the increases in the humidifier inlet air mass flow rate values since the air leaving the humidifier with the high moisture content carries more water vapor that condenses in the dehumidifier and this increases the productivity.

The accumulated water productivity for the HDH system at constant humidifier inlet water mass flow rate, constant condenser inlet water mass flow rate and variable humidifier inlet air mass flow rate is as shown in Figure 5-12. Since as the time passes the accumulated productivity increases due to more distilled water are produced.

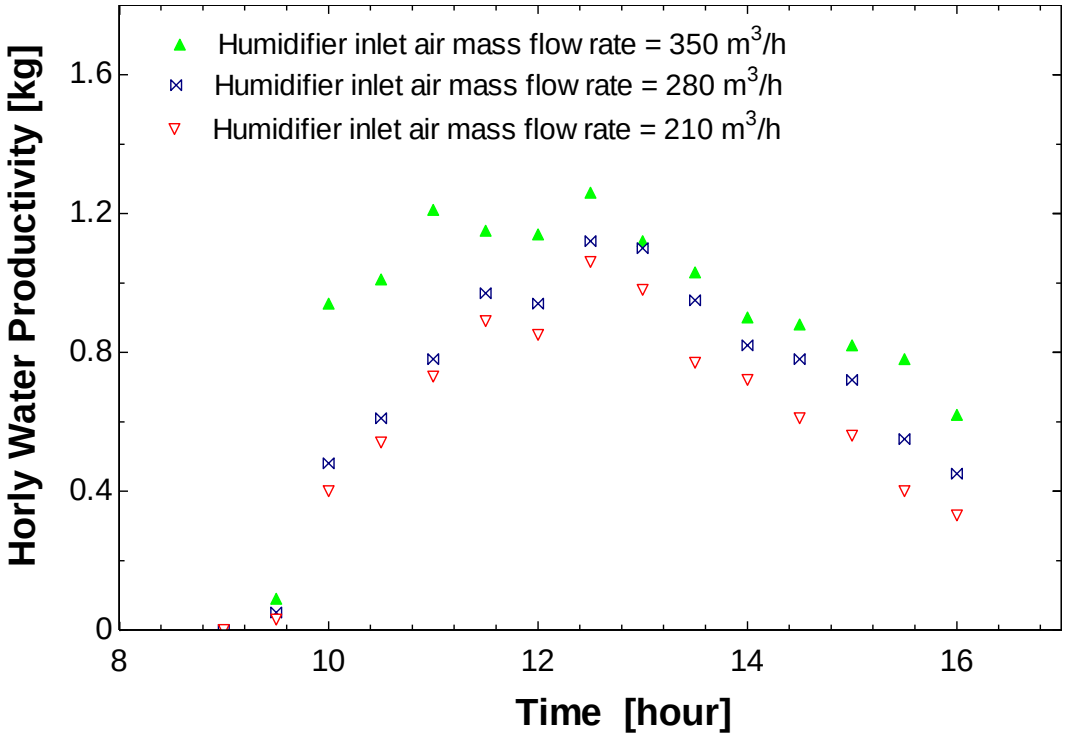

Figure 5-11 Hourly water productivity for different humidifier inlet air mass flow rate

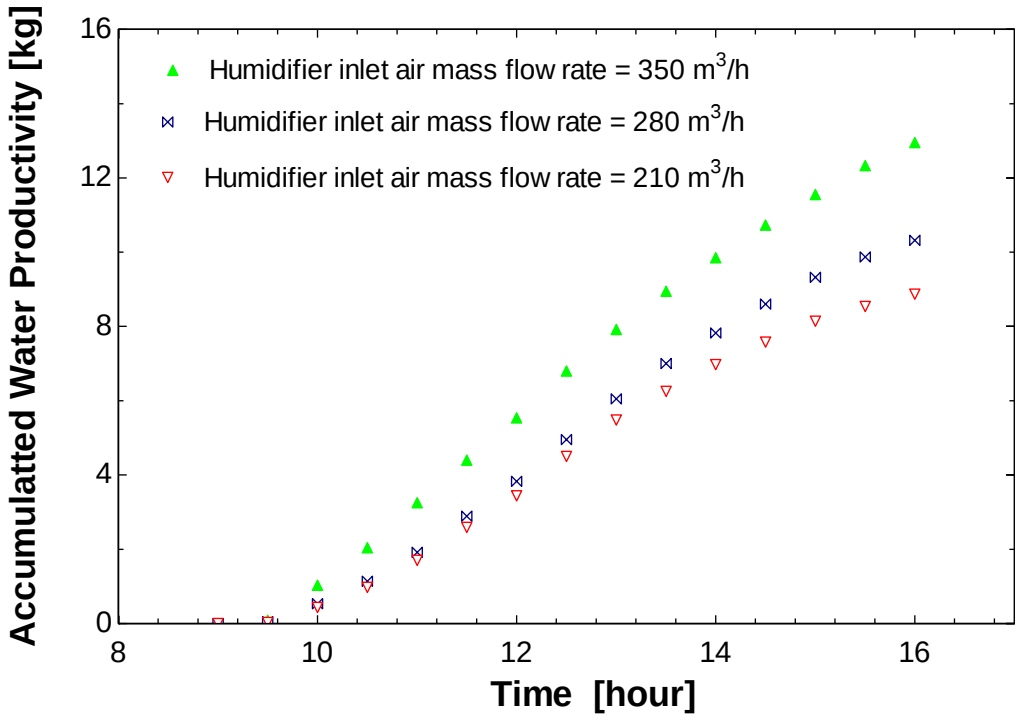

Figure 5-12 Accumulated water productivity for different humidifier inlet air flow rates

5.4 Condenser water mass flow rate

Figure 5-13 shows the effect of the cooling water mass flow rate on the hourly system productivity for fixed humidifier inlet water mass flow rate, humidifier inlet air mass flow rate and different values of the condenser inlet water mass flow rate. It is clear that increasing the cooling water mass flow rate significant drop the surface temperature of the shell and tube condenser. This results in an increase in the rate of the condensation of the water vapor on the shell and tube condenser surface and, thus, the system provides a higher yield.

The accumulated productivity of the system at constant humidifier inlet water mass flow rate, constant humidifier inlet air mass flow rate and selected values of condenser inlet water mass flow rate is shown in Figure 5-14. As the time elapses, the accumulated productivity increases due to more distilled water are produced.

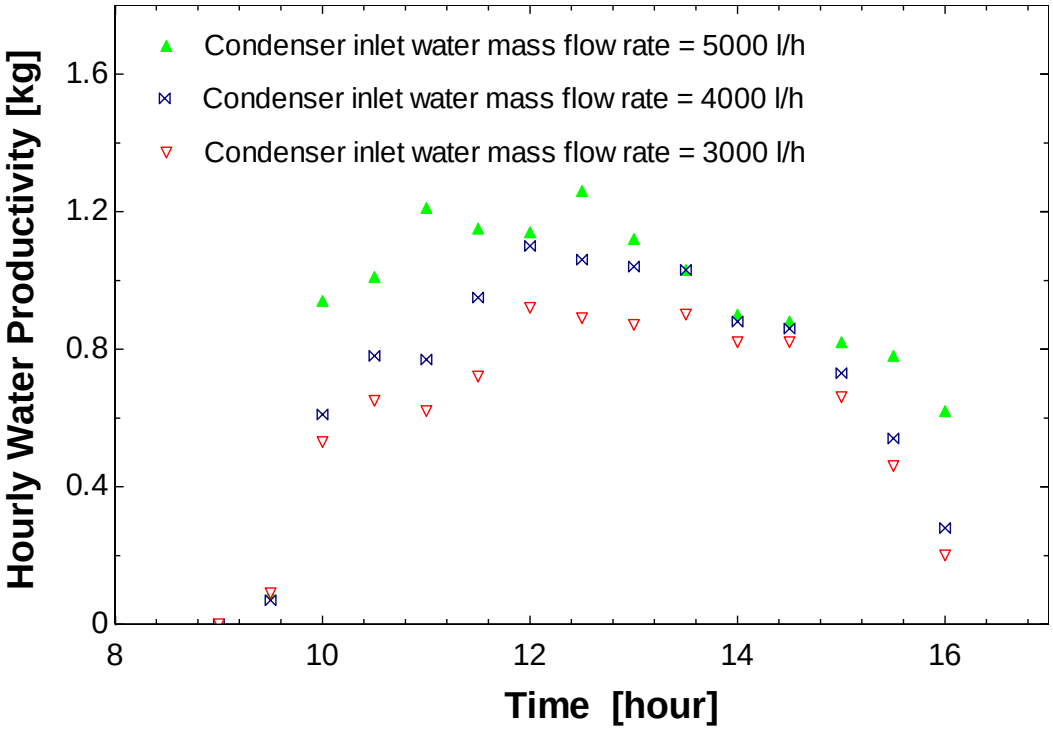

Figure 5-13 Hourly water productivity for different condenser inlet water mass flow rate

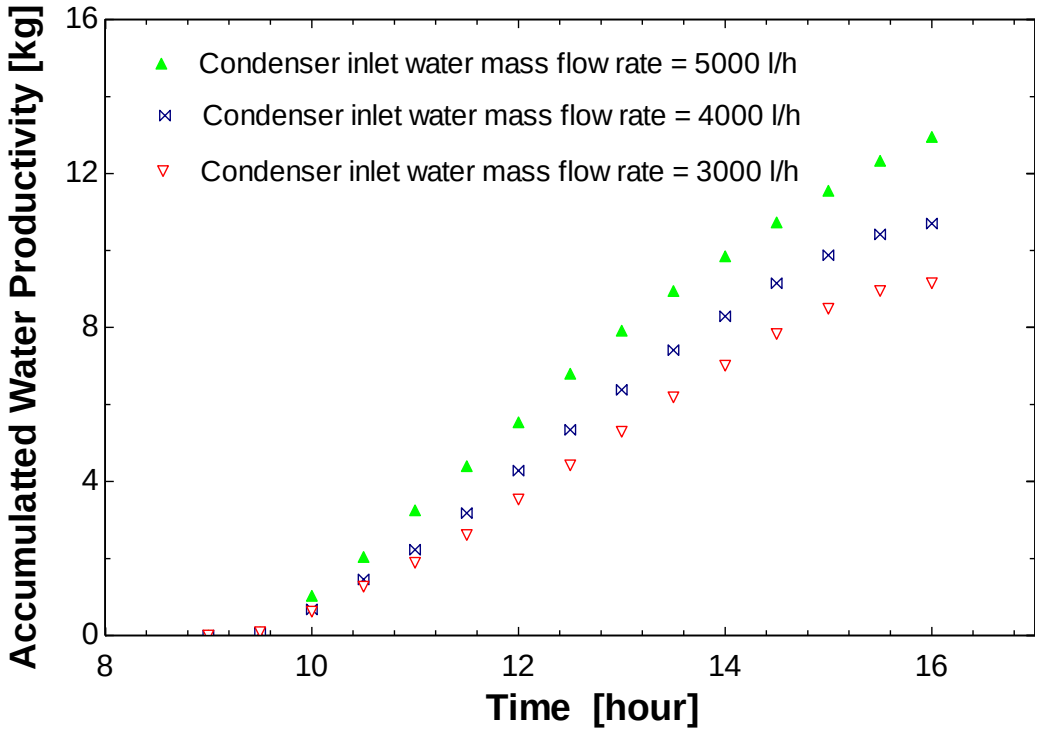

Figure 5-14 Accumulated water productivity at different condenser inlet water flow rates

Figure 5-15 represents the changes of the hourly solar air heater efficiency with time. It is noticed that the hourly solar air heater efficiency changes with time since both the actual and solar intensity from the sun also change with time.

The efficiency of the hourly solar air heater can be calculated using the following equations:

$$q_{ac} = m_a Cp_a (t_{a,o} - t_{a,i}) \quad (108)$$

$$q_{so} = I * A_s \quad (109)$$

$$\eta_s = \frac{q_{ac}}{q_{so}} \quad (110)$$

Figure 5-16 represents the changes in the hourly humidifier effectiveness with time. It is noticed that the hourly humidifier effectiveness is relatively constant since the enthalpy difference between the inlet and outlet of the humidifier is almost the same.

The hourly humidifier effectiveness can be calculated using the following equations:

$$\varepsilon_h = \frac{i_o - i_i}{i_{max} - i_i} \quad (111)$$

The maximum enthalpy calculated at the saturated humidifier outlet air temperature.

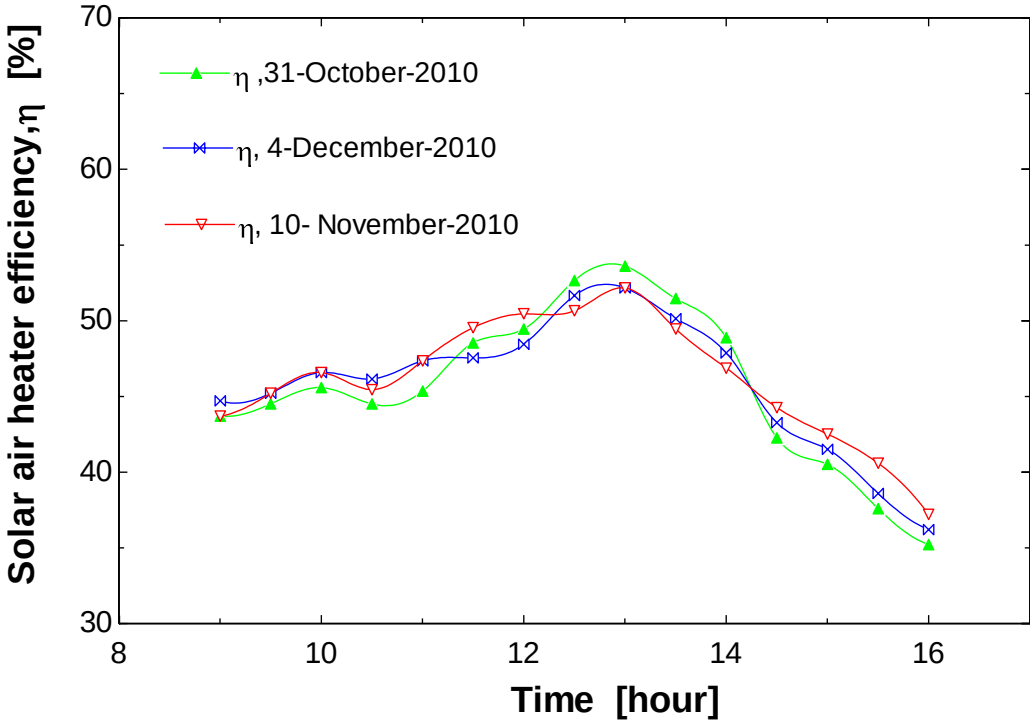

Figure 5-15 Solar air heater efficiency for three different days

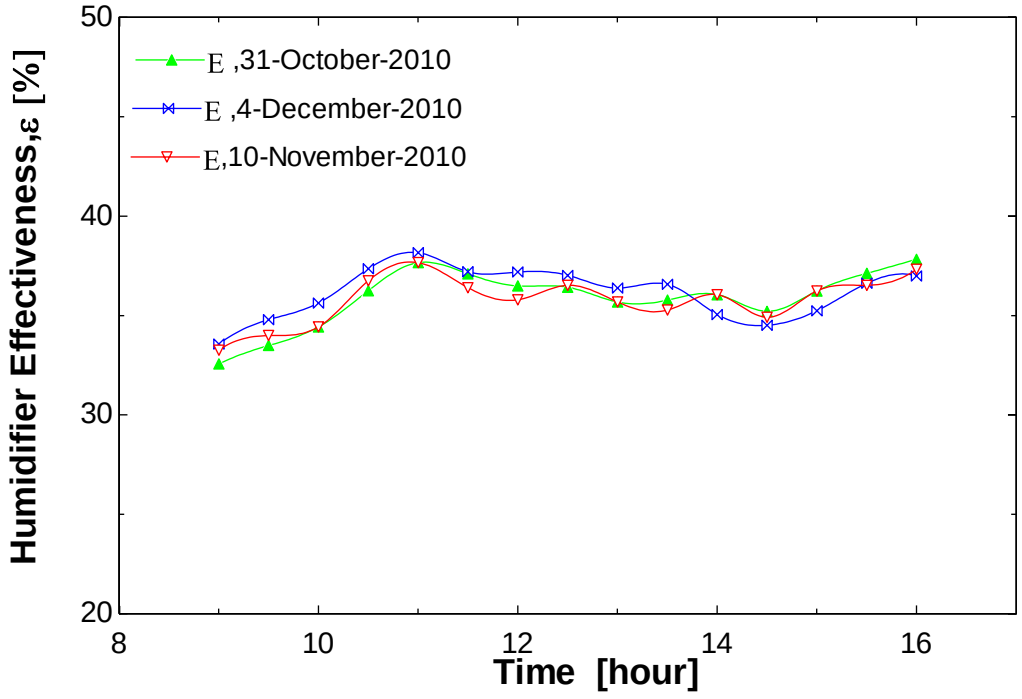

Figure 5-16 Humidifier effectiveness for three different days

Figure 5-17 represents the changes in the hourly condenser effectiveness with time. It is noticed that the hourly condenser effectiveness is relatively constant since the enthalpy difference between the inlet and outlet of the condenser is almost the same.

The hourly condenser effectiveness can be calculated using the following equations:

$$\varepsilon_c = \frac{i_i - i_o}{i_i - i_{min}} \quad (112)$$

The minimum enthalpy calculated at the saturated condenser inlet water temperature.

Validation of the theoretical simulation of the shell and tube condenser model was carried out by comparing the theoretical results with the experimental results of the HDH desalination system at the KFUPM beach.

Figure 5-18 represents the changes in the experimental and theoretical results of the hourly water productivity with time for one typical day. It is noticed that there is a good agreement between the experimental results from the solar HDH desalination system at the KFUPM beach and the simulation as shown in the figure.

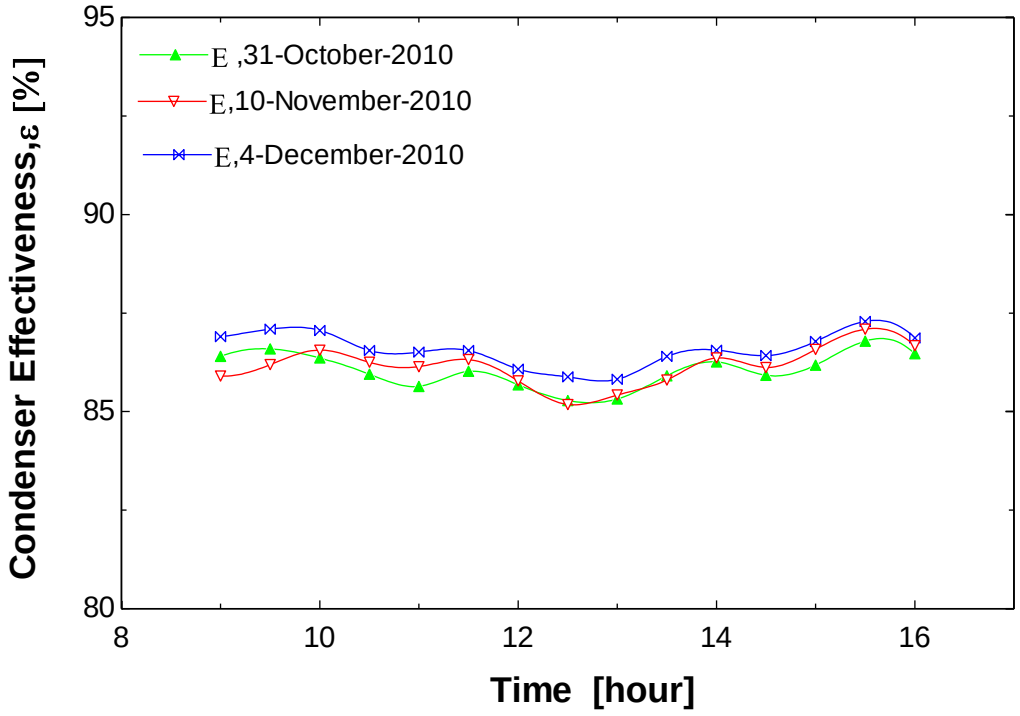

Figure 5-17 Condenser effectiveness for three different days

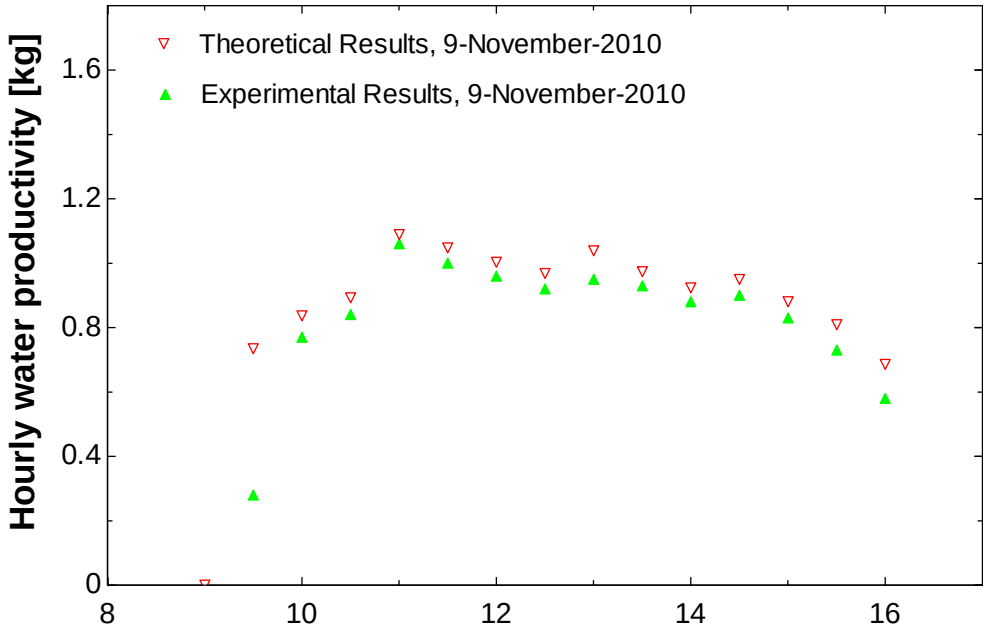

Figure 5-18 A comparison between the experimental and theoretical results of the hourly water productivity for one typical day

Table 5-3 Input parameters of the simulation of the shell and tube condenser

Input data	program values	Unit
Outside tube diameter	25.4	mm
Inside tube diameter	22.09	mm
Tube length	1.60	m
Shell inside diameter	270.0	mm
Number of tubes	28.0	-
Number of tube passes	2.0	-
Number of shell	1.0	-

The accumulated water productivity of the experimental HDH desalination system and the accumulated water productivity of the theoretical model are as shown in Figure 5-19. So as the time passes the accumulated water productivity increases due to more distilled water are produced.

Figure 5-20 represents the changes in the experimental and theoretical results of the condenser outlet air temperature with time for one typical day. Figure 5-21 represents the changes in the experimental and theoretical results of the condenser outlet water temperature with time for one typical day.

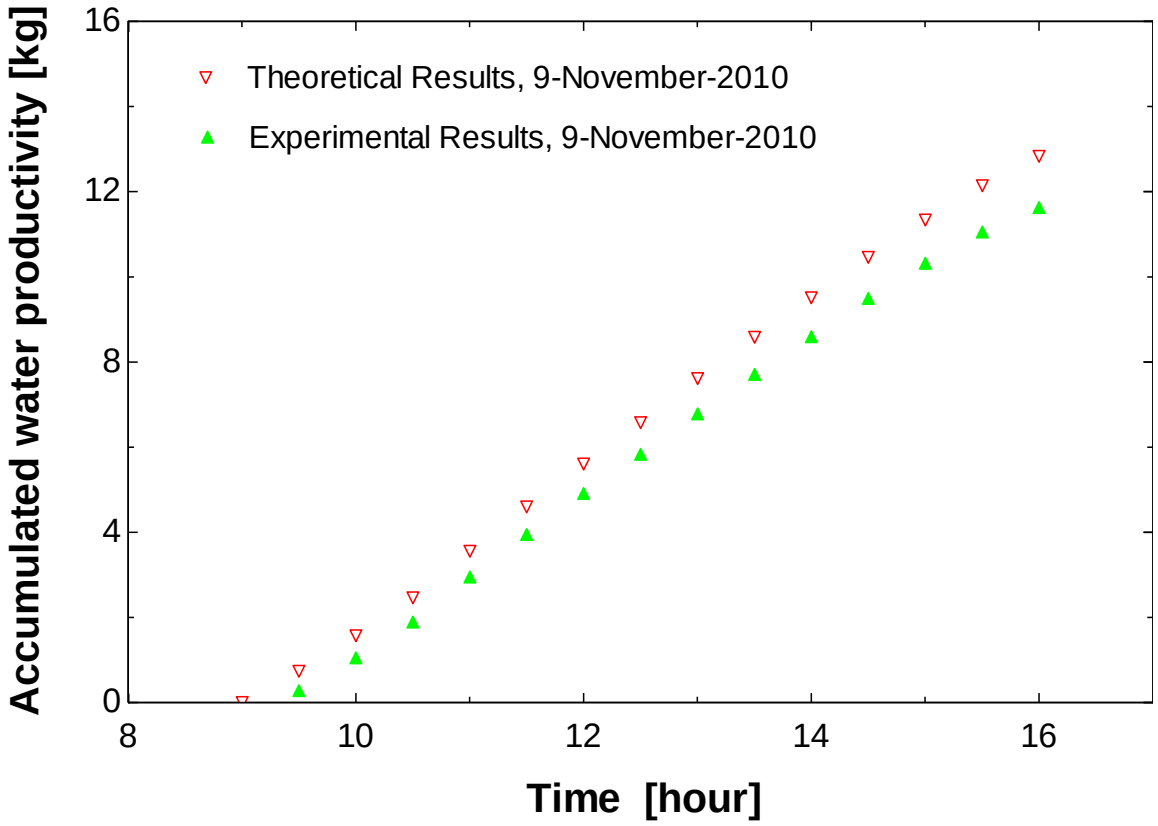

Figure 5-19 A comparison between the experimental and theoretical results of the accumulated water productivity for one typical day

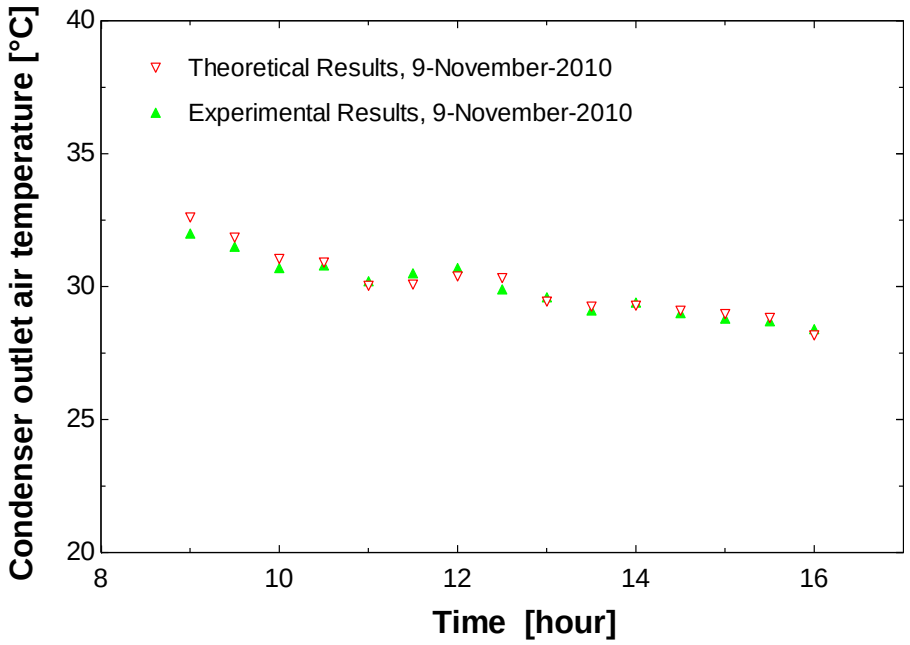

Figure 5-20 A comparison between the experimental and theoretical results of the condenser outlet air temperature for one typical day

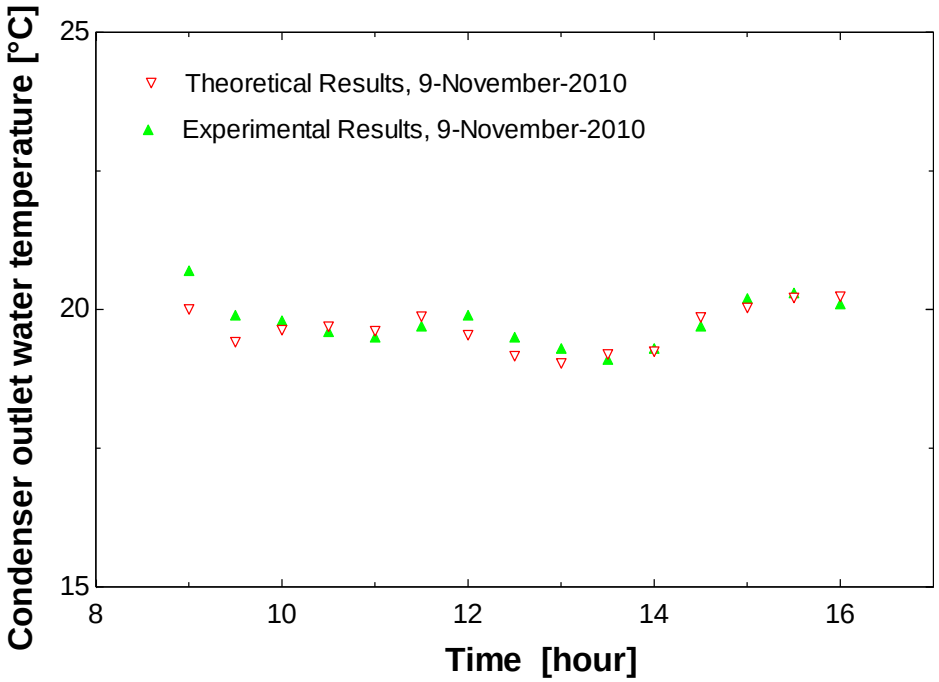

Figure 5-21 A comparison between the experimental and theoretical results of the condenser outlet water temperature for one typical day

The results of the chemical test that was carried out for three samples of water collected from the solar HDH desalination system in the environmental chemistry analytical laboratories at the Research Institute of the KFUPM University as shown in the following table.

Table 5-4 Chemical tests results

Test Name	Unit	Sample No.1	Sample No.2	Sample No.3
pH	----------	6.12	6.76	6.85
Conductivity – EC	S/m	155	30.4	34.8
Turbidity	NTU	0.15	0.16	0.1

Table 5-5 Total suspended solids (TSS) test for the three samples

Test Name	Unit	Sample No.1	Sample No.2	Sample No.3
Weight Difference	(mg)	0.0029	0.0002	0.0003
Total suspended solids	(mg/l)	14.5	1.0	1.50

Table 5-6 Total dissolved solids (TDS) test for the three samples

Test Name	Unit	Sample No.1	Sample No.2	Sample No.3
Weight Difference	(mg)	0.001	0.0008	0.0008
Total dissolved solids	(mg/l)	0.2	0.16	0.16

The final results of the analysis of Metals by ICP Instrument Samples were filtered and acidified with Nitric acid 5% is shown in the following table.

Table 5-7 Final results of the analysis of Metals by ICP Instrument

Metals	Units	Sample no. 1	Sample no. 2	Sample no. 3
As	mg/l	nd	nd	nd
Ca	mg/l	7.64	1.63	1.63
Cd	mg/l	nd	nd	0.014
Cr	mg/l	nd	nd	nd
Cu	mg/l	0.336	0.303	0.443
Fe	mg/l	0.023	0.017	0.005
Hg	mg/l	nd	nd	nd
K	mg/l	0.914	0.271	0.289
Mg	mg/l	1.58	0.384	0.369
Mn	mg/l	0.019	0.007	0.007
Na	mg/l	13.9	1.52	2.46
Pb	mg/l	nd	nd	nd
Se	mg/l	nd	nd	nd
Si	mg/l	0.308	0.091	0.087
Sr	mg/l	0.093	0.025	0.030
Zn	mg/l	0.156	0.168	0.133

Note: nd means not detected (below the detection limit of Instrument).

Table 5-8 Sample analysis results of inorganic metals test

Metals	Sample no. 1	Sample no. 2	Sample no. 3
F (ppm)	0.0218	0.0058	0.0021
Cl (ppm)	5.6618	0.5588	1.6864
NO_2 (ppm)	0.6379	0.3249	0.2251
NO_3 (ppm)	0.0842	0.0436	0.07
SO_4 (ppm)	18.6565	0.7955	1.7341
CO_3 (ppm)	0.0	0.0	0.0
HCO_3 (ppm)	52.34	23.17	22.47

CHAPTER 6

CONCLUSIONS AND RECOMMENDATIONS

6.1 Conclusions

Modeling of a plate fin tube heat exchanger and a shell and tube heat exchanger has been performed and validated against published data and experimental measurements. The effect of changing the air mass flow rate, water mass flow rate, inlet air temperature as well as inlet water temperature has been performed. Simulation results of the plate fin heat exchanger were compared with published results [69] where a very good agreement between the current results and published work was noticed where maximum percentage difference in these calculations does not exceed 8%.

A comparison between the performance of the shell and tube heat exchanger simulation results and published work in the literature [75] has also been made. The results show that the maximum percentage difference in this calculation between both models does not exceed 8%.

It was shown that increasing the air mass flow rate leads to an increase in the condensate flow till an optimum value is reached, and then it decreases. Increasing the water mass flow rate also increases the condensate flow rate.

On the other hand, increasing the air inlet temperature increases the condensate flow rate whereas increasing the inlet water temperature will decrease the condensate flow rate (product).

A sensitivity analysis was carried out for the most influential parameters that affect the performance of the fin plate tube heat exchanger. These results indicated that changes of the condensate flow rate are influenced by the inlet air temperature followed by the inlet relative humidity. In addition, transverse distance and inlet air velocity have an insignificant effect on the condensate flow rate. Other variables have a negligible effect on the condensate mass flow rate.

It is reported that increasing the vapor mass flow rate increases the condensate flow rate till an optimum value is reached and then, the condensate flow rate decreases.

The variation in the hourly productivity was measured and recorded with the changes in the solar intensity and ambient conditions (temperature and relative humidity) with time.

Increasing the humidifier inlet air mass flow rate increases the system productivity since more air carries more vapors toward the humidifier outlet. On the other hand, an increase in the condenser inlet water mass flow rate keeping the air mass flow rate constant increases the productivity of the heat exchanger. This is because the total heat transfer will increase by increasing the water mass flow rate. This means more heat will be absorbed transferred from the air side to the water side. Thus, the temperature of the air will decrease toward the dew point thus increasing the productivity of the system.

6.2 Recommendations

In order to increase the fresh water quantity produced from the current experimental setup, some modification may be carried out for this system. These may include

(1) Optimizing the air and water flow rates of the system to improve its performance.

(2) Adding more stages of heating and humidification to increase the moisture content leaving the humidifier(s) and hence increase the productivity.

(3) Trying different combinations of air and water loops such as closed air loop in combination with open or closed water flow loops.

Bibliography

[1] N. K. Nawayseh, M. M. Farid, A. A. Omar, and A. Sabirin, "Solar desalination based on humidification process- II. Computer simulation," Energy Conversion & Management, vol. 40, no. 13, pp. 1441-1461, 1999.

[2] N. K. Nawayseh, M. M. Farid, A. A. Omar, S. M. Al-Hallaj, and A. R. Tamimi, "A simulation study to improve the performance of a solar humidification-dehumidification desalination unit constructed in Jordan," Desalination, vol. 109, no. 3, pp. 277-284, 1997.

[3] H. Ben Bacha, M. Bouzguenda, M. S. Abid, and A. Y. Maalej, "Modelling and simulation of a water desalination station with solar multiple condensation evaporation cycle technique," Renewable energy, vol. 18, no. 3, pp. 349-365, 1999.

[4] Y. J. Dai, R. Z. Wang, and H. F. Zhang, "Parametric analysis to improve the performance of a solar desalination unit with humidification and dehumidification," Desalination, vol. 142, no. 2, pp. 107-118, 2002.

[5] M. M. Farid, S. Parekh, J. R. Selman, and S. Al-Hallaj, "Solar desalination with a humidification-dehumidification cycle: mathematical modeling of the unit," Desalination, vol. 151, no. 2, pp. 153-164, 2003.

[6] A. S. Nafey, H. E. S. Fath, S. O. El-Helaby, and A. Soliman, "Solar desalination using humidification dehumidification processes. Part I. An numerical investigation," Energy conversion and management, vol. 45, no. 7-8, pp. 1243-1261, 2004.

[7] H. E. S. Fath and A. Ghazy, "Solar desalination using humidification--dehumidification technology," Desalination, vol. 142, no. 2, pp. 119-133, 2002.

[8] C. Y. I. Solmus, "Theoretical investigation of a humidification-dehumidification desalination system configured by a double-pass flat plate solar air heater," Desalination, vol. 205, no. 13 2007.

[9] C. Y. I. Solmus, "A solar desalination system using humidification-dehumidification process: experimental study and comparison with the theoretical results," Desalination, vol. 220, no. 13 2008.

[10] E. Chafik, "A new seawater desalination process using solar energy," Desalination, vol. 153, no. 1, pp. 25-37, 2003.

[11] E. Chafik, "A new type of seawater desalination plants using solar energy," Desalination, vol. 156, no. 1-3, pp. 333-348, 2003.

[12] E. Chafik, "Design of palnts for solar desalination using the multi-stasge heating humidifing technique," Desalination, vol. 168, pp. 55-71, 2004.

[13] C. L. Gupta and H. P. Garg, "System design in solar water heaters with natural circulation," Solar Energy, vol. 12, no. 2, pp. 163-170, 1968.

[14] K. S. Ong, "A finite-difference method to evaluate the thermal performance of a solar water heater," Solar Energy, vol. 16, no. 3, pp. 137-147, 1974.

[15] K. S. Ong, "An improved computer program for the thermal performance of a solar water heater," Solar Energy, vol. 18, no. 3, pp. 183-191, 1976.

[16] A. I. Kudish, P. Santamaura, and P. Beaufort, "Direct measurement and analysis of thermosiphon flow," Solar Energy, vol. 35, no. 2, pp. 167-173, 1985.

[17] G. L. Morrison and J. E. Braun, "System modeling and operation characteristics of thermosyphon solar water heaters," Solar Energy, vol. 34, no. 4, pp. 389-405, 1985.

[18] P. A. Hobson and B. Norton, "A design nomogram for direct thermosyphon solar-energy water heaters," Solar Energy, vol. 43, no. 2, pp. 85-95, 1989.

[19] A. Shariah and B. Shalabi, "Optimal design for a thermosyphon solar water heater," Renewable energy, vol. 11, no. 3, pp. 351-361, 1997.

[20] J. Orfi, M. Laplante, H. Marmouch, N. Galanis, B. Benhamou, S. B. Nasrallah, and C. T. Nguyen, "Experimental and theoretical study of a humidification-dehumidification water desalination system using solar energy," Desalination, vol. 168, pp. 151-159, 2004.

[21] A. S. Nafey, H. E. S. Fath, S. O. El-Helaby, and A. Soliman, "Solar desalination using humidificationûdehumidification processes. Part II. An experimental investigation," Energy conversion and management, vol. 45, no. 7, pp. 1263-1277, 2004.

[22] H. Muller-Holst, M. Engelhardt, and W. Schlkopf, "Small-scale thermal seawater desalination simulation and optimization of system design," Desalination, vol. 122, no. 2, pp. 255-262, 1999.

[23] Treyable R .E., Mass Ttansfer Operation ,3ed, Mc Graw-Hill ,NY, Elsevier, 1980, pp. 255-262.

[24] F. Kreith and R. F. Boehm, "Direct Contact Heat Transfer, Washington: Hemisphere," Corp, 1988.

[25] M. A. Younis, M. A. Darwish, and F. Juwayhel, "Experimental and theoretical study of a humidification-dehumidification desalting system," Desalination, vol. 94, no. 1, pp. 11-24, 1993.

[26] S.A.El-Agouz, M. Abugderah," Experimental analysis of humidification process by air passing through seawater", Energy Conversion and Management, vol.49, no.12, pp. 3698-3703, 2008

[27] A. Lydersen, Mass transfer in engineering practice John Wiley & Sons, 1985.

[28] H. Muller-Holst, M. Engelhardt, M. Herve, and W. Scholkopf, "Solarthermal seawater desalination systems for decentralised use," Renewable energy, vol. 14, no. 1, pp. 311-318, 1998.

[29] F. C. McQuiston, "Finned tube heat exchangers: state of the art for the air side," ASHRAE Trans, vol. 17, no. 1,pp. 14-15, 1980.

[30] D. G. Rich, "The effect of fin spacing on the heat transfer and friction performance of multi-row, smooth plate fin-and-tube heat exchangers," ASHRAE Transactions, vol. 79, no. 2, pp. 137-145, 1973.

[31] D. G. Rich, "The effect of the number of tube rows on heat transfer performance of smooth plate fin-and-tube heat exchangers," ASHRAE Trans, vol. 81, no. 1, pp. 307-317, 1975.

[32] F. C. McQuiston, "Fin efficiency with combined heat and mass transfer," ASHRAE Transactions, vol. 81, no. 1, pp. 350-355, 1975.

[33] F. E. M. Saboya and E. M. Sparrow, "Transfer characteristics of two-row plate fin and tube heat exchanger configurations," International Journal of Heat and Mass Transfer, vol. 19, no. 1, pp. 41-49, 1976.

[34] F. C. McQuiston, "Heat mass and M oumentum transfer Data for five plate -fin tube transfer surface," ASHRAE Transiction Part 1, vol. 84, pp. 266-293, 1978.

[35] F. C. McQuiston, "Correlation of heat, mass and momentum transport coefficients for plate-fin-tube heat transfer surfaces with staggered tubes," ASHRAE Trans, vol. 84, no. 1, pp. 294-309, 1978.

[36] R. L. Webb, T. M. Rudy, and M. A. Kedzierski, "Prediction of the condensation coefficient on horizontal integral-fin tubes," Journal of Heat Transfer, vol. 107, p. 369, 1985.

[37] P. W. Eckels and T. J. Rabas, "Dehumidification: on the correlation of wet and dry transport processes in plate finned-tube heat exchangers," Journal of Heat Transfer, vol. 109, p. 575, 1987.

[38] J. E. R. Coney, C. G. W. Sheppard, and E. A. M. El-Shafei, "Fin performance with condensation from humid air: a numerical investigation," International Journal of Heat and Fluid Flow, vol. 10, no. 3, pp. 224-231, 1989.

[39] A. M. Jacobi and V. W. Goldschmidt, "Low Reynolds number heat and mass transfer measurements of an overall counterflow, baffled, finned-tube, condensing heat exchanger," International Journal of Heat and Mass Transfer, vol. 33, no. 4, pp. 755-765, 1990.

[40] D. R. Mirth and S. Ramadhyani, "Prediction of cooling-coil performance under condensing conditions," International Journal of Heat and Fluid Flow, vol. 14, no. 4, pp. 391-400, 1993.

[41] D. R. Mirth and S. Ramadhyani, "Correlations for predicting the air-side Nusselt numbers and friction factors in chilled-water cooling coils," Experimental Heat Transfer, vol. 7, no. 2, pp. 143-162, 1994.

[42] W. L. Fu, C. C. Wang, W. R. Chang, and C. T. Chang, "Effect of Anti-Corrosion Coating on the Thermal Characteristics of a Louvered Finned Tube Heat Exchangers Under Dehumidifying Conditions," ASME-PUBLICATIONS-HTD, vol. 320, pp. 75-82, 1995.

[43] Y. Seshimo, K. Ogawa, K. Marumoto, and M. Fujii, "Heat and mass transfer performances on plate fin and tube heat exchangers with dehumidification," Heat Transfer-Japanese Research, vol. 18, no. 5, pp. 79-94, 1989.

[44] G. Wu and T. Y. Bong, "Overall efficiency of a straight fin with combined heat and mass transfer," ASHRAE Transactions., no. 374,1994.

[45] M. Sen and K. T. Yang, "Applications of artificial neural networks and genetic algorithms in thermal engineering," CRC handbook of thermal engineering, pp. 620-661, 2000.

[46] Zhao, X.McClain, and R.L.Sen, "an artificial neural network model of heat exchanger," symposium of thermal scince and Engineering in Honor of chancellor-lin-tien, pp. 83-88, Dec.1995.

[47] G. Diaz, M. Sen, K. T. Yang, and R. L. McClain, "Simulation of heat exchanger performance by artificial neural networks," International Journal of Heating Ventilating Air Conditioning and Refrigerating Research, vol. 5, no. 3, pp. 195-208, 1999.

[48] J. Y. Kim and T. H. Song, "Effect of tube alignment on the heat mass transfer from a plate fin and two-tube assembly: naphthalene sublimation results," International Journal of Heat and Mass Transfer, vol. 46, no. 16, pp. 3051-3059, 2003.

[49] M. S. Mon and U. Gross, "Numerical study of fin-spacing effects in annular-finned tube heat exchangers," International Journal of Heat and Mass Transfer, vol. 47, no. 8-9, pp. 1953-1964, 2004.

[50] Y. Kim, "Heat transfer characteristics of flat plate finned-tube heat exchangers with large fin pitch," International Journal of Refrigeration, vol. 28, no. 6, pp. 851-858, 2005.

[51] G. Xie, Q. Wang, and B. Sunden, "Parametric study and multiple correlations on air-side heat transfer and friction characteristics of fin and tube heat exchangers with large number of large diameter tube rows," Applied Thermal Engineering, vol. 29, no. 1, pp. 1-16, 2009.

[52] D. K. Yang, K. S. Lee, and S. Song, "Fin spacing optimization of a fin tube heat exchanger under frosting conditions," International Journal of Heat and Mass Transfer, vol. 49, no. 15-16, pp. 2619-2625, 2006.

[53] D. Q. Kern, Process heat transfer Tata McGraw-Hill, 2002.

[54] T. Tinker, "Shell side characteristics of shell and tube heat exchangers, parts I, II and III, general discussion of heat transfer," Proc. Inst. Mech. Eng. , London, 1951.

[55] K. J. Bell, "Final report of the cooperative research program on shell and tube heat exchangers," Bulletin, vol. 5 1963.

[56] E. A. D. Saunders, Heat exchangers: selection, design & construction Halsted Pr, 1988.

[57] J. Taborek, "Recommended method: principles and limitations," Hedh: Heat Exchanger Design Handbook, 2002.

[58] M. J. N. Wills, D. Johnston, and A. Harwell, "A new and accurate hand calculation method for shellside pressure drop and flow distribution," American Society of Mechanical Engineers,p. 67,1984.

[59] G. F. Hewitt, "Flow stream analysis method for segmentally baffled shell and tube heat exchangers," Hedh: Heat Exchanger Design Handbook, 2002.

[60] M. Reppich and S. Zagermann, "A new design method for segmentally baffled heat exchangers," Computers & Chemical Engineering, vol. 19, pp. 137-142, 1995.

[61] E. S. Gaddis and V. Gnielinski, "Pressure drop on the shell side of shell and tube heat exchangers with segmental baffles," Chemical Engineering and Processing, vol. 36, no. 2, pp. 149-159, 1997.

[62] E. S. Gaddis and V. Gnielinski, "Pressure drop in cross flow across tube bundles," Int. Chem. Eng, vol. 25, no. 1, pp. 1-15, 1985.

[63] H. Li and V. Kottke, "Local heat transfer in the first baffle compartment of the shell and tube heat exchangers for staggered tube arrangement," Experimental Thermal and Fluid Science, vol. 16, no. 4, pp. 342-348, 1998.

[64] H. Li and V. Kottke, "Visualization and determination of local heat transfer coefficients in shell and tube heat exchangers for staggered tube arrangement by mass transfer measurements," Experimental Thermal and Fluid Science, vol. 17, no. 3, pp. 210-216, 1998.

[65] H. Li and V. Kottke, "Effect of the leakage on pressure drop and local heat transfer in shell and tube heat exchangers for staggered tube arrangement," International Journal of Heat and Mass Transfer, vol. 41, no. 2, pp. 425-434, 1998.

[66] H. Li and V. Kottke, "Effect of baffle spacing on pressure drop and local heat transfer in shell and tube heat exchangers for staggered tube arrangement," International Journal of Heat and Mass Transfer, vol. 41, no. 10, pp. 1303-1311, 1998.

[67] G. Diaz, M. Sen, K. T. Yang, and R. L. McClain, "Dynamic prediction and control of heat exchangers using artificial neural networks," International Journal of Heat and Mass Transfer, vol. 44, no. 9, pp. 1671-1679, 2001.

[68] M. Ayoubi, "Dynamic Multi-Layer Perceptron Networks: Application to the Nonlinear Identification and Predictive Control of a Heat Exchanger," Applications of neural adaptive control technology, p. 205, 1997.

[69] F. C. McQuiston, J. D. Parker, and V. Heating, "Air Conditioning Analysis and Design," John Wiley & Sons, New York, 1988.

[70] F. P. Incropera, D. P. DeWitt, T. L. Bergman, and A. S. Lavine, "Fundamentals of heat and mass transfer," 1996.

[71] G. Schmidt and S. J. Thannhauser, "A method for the determination of desoxyribonucleic acid, ribonucleic acid, and phosphoproteins in animal tissues," Journal of Biological Chemistry, vol. 161, no. 1, p. 83, 1945.

[72] A. Saltelli, M. Ratto, T. Andres, F. Campolongo, J. Cariboni, D. Gatelli, M. Saisana, and S. Tarantola, Global sensitivity analysis: the primer Wiley-Interscience, 2008.

[73] S. A. Klein and F. L. Alvarado, "EES-engineering equation solver," F-chart software, 2002.

[74] M. G. Morgan, M. Henrion, and M. Small, Uncertainty: a guide to dealing with uncertainty in quantitative risk and policy analysis Cambridge University Press, 1990.

[75] R. W. Serth, Process heat transfer: principles and applications Academic Press, 2007.

[76] R. A. Bowman, A. C. Mueller, and W. M. Nagle, "Mean temperature difference in design," Trans. ASME, vol. 62, no. 4, pp. 283-294, 1940.

[77] J. Taborek, "Shell-and-tube heat exchangers: single-phase flow," Heat exchanger design handbook, vol. 3, pp. 1-3, 1988.

Vita

Name: Islam Shabaneh

Nationality: Jordanian

Current Address: Dhahran - Saudi Arabia

Permanent Address: Hebron - Palestine

Email: islam_ppu@hotmail.com

Mobile: +966598503713

ACADEMIC QUALIFICATIONS

- Master of Science: King Fahd University of Petroleum and Mineral – 2011

1. Major: Mechanical Engineering
2. Minor: Thermo-Fluid Engineering

- Bachelors of Science: Palestine Polytechnic University –2007 Graduate

1. Major: Mechanical Engineering
2. Minor: Air conditioning & Refrigeration Engineering